ELEMENTAL COMPOSITION OF SOLAR ENERGETIC PARTICLES

Thesis by

Walter Richardson Cook III

In Partial Fulfillment of the Requirements

for the Degree of

Doctor of Philosophy

California Institute of Technology

Pasadena, California

1981

(Submitted November 3, 1980)

SRL 80-5

Acknowledgements

This thesis is based on experiments aboard the Voyager 1 and 2 spacecraft and therefore owes much to the people across the country who have contributed to the outstanding success of the Voyager mission. Although I cannot individually thank them, I gratefully acknowledge their excellent work.

Among those who have made special contributions to this thesis and to my education, foremost is my advisor Dr. Rochus Vogt. I especially thank Dr. Vogt for his scientific leadership as the principal investigator of the Voyager Cosmic Ray Subsystem (CRS), for his thoughts on science and people, and for encouraging independence throughout my graduate career. I am particularly grateful to Dr. Vogt for providing the opportunity for me to participate in the many phases of the Voyager experiment, from instrument design, fabrication, testing and calibration, to data analysis and the study of scientific results.

I also sincerely thank Dr. Edward Stone and Dr. Richard Mewaldt. Dr. Stone has served in many ways as my co-advisor. As a CRS co-investigator he designed the Low Energy Telescopes which provided the data for this thesis. As the Voyager project scientist he has not only made major contributions to this work, but is largely responsible for the scientific success of the entire Voyager mission. Dr. Mewaldt has provided valuable ideas, comments and criticism throughout this work. His advice and help during my early days in the lab are very much appreciated.

There are many others at Caltech who have made my work both enjoyable and rewarding. Bill Althouse was responsible for much of the technical design and implementation of the CRS experiment. I have valued his insights into electronics, mechanical design and experimental techniques. I have enjoyed working closely with Drs. Tom Garrard and Allan Cummings throughout all the phases of the Voyager project. Dr. Garrard was in charge of, among many other things, the Voyager data processing system — I particularly thank him for his cooperation in matters of the computer. Dr. Cummings had major responsibility for the assembly and testing of the Voyager Lower Energy Telescopes and therefore deserves much of the credit for their nearly flawless performance during the observations of this work.

I appreciate the many contributions of my fellow graduate students. I particularly thank Neil Gehrels for his help during the accelerator calibration of the Voyager Electron Telescope and his analysis of the Low Energy Telescope laboratory calibrations; Jim Povlis for the analysis and organization of the CRS electronic calibration results; and John Spalding for valuable discussions of data analysis techniques. I also thank former graduate students Dr. Frank Marshall and Dr. Steward Hartman for their help and friendship during my first years of graduate study.

A main part of my training in experimental physics was the calibration of the Voyager Electron Telescope at an electron linear accelerator. I especially thank those who helped in that effort: Bill Althouse, Dr. Allan Cummings, Neil Gehrels, Brownlee Gauld, Neil Hickey, Marty Smith, and Dr. Rochus Vogt.

In addition, I thank all the other members of the Space Radiation Laboratory staff: In particular, Tom Aufrance and Brownlee Gauld for their contributions to the Voyager data processing software; Susan McCurdy for her patience and help; and Mark Walther for his assistance with the computers.

The Voyager CRS is the result of a collaboration of research groups at Caltech, Goddard Space Flight Center, the University of Arizona, and the University of New Hampshire. I have appreciated my occasional opportunities for contact with people from these groups including Don Stilwell, Bill Davis, Nan Lal and CRS co-investigators Dr. Frank McDonald, Dr. Jim Trainor, Dr. Bonnard Teegarden, and Dr. Bill Webber.

This work has been supported in part by the National Aeronautics and Space Administration under contract NAS7-100 and grant NGR 05-002-160. I gratefully acknowledge tuition scholarships from the California Institute of Technology.

Finally, I thank the people who are very dear to me - my parents Richard and Jean and my brothers Steve and Dave - for their love, encouragement, and enthusiasm over the years.

Most of all I thank Helene R. Schember. Her love and encouragement, her careful reading and criticism of the text, and her extensive knowledge of the computer programs which I have used to edit and type this thesis have been invaluable to me.

Abstract

The Low Energy Telescopes on the Voyager spacecraft are used to measure the elemental composition ($2 \leq Z \leq 28$) and energy spectra (5 to 15 MeV/nucleon) of solar energetic particles (SEPs) in seven large flare events. Four flare events are selected which have SEP abundance ratios approximately independent of energy/nucleon. The abundances for these events are compared from flare to flare and are compared to solar abundances from other sources: spectroscopy of the photosphere and corona, and solar wind measurements.

The selected SEP composition results may be described by an average composition plus a systematic flare-to-flare deviation about the average. For each of the four events, the ratios of the SEP abundances to the four-flare average SEP abundances are approximately monotonic functions of nuclear charge Z in the range $6 \leq Z \leq 28$. An exception to this Z-dependent trend occurs for He, whose abundance relative to Si is nearly the same in all four events.

The four-flare average SEP composition is significantly different from the solar composition determined by photospheric spectroscopy: The elements C, N and O are depleted in SEPs by a factor of about five relative to the elements Na, Mg, Al, Si, Ca, Cr, Fe and Ni. For some elemental abundance ratios (e.g. Mg/O), the difference between SEP and photospheric results is persistent from flare to flare and is apparently not due to a systematic difference in SEP energy/nucleon spectra between the elements, nor to propagation effects which would result in a time-dependent abundance ratio in

individual flare events.

The four-flare average SEP composition is in agreement with solar wind abundance results and with a number of recent coronal abundance measurements. The evidence for a common depletion of oxygen in SEPs, the corona and the solar wind relative to the photosphere suggests that the SEPs originate in the corona and that both the SEPs and solar wind sample a coronal composition which is significantly and persistently different from that of the photosphere.

Table of Contents

Chapter 1

Introduction

The energetic particles which are often ejected from solar flares constitute a sample of solar material which may be analyzed to yield information on the elemental and isotopic composition of the solar atmosphere -- information that impacts a wide range of astrophysical problems from the history of the solar system, to solar structure and dynamics, to nucleosynthesis.

Following the pioneering spectroscopic study by H. N. Russell (1929), the composition of the sun has been the subject of extensive experimental and theoretical investigations (see, e.g., Claas 1951, and Goldberg, Muller and Aller 1960), yet today our knowledge of solar composition remains inadequate. Currently, solar composition information is obtained using a number of techniques including spectroscopy of the photosphere and corona, and measurements of solar wind and of energetic particles from solar flares (see the review by Ross and Aller 1976, the update by Aller 1980 and references therein). None of the techniques are free of difficulty: Spectroscopic abundance determinations are (a) subject to inaccuracies in modeling the temperature and density structure of the solar atmosphere and to uncertainties in our knowledge of the spectral line formation mechanisms and atomic transition probabilities, and are (b) particularly difficult to obtain for some elements -- most notably helium, the second most abundant solar constituent. While the solar wind and energetic flare particles are samples of solar material whose composition is directly measured, there is the concern that these

samples may be biased since in both cases the elemental composition varies and may be influenced by acceleration effects which are currently not understood.

The potential of solar energetic particle (SEP) measurements as a source of solar composition information was first explored in the early 1960's using rocket-borne nuclear emulsion experiments with energy thresholds near 40 MeV/nucleon. The early work (see the reviews by Biswas and Fichtel 1965; Bertsch, Fichtel and Reames 1972) suggested that, for nuclei with nearly the same nuclear charge to mass ratio (namely most of the abundant nuclei except protons), the SEPs might indeed represent an unbiased sample of solar material. In six different flare events, the ratios of the numbers of He nuclei to medium group nuclei (M = C + N + O), when counted in common energy/nucleon (i.e. particle speed) intervals, were found to be (a) approximately independent of the choice of the energy/nucleon interval and (b) nearly constant from flare to flare (Biswas, Fichtel and Guss 1962; Biswas et. al. 1963; Biswas, Fichtel and Guss 1966; Durgaprasad et. al. 1968; Bertsch, Fichtel and Reames 1972). Combining the measured SEP He/M ratio (= 58± 5) with the spectroscopically determined M/H ratio, Bertsch, Fichtel and Reames (1972) obtained H/He = 16± 2, one of the few available estimates of the solar H/He abundance ratio. The early emulsion measurements achieved only poor statistical accuracy and charge resolution for the elements Ne, Mg, Si and Fe, but suggested that the SEP abundances of these elements relative to the M group nuclei were roughly constant from flare to flare and similar to spectroscopic abundance results (Biswas and Fichtel 1965; Bertsch,

Fichtel and Reames 1972). In contrast to the apparent constancy of SEP composition for He and heavier nuclei, the SEP proton to He nuclei ratio was found to vary (by factors of 10 to 100) from flare to flare and as a function of time and energy/nucleon in single flare events (see, e.g., Biswas and Fichtel 1965; Fichtel and McDonald 1967).

The above results suggested that during acceleration and propagation to earth the SEPs were fully stripped of electrons and interacted mainly with large scale electromagnetic fields. In this case most of the abundant nuclei, except protons, would have nearly equal charge to mass ratios and would be affected almost identically by the electromagnetic fields, no matter how complex. However, the charge to mass ratio of protons would be a factor of two larger than that of the other abundant nuclei, and this difference might account for the observed variability of the SEP proton to He (or heavier) nuclei ratio. The early SEP results also suggested that processes which do not scale as the charge to mass ratio (such as thermal particle acceleration, or particle deceleration by Coulomb interactions) were not very important during SEP acceleration and propagation.

However, following the early nuclear emulsion results, a large amount of research has indicated that, even for elemental species with the same nuclear charge to mass ratios, the SEP elemental composition does vary from flare to flare (see, e.g., Armstrong and Krimigis 1971; Armstrong et. al. 1972; Mogro-Campero and Simpson 1972b; Bertsch et. al. 1973; Teegarden, von Rosenvinge and McDonald 1973; Crawford et. al. 1975) and sometimes varies with time, space, and/or energy per nucleon in single flare events (see, e.g., Bertsch, Biswas and Reames

1974; Van Allen, Venketarangan and Venkatesan 1974; Crawford et. al. 1975; Armstrong et. al. 1976; O'Gallagher et. al. 1976; Scholer et. al. 1978). Some of the more extreme SEP elemental composition anomalies are associated with large ^3He enhancements (Hovestadt et. al. 1975, Hurford et. al. 1975; Zwickl et. al. 1978). The few reported charge state measurements of SEPs are for energies below about 1 MeV/nucleon and indicate that while C and O nuclei are almost fully stripped, iron nuclei retain more than half their electrons (Sciambi et. al. 1977; Gloeckler et. al. 1976).

This apparent complexity, and the availability of high quality SEP composition measurements for only a small number of flare events, has made it difficult to determine which features of SEP composition are the same from flare to flare and which are variable. One area of uncertainty is the energy dependence of SEP composition. Until recently, the most extensive work in this area was performed using plastic and glass track detectors and nuclear emulsions aboard rockets and Apollo spacecraft. Crawford et. al. (1975) summarized this work and concluded that, above an energy E_0 (which ranged between about 5 and 20 MeV/nucleon in five different flare events), the SEP composition was (a) approximately independent of energy/nucleon, (b) roughly constant from flare to flare and (c) the same as spectroscopic composition results within factors of two to three. However, below energy E_0, they found that the heavy elements were enhanced by an amount which varied from flare to flare, but always increased with decreasing energy/nucleon and increasing nuclear charge Z (see Figure 1.1 which shows data from one of the five flares). In contrast, Mason,

Figure 1.1

SEP composition measurements for the 25 January 1971 solar flare event, showing the enhancement of heavy elements, such as Fe, at energies below about 15 MeV/nucleon (taken from Crawford et. al. 1975). The flux measurements of He nuclei by Lanzerotti, Maclennan and Graedel (1972) were performed with an instrument aboard the IMP 5 satellite. The other data, including those of Bertsch et. al. (1973), were obtained during a rocket flight. (The smooth curves drawn through the data are meant only to guide the eye.)

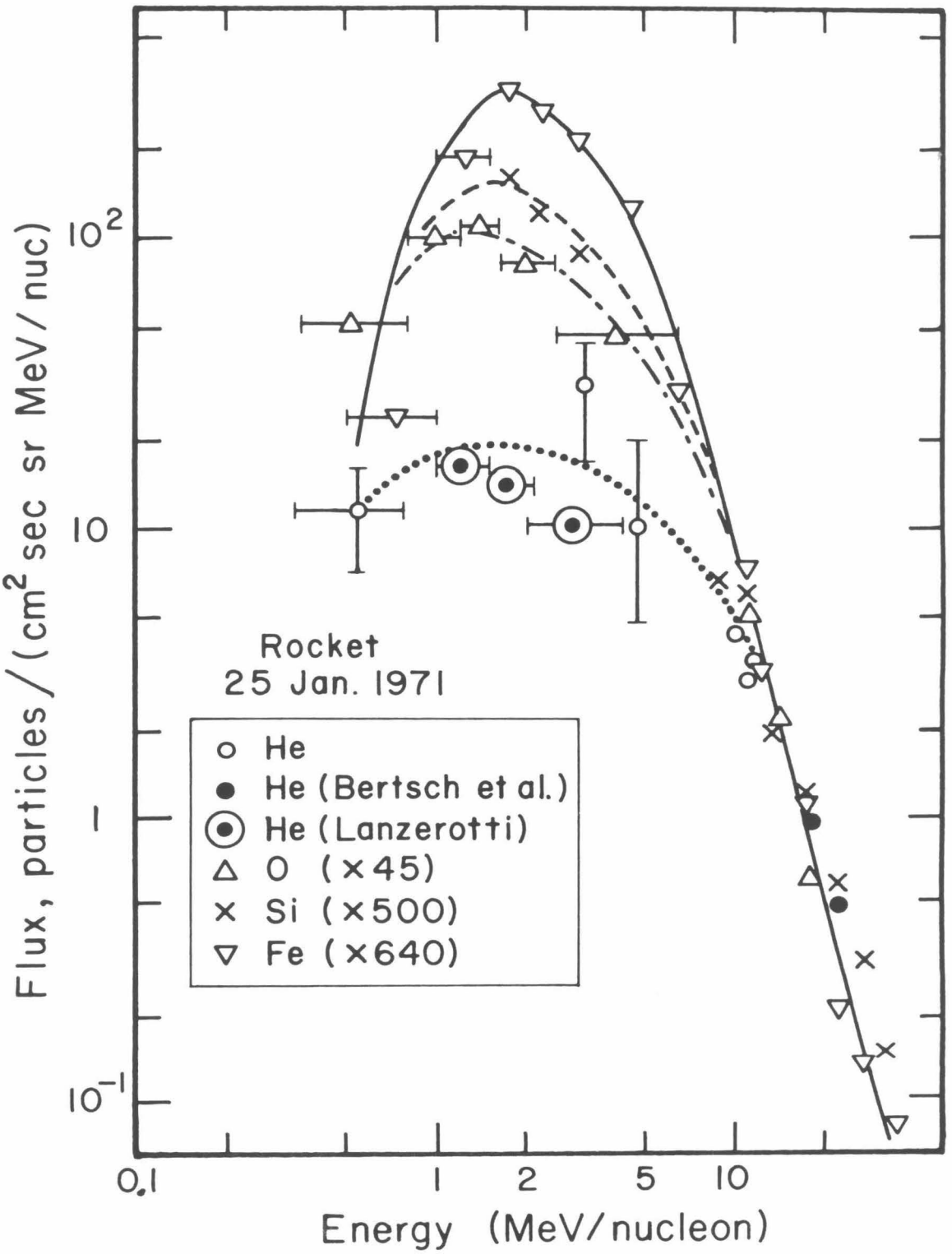
Flux, particles / (cm² sec sr MeV/nuc)
10²
10
1
10⁻¹
0.1
1
2
5
10
Energy (MeV/nucleon)
Rocket
25 Jan. 1971
He
He (Bertsch et al.)
He (Lanzerotti)
O (×45)
Si (×500)
Fe (×640)

Hovestadt and Gloeckler (1979), in a satellite study of flare events in the 1973 to 1977 period, found that the average SEP composition for the abundant elements from He through Fe was essentially the same at 1 MeV/nucleon as that measured by others above 10 MeV/nucleon. Further, heavy element enhancements which were found only at low energies by Crawford et. al. (1975) have been reported above 25 MeV/nucleon in one flare event (Bertsch and Reames 1977) and, in another event, were found to extend from 25 to above 100 MeV/nucleon, independent of energy/nucleon (Dietrich and Simpson 1978).

Another area of uncertainty is the relationship of SEP composition to the solar composition values which have been determined by other means. Crawford et. al. (1975) compared their best estimate of SEP composition above 15 MeV/nucleon with their best estimate of solar atmosphere composition based on spectroscopic data and concluded that the differences did not correlate with either first ionization potential or nuclear charge Z, and were small enough (factors of two to three) to result from errors in the spectroscopic abundances. On the other hand, Webber (1975) found that the differences between his best estimates of SEP and solar atmosphere composition were significant and were correlated with first ionization potential -- the elements with high first ionization potentials were found to be depleted in SEPs (see Figure 1.2). Averaging over seven flare events Mogro-Campero and Simpson (1972a,b) reported still different results -- the SEP abundances of the heavy elements were enhanced relative to "solar system" composition (derived from a mixture of solar spectroscopic data, meteoritic data, earlier SEP

Figure 1.2

A comparison of solar energetic particle (SEP) abundances to solar atmosphere (SA) abundances determined by spectroscopy, showing a relative depletion in SEPs of elements with high first ionization potential (taken from Webber 1975).

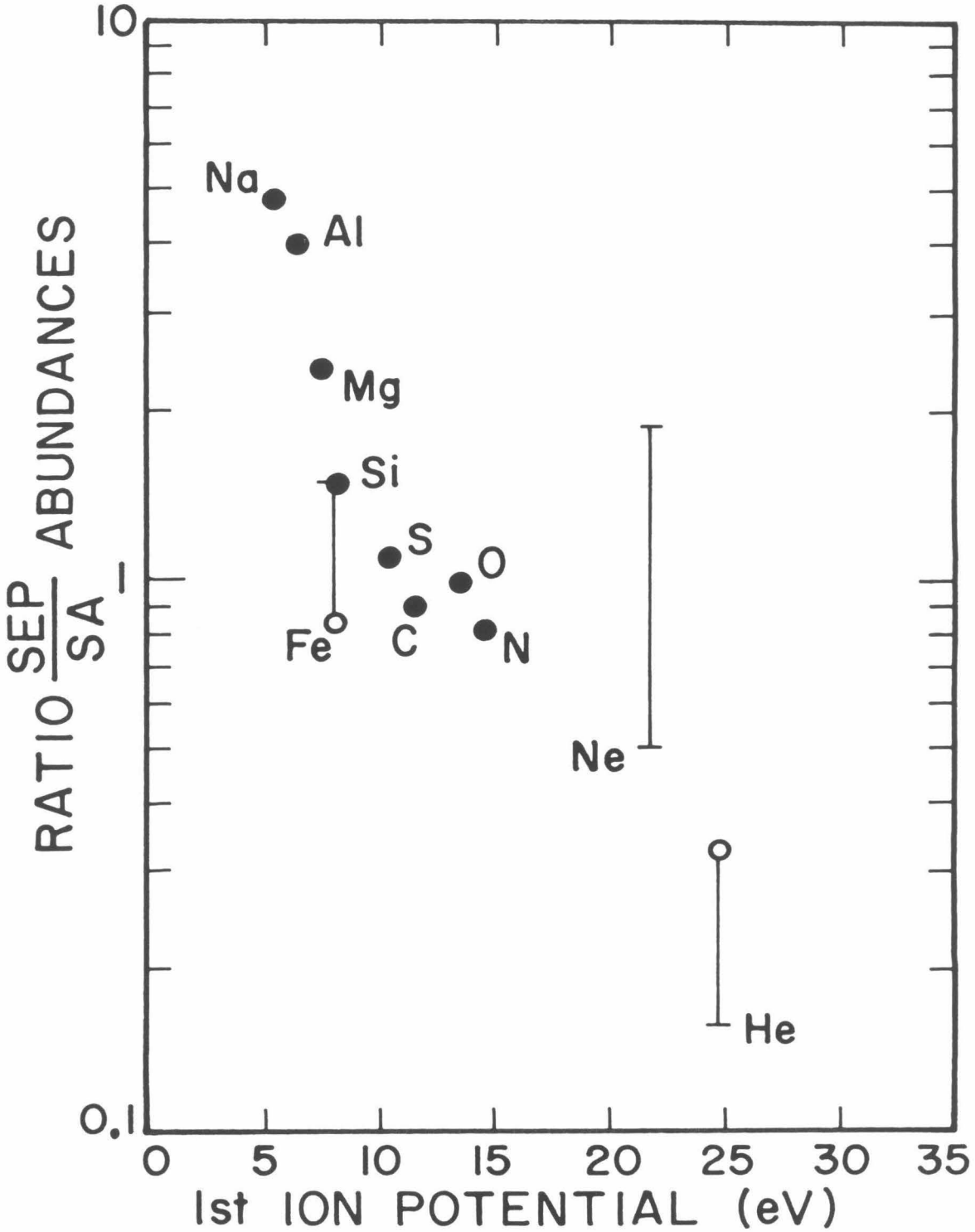
10
0.1
RATIO SEP/SA ABUNDANCES
Na
Al
Mg
Si
S
O
Fe
C
N
Ne
He
0
5
10
15
20
25
30
35
1st ION POTENTIAL (eV)

results, and nucleosynthesis theory; Cameron 1968) by an amount which increased as an approximately monotonic function of nuclear charge Z, for the abundant nuclei from carbon through iron. Similar heavy element enhancements were reported by Bertsch and Reames (1977) and Dietrich and Simpson (1978); see Figure 1.3. Furthermore, Dietrich and Simpson (1978) claimed an additional enhancement of the rare odd-Z nuclei, such as B, F, Na, and Al, by amounts consistent with the production of these nuclei in spallation reactions of the other even-Z nuclei during passage through an estimated 0.6 gm/cm^2 of solar atmospheric material -- a claim which has been disputed by Cook et. al. (1979) and McGuire, von Rosenvinge and McDonald (1979) (also see Section 4.4.2 of this thesis).

The above comments indicate the need to study SEP composition in a large number of flare events with a single, high-quality experiment and common analysis criteria, as is done in this thesis. Here, we present SEP composition measurements for seven large flare events which occurred in the September 1977 to May 1978 period. The measurements were performed in interplanetary space with advanced instrumentation on the Voyager 1 and 2 spacecraft and cover the nuclear charge range from He (Z=2) through Ni (Z=28) with the best combination of charge resolution, background rejection and statistical accuracy achieved to date. Thus, for the first time, we are able to study statistically significant measurements of 15 different elemental species (He, C, N, O, Ne, Na, Mg, Al, Si, S, Ar, Ca, Cr, Fe, and Ni) in seven individual flare events.

With the goal of understanding the relationship between SEP

Figure 1.3

The ratio (Enhancement Factor, Q) of solar energetic particle (SEP) abundance to "solar system" abundance plotted versus nuclear charge Z, for the 24 September 1977 flare event (taken from Dietrich and Simpson 1978). The use of "solar system" abundances which were a mixture of results from different sources (including earlier SEP data for the elements Ne, Mg, and Si) led Dietrich and Simpson to claim that (a) the enhancement of even–Z nuclei in SEPs increased as an approximately monotonic function of Z and (b) the rarer odd–Z nuclei Na and Al were additionally enhanced in SEPs as the result of spallation of even–Z nuclei in the solar atmosphere. Cook et. al. (1979) and McGuire, von Rosenvinge and McDonald (1979) obtained different conclusions (see section 4.4.2 of this thesis).

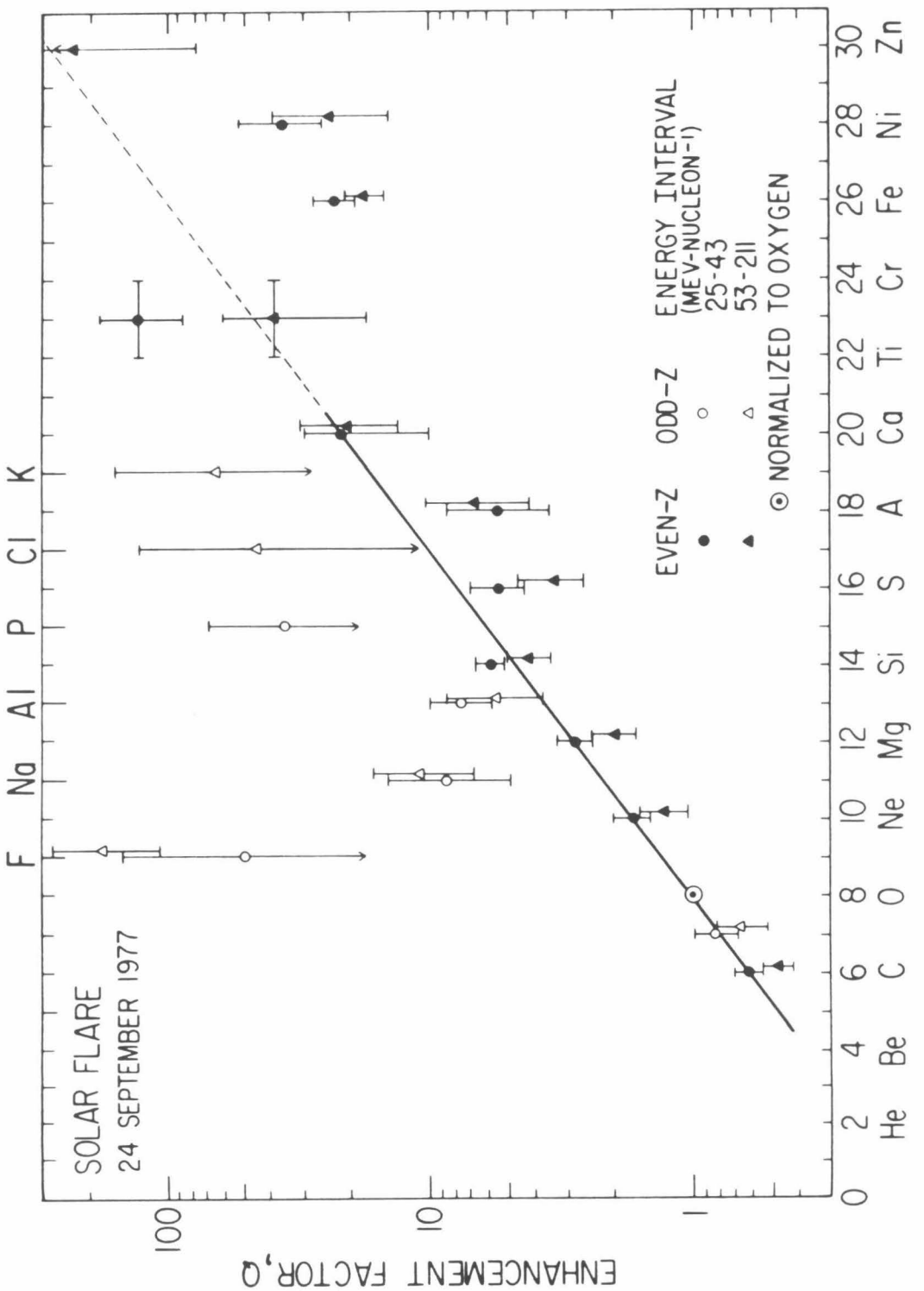
SOLAR FLARE
24 SEPTEMBER 1977
EVEN-Z ODD-Z ENERGY INTERVAL (MEV-NUCLEON-1)
25-43
53-211
⊙ NORMALIZED TO OXYGEN
ENHANCEMENT FACTOR, Q
NUCLEAR CHARGE, Z
100
10
1
0 2 4 6 8 10 12 14 16 18 20 22 24 26 28 30
He Be C O Ne Mg Si S A Ca Ti Cr Fe Ni Zn
F Na Al P Cl K

elemental composition and the composition of the sun we proceed in this thesis according to the following scheme:

(1) We select only large flare events. In addition to affording the necessary statistical accuracy, large flare events show less SEP compositional variability than smaller events (Zwickl et. al. 1978; Mason, Hovestadt and Gloeckler 1979). Furthermore, extreme SEP compositional anomalies associated with ^{3}He enhancements appear to occur only in relatively small events (Hurford et. al. 1975, Zwickl et. al. 1978). Thus, while the study of smaller events should ultimately provide insight into details of flare acceleration mechanisms and small scale solar atmospheric inhomogeneities, the larger events (where energetic particle acceleration may occur over large portions of the solar atmosphere) are more suitable for the study of global composition.

(2) We attempt to minimize the effects of possible SEP "acceleration/propagation bias" by (a) the selection of averaging time periods for each flare which exclude times when the composition is likely to be affected by propagation and (b) the rejection of those flare events in which the measured SEP composition is dependent on energy/nucleon. Here, the term "acceleration/propagation bias" refers to any effect which causes the SEP elemental composition, in a fixed energy/nucleon interval, to differ from the composition of the pre-accelerated plasma at the SEP flare acceleration site. By examining the measured SEP composition as a function of time and energy/nucleon in each flare event we seek to both gauge the extent of possible acceleration/propagation biases and minimize their effect.

(3) We compare SEP composition measurements among the different flare events.

(4) We compare our SEP composition measurements to solar abundance measurements from other sources -- (a) spectroscopic results from the photosphere, (b) spectroscopic results for the corona, and (c) solar wind measurements.

The main result is the discovery of large persistent differences between SEP elemental composition and the results of photospheric spectroscopy (which are currently considered the most reliable of the different types of solar abundance measurements). The differences are apparently not due to any acceleration/propagation bias which we could detect in our energy range, but are roughly ordered by first ionization potential -- an atomic parameter which plays a major role in the physics of the photosphere. These results suggest that (a) the composition of the SEP acceleration site is persistently different from that measured for the photosphere and/or (b) there is a persistent SEP acceleration bias operating at energies well outside our range of observation. The agreement we find among our SEP elemental composition results, solar wind data and a number of recent coronal abundance measurements favors possibility (a) and suggests (assuming the correctness of the photospheric composition results) that the SEPs originate in the corona, sampling a coronal composition which is significantly different from that of the photosphere.

Brief accounts of this work have been published in the proceedings of the International Cosmic Ray Conference, Kyoto, Japan

(Cook et. al. 1979) and in the Astrophysical Journal (Letters) (Cook, Stone and Vogt, 1980). In addition, Mewaldt (1980) reviewed recent progress in SEP elemental and isotopic composition measurements, including preliminary results of this work.

Chapter 2

The Experiment

2.1 The Spacecraft

The observations reported in this thesis were performed with the Low Energy Telescopes (LETs) of the cosmic ray detector systems aboard the Voyager 1 and 2 spacecraft. The Voyagers were launched toward the outer heliosphere in the fall of 1977 and followed trajectories nearly in the ecliptic plane (see Figure 2.1). The spacecraft are three-axis stabilized. All of the observations reported here were obtained during the September 1977 to May 1978 period when both spacecraft were in interplanetary space, well beyond the influence of the earth's magnetic field.

2.2 The Voyager Cosmic Ray Subsystems

The essentially identical Cosmic Ray Subsystems (CRS, see Stone et. al. 1977) on Voyagers 1 and 2 each consist of four Low Energy Telescopes (LETs), two High Energy Telescopes (HETs), the Electron Telescope (TET), and their associated electronic data systems. Together these telescopes measure the energy spectrum of electrons from 3–110 MeV and the energy spectra and elemental composition of nuclei from hydrogen through nickel over an energy range from 3–500 MeV/nucleon. The telescopes, shown in schematic cross section in Figure 2.2, employ silicon solid-state detectors exclusively and are designed to achieve (1) the reliability required for the anticipated 20 year mission life, (2) excellent charge and energy resolution, and (3)

Figure 2.1

The trajectories of the Voyager 1 and 2 spacecraft from launch to Jupiter encounter. The data for this work were obtained in the September 1977 to May 1978 time period.

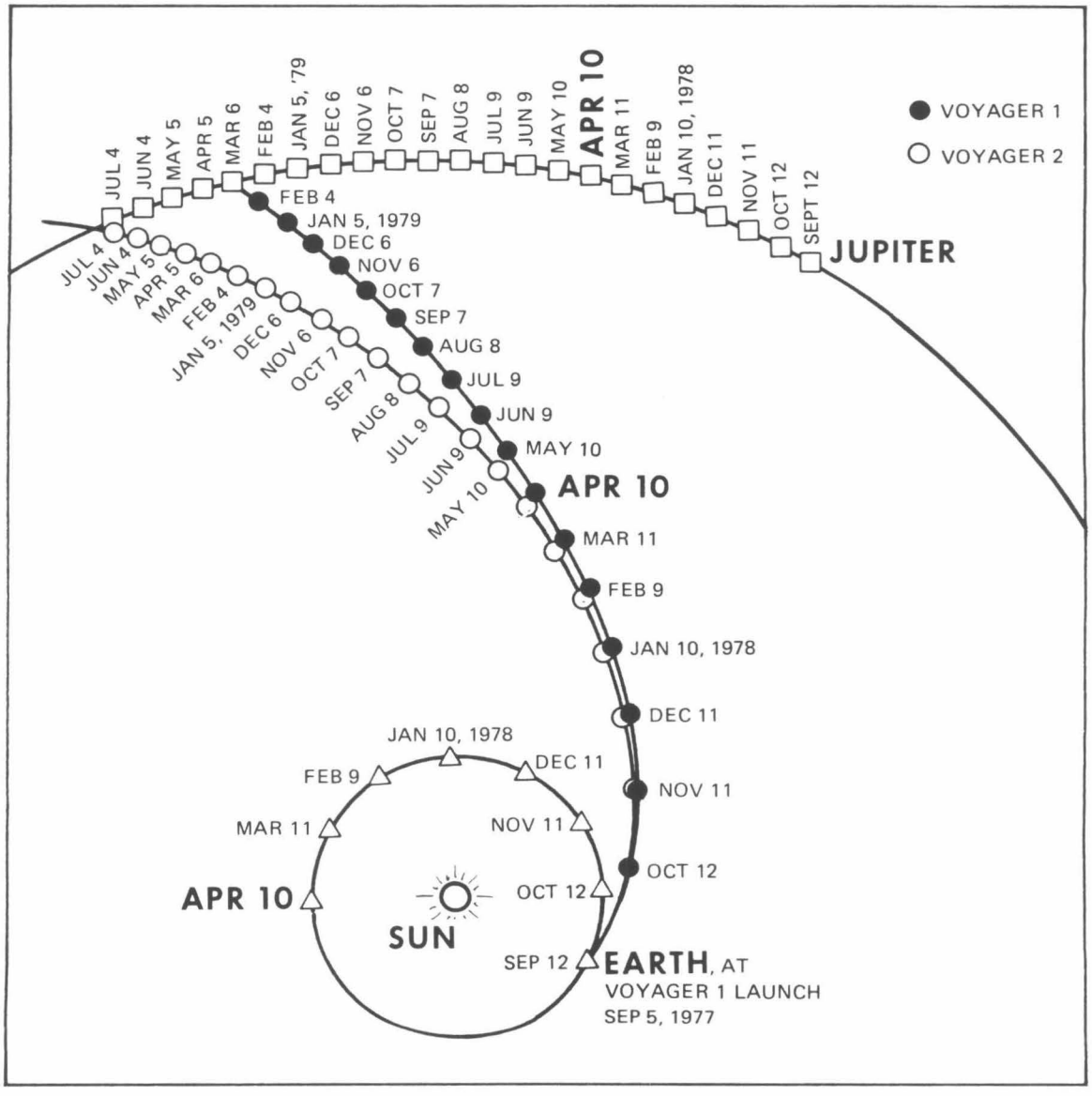
VOYAGER 1
VOYAGER 2
JUPITER
JUL 4
JUN 4
MAY 5
APR 5
MAR 6
FEB 4
JAN 5, '79
DEC 6
NOV 6
OCT 7
SEP 7
AUG 8
JUL 9
JUN 9
MAY 10
APR 10
MAR 11
FEB 9
JAN 10, 1978
DEC 11
NOV 11
OCT 12
SEPT 12
JAN 5, 1979
SUN
EARTH, AT
VOYAGER 1 LAUNCH
SEP 5, 1977

Figure 2.2

Schematic cross sections of the particle telescopes of the Voyager Cosmic Ray Subsystem.

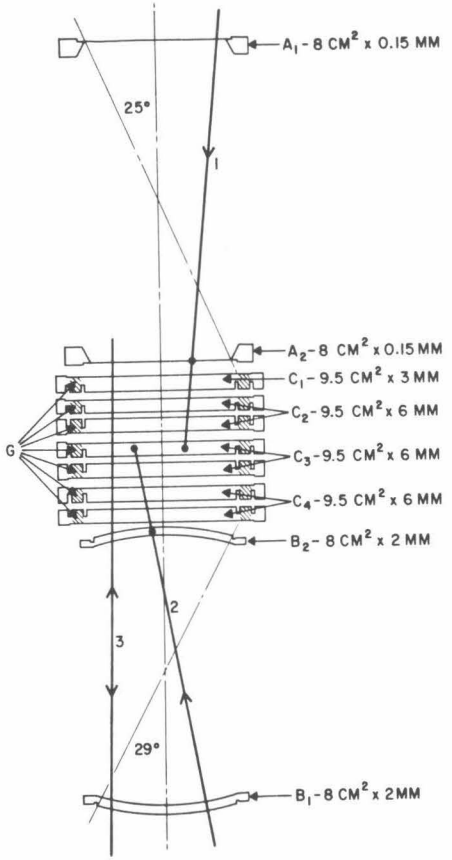

HIGH ENERGY TELESCOPE (HET)

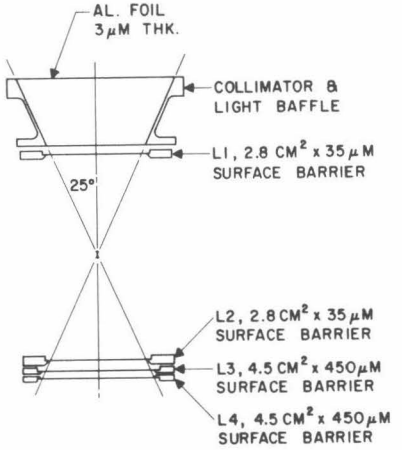

LOW ENERGY TELESCOPE (LET)

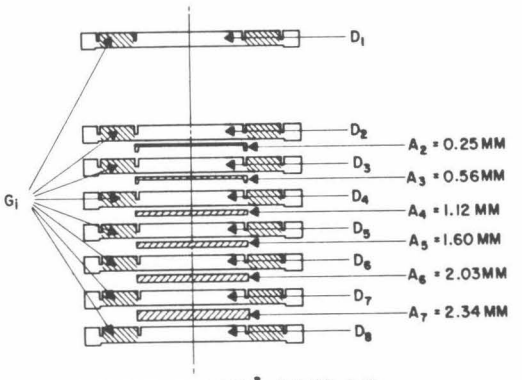

D_i = DETECTORS, 4.5 CM² x 3.0 MM, LiD

A_i = TUNGSTEN ABSORBER (ρ = 18.0 g/CM³)

G_i = GUARD DETECTORS, 3.0 MM, LiD

THE ELECTRON TELESCOPE (TET)

the high count rate capability necessary during large solar flares and passage through the Jovian and Saturnian magnetospheres.

The Voyager CRS is the result of a collaboration of scientists and engineers at the California Institute of Technology, the Goddard Space Flight Center, the University of Arizona, and the University of New Hampshire.

2.3 The Low Energy Telescope System

The LET system on each Voyager spacecraft incorporates four nominally identical charged particle telescopes (A, B, C and D) which use the $\frac{dE}{dx}-E$ technique (described in the next section) to measure the kinetic energy and the nuclear charge Z of individual incident nuclei in the range $1 \leq Z \leq 28$. The kinetic energy range of response varies from about 3–8 MeV/nucleon for protons and helium nuclei to about 5–30 MeV/nucleon for iron nuclei. The four telescopes, in addition to having a relatively large combined geometry factor of 1.7 cm^2 steradian, are oriented at different viewing angles to provide three dimensional information on energetic particle streaming patterns.

Each LET (see Figure 2.2) contains four totally depleted silicon surface barrier detectors, labeled L1–L4. L1 and L2 are nominally identical 35 μm thick detectors of the "keyhole" design, where the active area is precisely defined by the location of vapor–deposited aluminum and gold contacts of about two centimeters diameter. L3 and L4 are 450 μm thick detectors with active areas about 2.4 centimeters in

diameter. A thin (3μm) aluminum foil covers the top of each LET, protecting the detectors from sunlight and providing thermal control.

The detectors L1–L3 are connected through charge sensitive preamplifiers and shaping amplifiers to linear 4096 channel pulse height analyzers (see Figure 2.3). Threshold circuits connected to the L1–L4 amplifier outputs provide digital signals to coincidence circuitry which determines when pulse height analysis occurs. Pulse height analyzed (PHA) events are automatically sorted into two groups, $Z < 3$ (protons and alphas) and $Z \geq 3$ (lithium through nickel), by the discrimination of an appropriate linear combination of the L1, L2 and L3 analog signals. The PHA events are temporarily stored in separate $Z < 3$ and $Z \geq 3$ buffers which are sequentially polled for readout into the Voyager telemetry stream. Thus, during times of high counting rate (e.g. major solar flare events) when the PHA event readout rate is limited by telemetry, the occurrence of the relatively rare $Z \geq 3$ PHA events is enhanced in a predictable way. A rate accumulator system monitors single detector and various coincidence counting rates, including those needed to normalize the PHA event sample to obtain absolute flux measurements. (Details on the CRS electronic data system are given in Stilwell et. al. 1979)

Throughout the observation periods reported here the basic requirement for pulse height analysis (which can be controlled by ground command) was a coincidence of discriminator signals from detectors L1 and L2. L4 was at all times in anticoincidence so that normally only particles entering L1 and stopping in either L2 or L3 were pulse height analyzed.

Figure 2.3

Schematic diagram of one HET/LET electronic system. An identical system serves the other HET and two LETs. Note that the HET and LET systems share post amplifiers and pulse height analyzers.

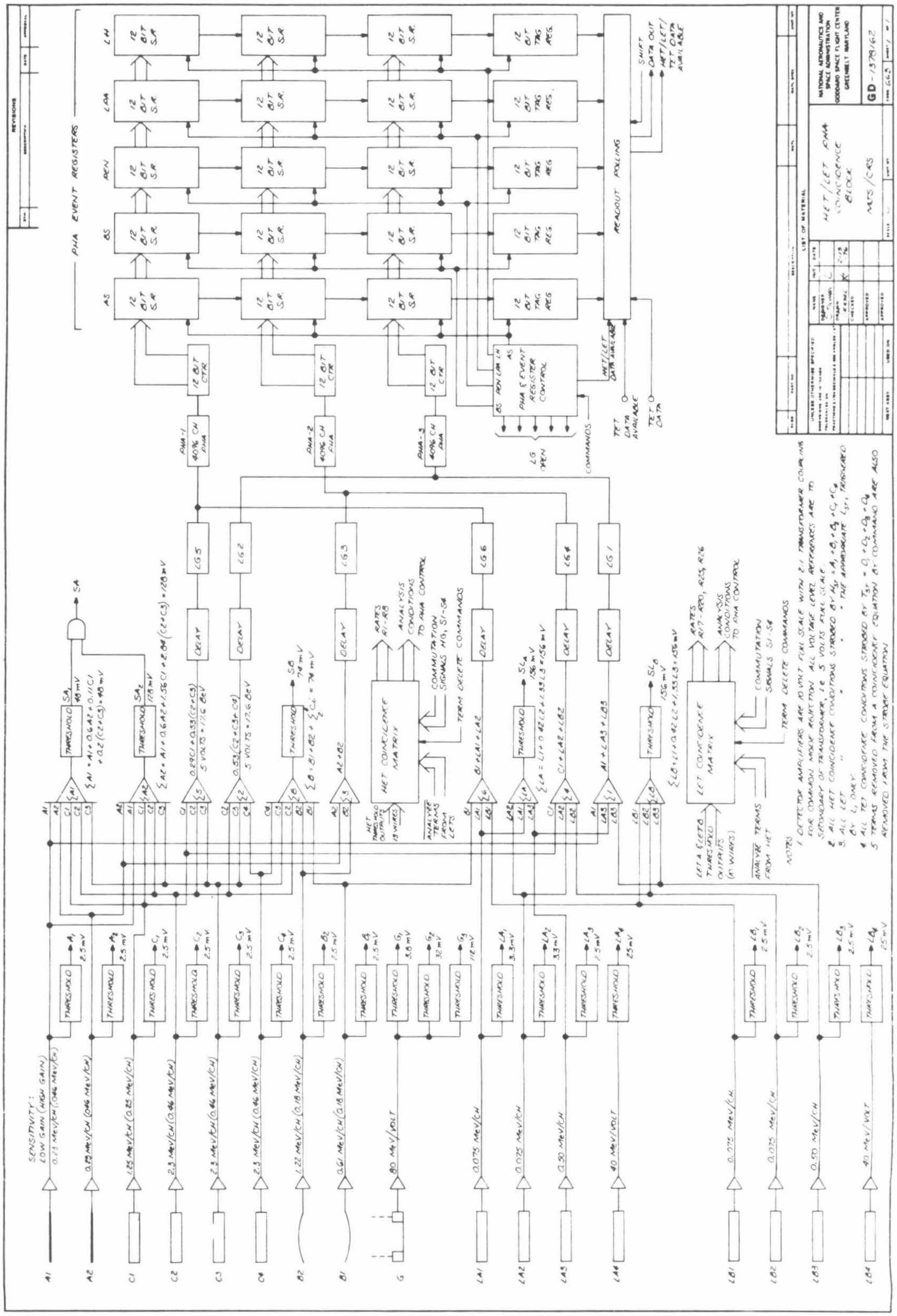
PHA EVENT REGISTERS
AS
BS
REN
LAA
LH
12 BIT S.R.
12 BIT TAG REG
READOUT POLLING
SHIFT
DATA OUT
HET/LET/TET DATA AVAILABLE
12 BIT CTR
PHA-1 4096 CH PHA
PHA-2 4096 CH PHA
PHA-3 4096 CH PHA
PHA EVENT REGISTER CONTROL
HET/LET DATA AVAILABLE
TET DATA AVAILABLE
TET DATA
LG OPEN
COMMANDS
LG5
LG2
LG3
LG6
LG4
LG1
DELAY
HET COINCIDENCE MATRIX
LET COINCIDENCE MATRIX
THRESHOLD
SENSITIVITY:
LOW GAIN (HIGH GAIN)
COMMUTATION SIGNALS
TERM DELETE COMMANDS
ANALYSIS CONDITIONS TO PHA CONTROL
ANALYZE TERMS FROM LETS
ANALYZE TERMS FROM HET
A1
A2
C1
C2
C3
C4
B2
B1
G
LA1
LA2
LA3
LA4
LB1
LB2
LB3
LB4
NOTES
NATIONAL AERONAUTICS AND SPACE ADMINISTRATION
GODDARD SPACE FLIGHT CENTER
GREENBELT MARYLAND
HET/LET PHA COINCIDENCE BLOCK
GD-1378162
REVISIONS
LIST OF MATERIAL

The nominal characteristics of detectors L1–L4, and their corresponding discriminator thresholds and PHA channel widths are listed in Table 2.1. (The actual values of most of these parameters were measured as discussed in the calibration section of this chapter.)

2.4 The $\frac{dE}{dx}$–E Technique

The charge and energy of individual incident nuclei are measured using the $\frac{dE}{dx}$–E technique as illustrated in Figure 2.4. An incident nucleus (nuclear charge Z, mass M, and velocity v) penetrates a thin front detector of thickness L, and then deposits most of its initial energy and stops in a second detector. The (non–relativistic) ionization energy loss ΔE measured in the thin detector is roughly proportional to LZ^2/v^2 while the total energy $E=Mv^2/2$ is the sum of ΔE and the residual energy E′ measured in the second detector. Therefore, the product $\Delta E \times E$ is roughly proportional to LZ^2M and is strongly dependent on Z. The response of a typical LET is illustrated in Figure 2.5, a plot of the energy deposited in L1 (ΔE) versus the sum of the energies deposited in L2 and L3 (E′) for a raw sample of $Z \geq 3$ events from LET C of Voyager 1. The "tracks" of the relatively abundant elements C, N, O, Ne, Mg, Si, S and Fe are apparent, as are the less populated tracks of Na, Al, Ar and Ca. The finite width of the tracks is mainly due to the variation of particle incidence angles and detector thickness non–uniformities, which both contribute to a variation of the pathlength, L.

For nuclei which penetrate both detectors L1 and L2, and then stop

TABLE 2.1

LET Detector and Electronics

Nominal Data

	Detector			
	L1	L2	L3	L4
Thickness (μm)	35	35	450	450
Active Diameter (cm)	2.0	2.0	2.4	2.4
Discriminator Threshold (KeV)	200	200	1000	300
PHA Channel Width (KeV)	70	70	500	-

$\frac{dE}{dx}$ - E TECHNIQUE

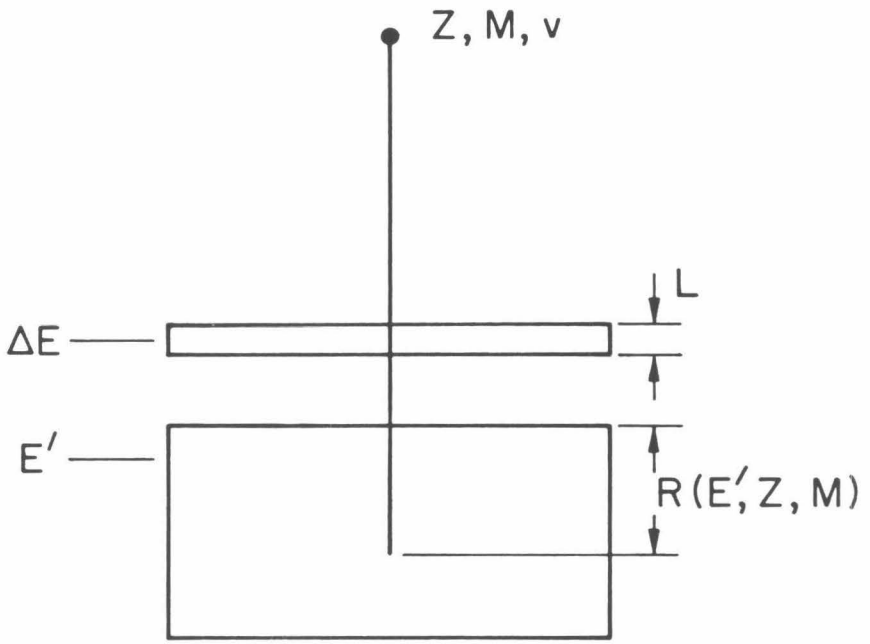

Approximate Calculation:

$$\left.\begin{aligned} \Delta E &\propto LZ^2/v^2 \\ \Delta E + E' &= E \simeq \tfrac{1}{2}Mv^2 \end{aligned}\right\} \Rightarrow \Delta E \cdot E \propto LZ^2 M$$

In practice, the charge, Z, is calculated by solving:

$$L = R(\Delta E + E', Z, M) - R(E', Z, M)$$

$$\text{with } M = f(Z) \cong 2Z$$

Figure 2.4

Figure 2.5

The $\frac{dE}{dx}$–E response of a typical LET. The energy deposited in detector L1 (ΔE) is plotted versus the sum of the energies deposited in detectors L2 and L3 (E′), for a sample of $Z \geq 3$ PHA events from LET C of Voyager 1. To prevent plot saturation, only every tenth event was plotted for elements oxygen and below.

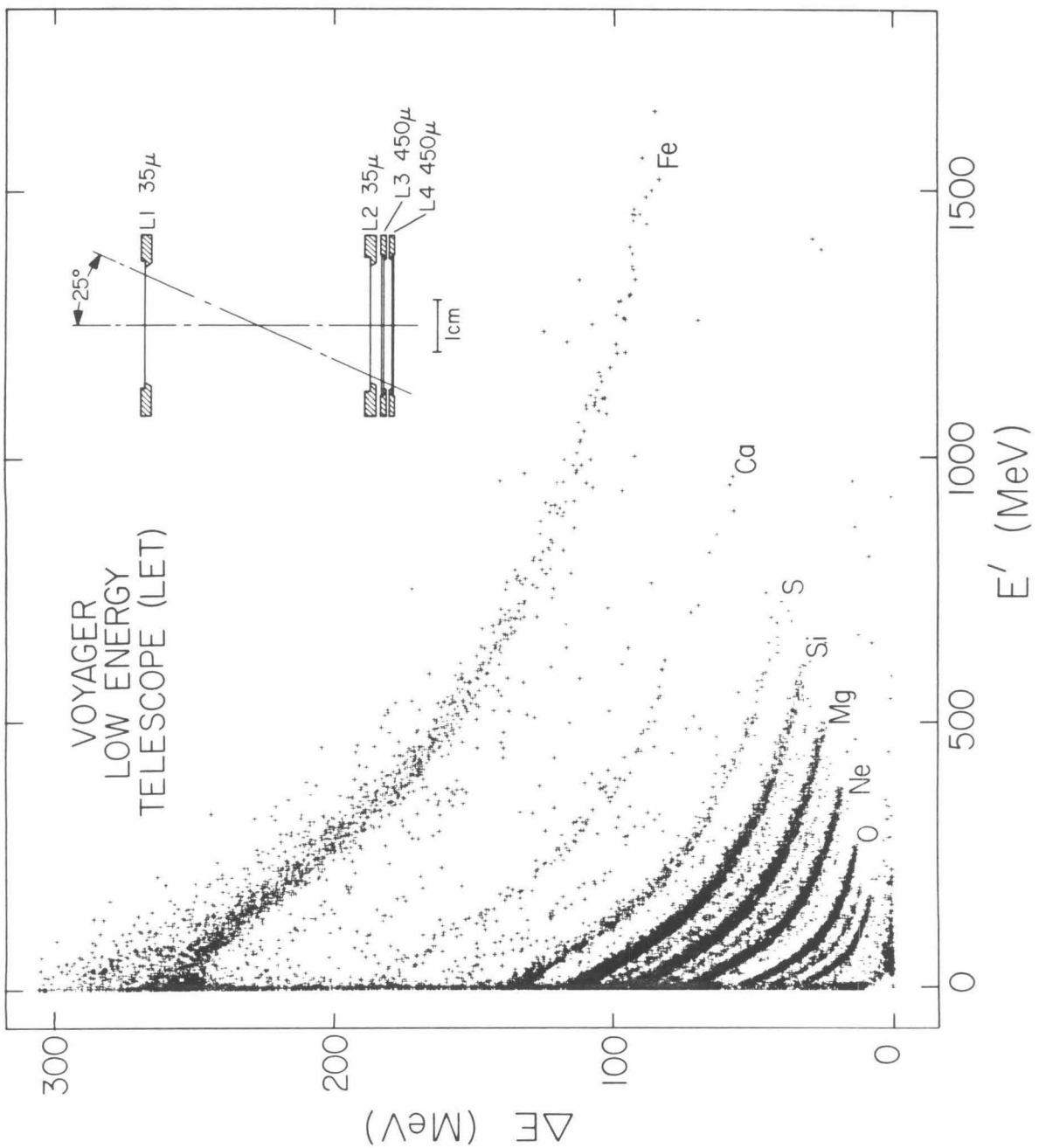
VOYAGER
LOW ENERGY
TELESCOPE (LET)
25°
L1 35μ
L2 35μ
L3 450μ
L4 450μ
1cm
Fe
Ca
S
Si
Mg
Ne
O
ΔE (MeV)
E′ (MeV)
300
200
100
0
0
500
1000
1500

in L3, two independent ΔE measurements are obtained. This redundant information improves the charge resolution and significantly reduces background for the rarer elements (as will be seen in Section 3.5).

2.5 Calibrations

2.5.1 Detector Thicknesses and Areas

The thickness and area of each LET detector was measured as described in detail by Gehrels (1980). The measurements are briefly discussed below.

The thickness ($\approx$ 35 μm) of each of the L1 and L2 detectors was determined using laboratory measurements of the energy deposited by penetrating 8.78 MeV alpha particles from a ^{212}Po source, together with the alpha particle range–energy relation of Vidor (1975). For each detector, a sequence of aluminum masks was used to obtain separate exposures of six concentric, but non–overlapping, annular regions, which together covered the entire detector. The mean of the alpha particle energy loss distribution from each annular region was used to determine the average thickness of the annulus, while the spread of the distribution was used to estimate the rms of the thickness variations of the annular region. These data were then used to compute the mean pathlength in the detector and the rms variation in the pathlength expected for particles of an isotropic flux penetrating both L1 and L2. The mean pathlength measurements were reproducible with a sigma of about 0.2 percent. The main systematic error is due to uncertainty in the alpha particle

range–energy relation. For example, use of the range–energy relation obtained by scaling the proton range–energy relation of Janni (1966) gives 3 percent larger mean pathlengths than those listed in Gehrels (1980), while the alpha range–energy relation of Ziegler (1977) gives 6 percent larger results.

The thickness ($\approx$ 450 μm) of each of the L3 and L4 detectors was measured relative to a standard gauge–block using capacitive probes and a precision micrometer. For each detector the thickness was measured at the center and at four positions around the edge, and the mean pathlength and rms variation of the pathlength for an isotropic flux of particles penetrating both L1 and L2 was calculated by assuming that the detector surfaces were, to first approximation, spherical sections. The thickness measurements were reproducible with about a 2 μm sigma.

A travelling microscope was used to measure the dimensions of the Al and Au contacts which define the active areas of the L1 and L2 detectors. In addition, the relative areas of all L1 and L2 detectors were obtained more precisely by placing each detector a standard distance from an ^{241}Am source and measuring the counting rate of 5.5 MeV alpha particles. These data and the L1–L2 separation distances measured during the LET assembly process were used to calculate the LET geometry factors listed in Gehrels (1980).

2.5.2 Detector Dead Layers

For silicon surface barrier detectors the thickness of the dead

layers is very nearly equal to the thickness of the front (Au) and back (Al) electrodes. These thicknesses were specified for the LET detectors by their manufacturer, ORTEC, and were all within the range 40.0± 0.6 $\mu g/cm^2$. Since this is only about 0.5 percent of the total thickness of the LET 35 μm detectors, the effect of the dead layers was not explicitly included in the particle energy measurements discussed later.

2.5.3 LET Window Thicknesses

The thickness of the thin Al window at the top of each LET was not measured in the laboratory. However, in determining particle incidence energies, a correction was made for energy loss in a window of thickness 3 μm; the thickness specified by the manufacturer. The energy correction was largest (about 8 percent) for nickel nuclei near their two detector threshold of 5 MeV/nucleon, but decreased rapidly with increasing energy and was only 3.5 percent for nickel nuclei at their three detector threshold of 8.7 MeV/nucleon.

2.5.4 Electronic Energy Calibration

The LET preamp–postamp–pulse height analyzer chains were calibrated in the laboratory as described in Povlis (1980). A precision pulser was used to inject a charge pulse into a preamp input and the corresponding pulse height was read out. For each LET detector i, the input charge amplitude Q_i corresponding to a channel threshold P was obtained for about 20 selected channels at two temperatures: T = 0 °C and 20 °C. For each detector the charge

$Q_i(P,T)$ was linear in P to within 2 percent of full scale and $Q_i(P,0)$ was 1 to 2 percent larger than $Q_i(P,20)$. An estimate $E_{cal,i}$ of the energy which, when deposited in LET detector i by an incident nucleus, would give a pulse height, P, was obtained using:

$$E_{cal,i}(P,T) = E_q \cdot Q_i(P,T) \qquad (2.1)$$

where E_q is ratio of the ionization energy deposited to charge output for silicon detectors. The main uncertainty in this calibration was in the absolute amplitude of the calibrating charge pulses[1]; the uncertainty in their relative amplitudes was negligible due to the linearity and zero offset of the precision pulser. Also negligible, in the LETs' energy range, is the error which results from the approximation that the charge output of silicon detectors is proportional to the energy deposited[2]. Thus, the relation between energy deposited and pulse height was taken to be:

$$E_i(P,T) = F_i \cdot E_{cal,i}(P,T)$$

where the F_i were determined using oxygen PHA events as described in the next chapter.

---

1. The uncertainty in the absolute amplitude of the calibration charge pulses was due to the uncertainty in the capacitance of the test capacitors (a different one for each preamp) used to couple the precision pulser to the preamp inputs.

2. The pulse height response characteristics for heavy ions in silicon surface barrier detectors has been studied (Kaufman et. al. 1974, and references therein) by comparing the true energy E_t of incident heavy ions of carbon through uranium to the alpha particle energy E_a yielding the same pulse height. The energy defect, $E_t - E_a$, was essentially zero for carbon and oxygen ions but increased with nuclear charge and was about 2 MeV for nickel ions near 1 MeV/nucleon. The size of the defect

was roughly independent of energy, suggesting that at the LETs' threshold for nickel (about 5 MeV/nucleon) the percentage defect would be only about 1 percent.

Chapter 3

Data Analysis

3.1 Overview

The various steps in the data analysis are shown schematically in Figure 3.1 and include (1) the completion of the energy versus pulse height calibrations using oxygen PHA events acquired in-flight, (2) the use of in-flight neon, magnesium, silicon and iron PHA events to obtain a charge calibration of the experiment, (3) the selection of PHA events by "two parameter" $(\frac{dE}{dx}-E)$ analysis for flux and abundance measurements of the elements C, O, Ne, Mg, Si, and Fe over the full LET energy range, and (4) the selection of PHA events by "three parameter" $(\frac{dE}{dx}-\frac{dE}{dx}-E)$ analysis for very low background flux and abundance measurements of helium through nickel.

3.2 In-flight Energy Calibration

As discussed earlier, the relation between energy, E_i and pulse height, P, for each LET detector, i, was taken to be:

$$E_i(P,T) = F_i \cdot E_{cal,i}(P,T) . \qquad (3.1)$$

The functions $E_{cal,i}$ were measured (as discussed in Section 2.5.4) at about twenty selected channel thresholds and two different temperatures during the laboratory electronic calibration and, throughout this work, were extended to intermediate values of P and T by linear interpolation. The F_i were obtained by least squares fits which optimized the agreement between the locations of the in-flight

DATA ANALYSIS

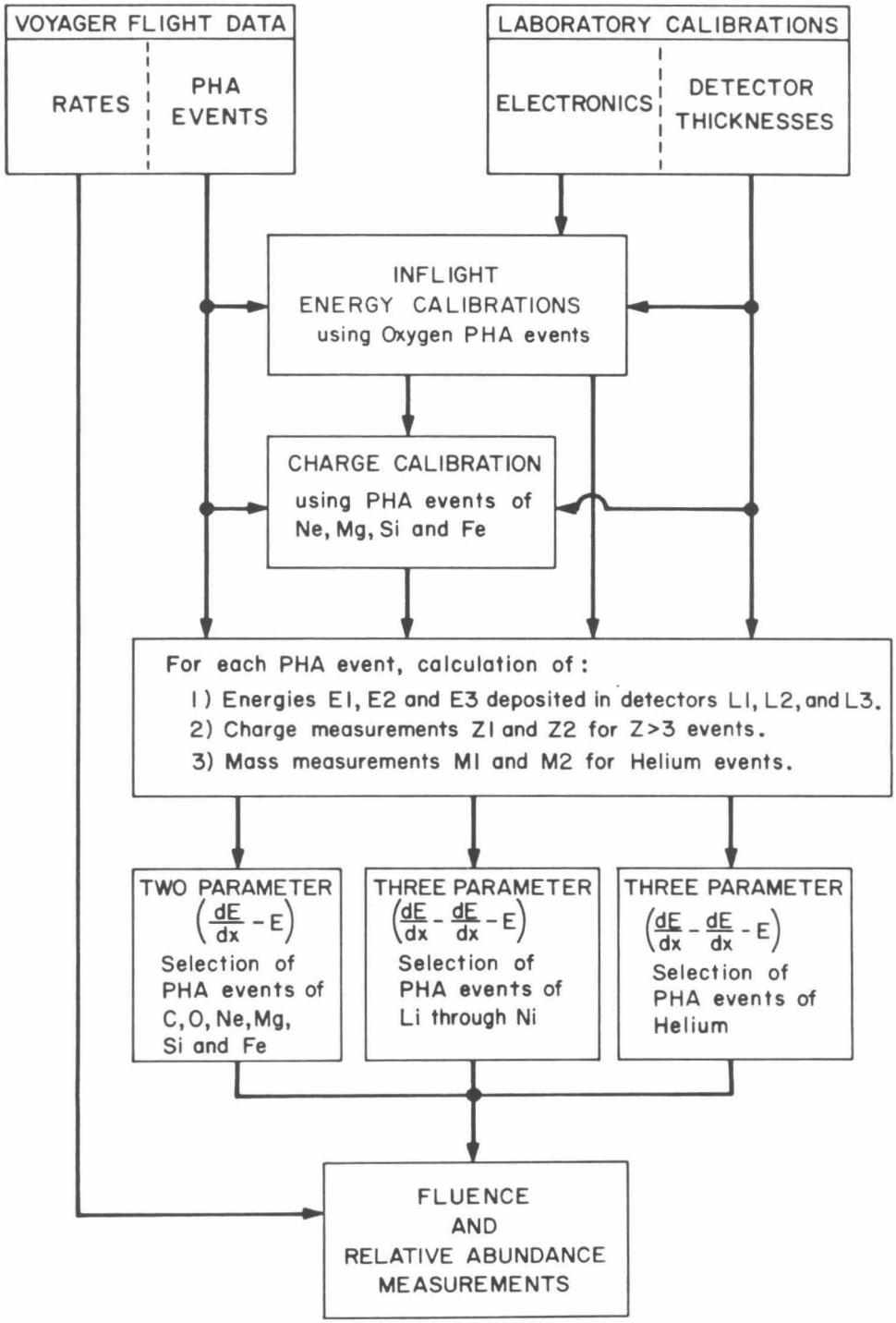

Figure 3.1

oxygen "tracks" (e.g., see Figure 2.5) and those calculated using equation (3.1) together with the oxygen range–energy relation of Vidor (1975) and the L1 and L2 detector mean pathlength measurements discussed earlier. The method is described below, using LET C of Voyager 1 as an example.

Figure 3.2 illustrates the iterative technique used to obtain the location of the oxygen track on a plot of L2 versus L3 pulse height. In the first pass (Figure 3.2a), candidate oxygen PHA events were selected using curves which loosely bracketed the track. The selected events were used to define a preliminary oxygen track location in tabular form (Figure 3.2b) by calculating the mean pulse heights $(\overline{P}_{L2}, \overline{P}_{L3})_j$ and the standard deviation of the L2 pulse heights S_j, for each group j, of N_j (≈ 20) PHA events with adjacent L3 pulse heights. The S_j were smoothed by averaging each consecutive set of ten values along the track, and the smoothed values were used to define the final selection curves at about ± 2.5 sigma from the tabulated track center. The events selected using these curves are shown in Figure 3.2c and were used to calculate the final track shown in Figure 3.2d. The L1 versus L3 oxygen track was obtained in a similar way.

The first step of fitting the L2 versus L3 oxygen track was to convert the mean pulse heights and sigmas to energies using the laboratory electronics calibration, i.e. equation (2.1):

$$(\overline{P}_{L2}, \overline{P}_{L3}, S)_j \rightarrow (\overline{E}_{cal,L2}, \overline{E}_{cal,L3}, \sigma)_j$$

where σ_j is the statistical uncertainty in $\overline{E}_{cal,L2,j}$. Then, for oxygen nuclei, the relationship between the average energy $\overline{E}_{L2}$, deposited in L2

Figure 3.2

The selection of PHA events from flight data to define the location of the oxygen track (see text).

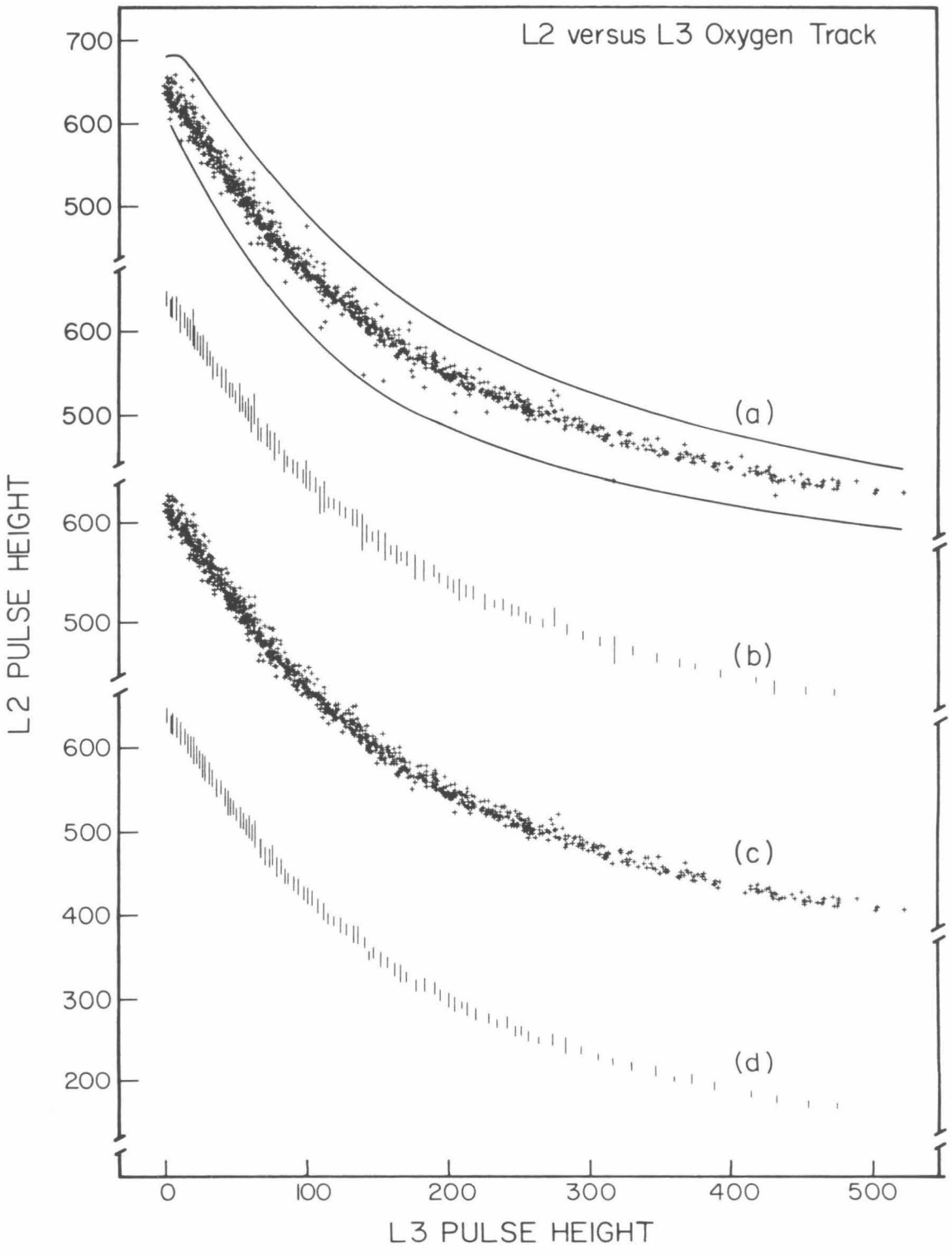
L2 versus L3 Oxygen Track
L2 PULSE HEIGHT
L3 PULSE HEIGHT
700
600
500
600
500
600
500
600
500
400
300
200
0
100
200
300
400
500
(a)
(b)
(c)
(d)

and the average energy $\overline{E}_{L3}$, deposited in L3 was calculated using:

$$\overline{E}_{L2} = R^{-1}[R(\overline{E}_{L3}) + T_{L2}]$$
$$\equiv f(\overline{E}_{L3})$$

where R is the oxygen range–energy relation of Vidor (1975), and T_{L2} is the L2 detector mean pathlength (see Section 2.5.1). Finally, F_{L2} and F_{L3} could be found by minimizing:

$$\chi^2_{2,3}(F_{L2}, F_{L3}) = \sum_j \left[\frac{f(F_{L3} \cdot E_{cal,L3,j})}{F_{L2}} - E_{L2,cal,j} \right] / \sigma_j^2$$

Similarly, F_{L1} and a second determination of F_{L3} could be obtained from the L1 versus L3 oxygen track.

For the Voyager 2 LETs, the F_i determined for two different flare periods (September 19 through 27 of 1977 and February 13 through 20 of 1978) were found to differ by less than 1 percent. However, the values of F_{L3} from the L1 versus L3 tracks were systematically larger then those obtained from the L2 versus L3 tracks by about 2 percent. The finally adopted values of F_i (listed in Table 3.1) were obtained by minimizing:

$$\chi^2(F_{L1}, F_{L2}, F_{L3}) = \left[\chi^2_{1,3}(F_{L1}, F_{L3}) + \chi^2_{2,3}(F_{L2}, F_{L3}) \right]_{period1}$$
$$+ \left[\chi^2_{1,3}(F_{L1}, F_{L3}) + \chi^2_{2,3}(F_{L2}, F_{L3}) \right]_{period2}$$

The good agreement obtained between the oxygen tracks and the fits calculated using the adopted F_i is shown in Figure 3.3, for LET C of Voyager 1.

TABLE 3.1

LET Gain Correction Factors

	F_{L1}	F_{L2}	F_{L3}
Voyager 1			
LET A	0.9719	0.9864	0.9278
LET B	0.9893	0.9921	0.8930
LET C	1.0320	1.0164	0.9035
LET D	1.0010	0.9733	0.9695
Voyager 2			
LET A	0.9421	0.9740	0.9303
LET B	0.9836	0.9561	0.9007
LET C	0.9519	1.0124	0.9340
LET D	1.0049	1.0406	0.9377

Figure 3.3

Comparison of the oxygen track obtained from flight data (DATA) and the calculated oxygen track (FIT) for LET C of Voyager 1 (see text).

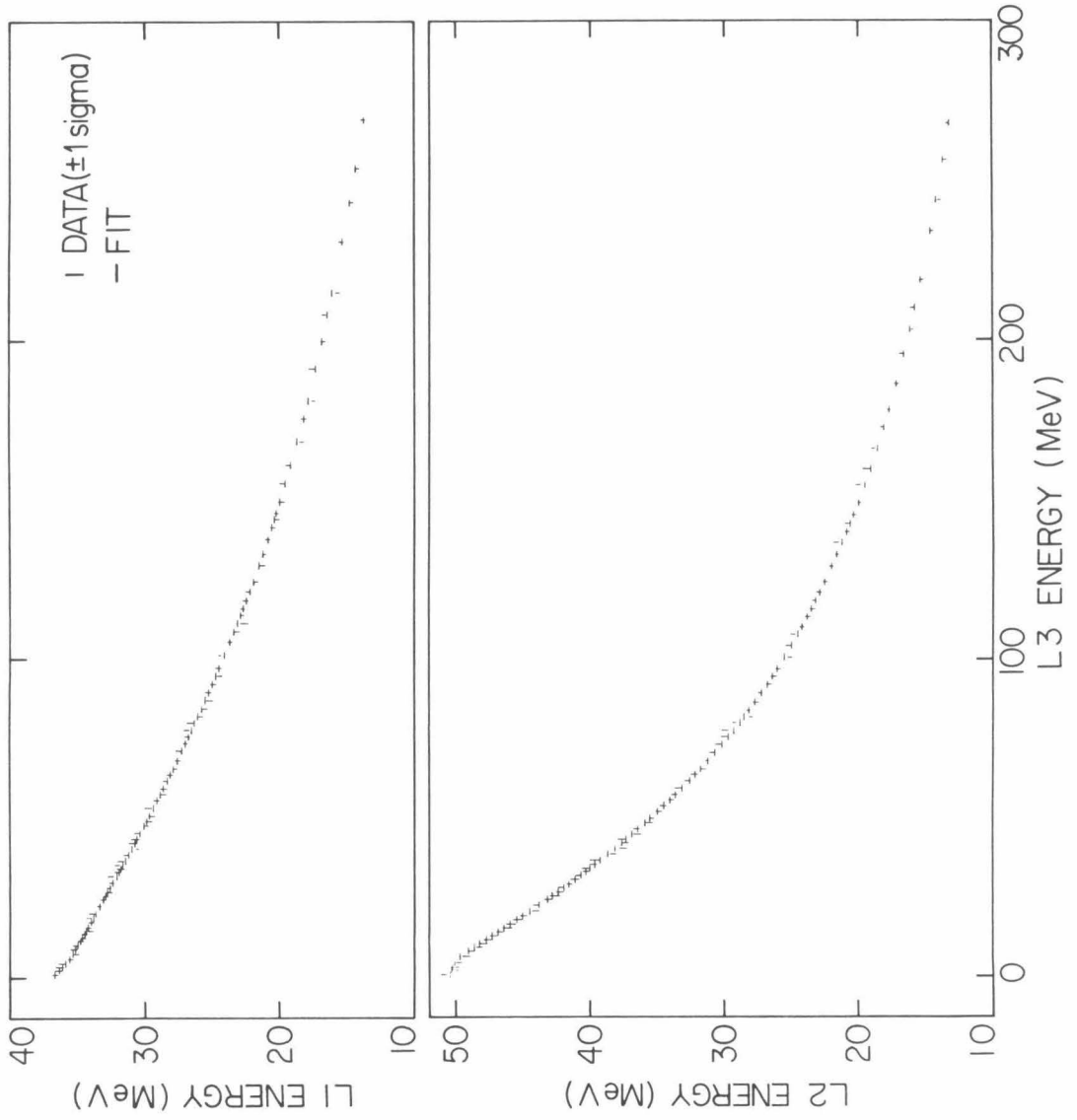
I DATA(±1 sigma)
– FIT
L1 ENERGY (MeV)
L2 ENERGY (MeV)
L3 ENERGY (MeV)
40
30
20
10
50
40
30
20
10
0
100
200
300

Since the energy calibration of the L3 detectors was performed without making use of the L3 detector thicknesses (which were accurately measured in the laboratory; see Section 2.5.1) it was possible to obtain an independent check on the possible systematic errors accumulated during the entire energy calibration procedure. This was done as illustrated in Figure 3.4 which shows a histogram of the energy deposited by oxygen nuclei in detector L3 of Voyager 1 LET C. The high energy cutoff results from the penetration of oxygen nuclei into the anticoincidence detector L4. For each L3 detector, the predicted cutoff energy E_c' (calculated using the oxygen range–energy relation of Vidor 1975 together with the L3 detector mean pathlength measurements) was compared to the observed cutoff energy energy E_c (the energy at which the response has roughly halved). The observed cutoff energies, E_c , were systematically about 3 percent lower than the predicted cutoff energies, E_c' , indicating that absolute systematic errors on the order of 3 percent were accumulated in the calibration procedure. The effect of such possible errors on the observations is discussed in Chapter 4.

The rms uncertainties due the finite number of PHA events used to define the oxygen tracks are only about 0.1 percent for the F_{L1} and F_{L2} and 0.2 percent for the F_{L3}.

3.3 The Charge Calibration

For each PHA event, the energies E_{L1}, E_{L2} and E_{L3} (if L3 was triggered) were obtained from the corresponding L1, L2 and L3 detector pulse heights using the energy calibrations established in the

Figure 3.4

A histogram of the energy deposited by oxygen nuclei in detector L3 of Voyager 1 LET C. The histogram cuts off at high energies due to the penetration of oxygen nuclei through L3 into anti-coincidence detector L4. E_c and E_c' are the observed and predicted cutoff energies respectively (see text).

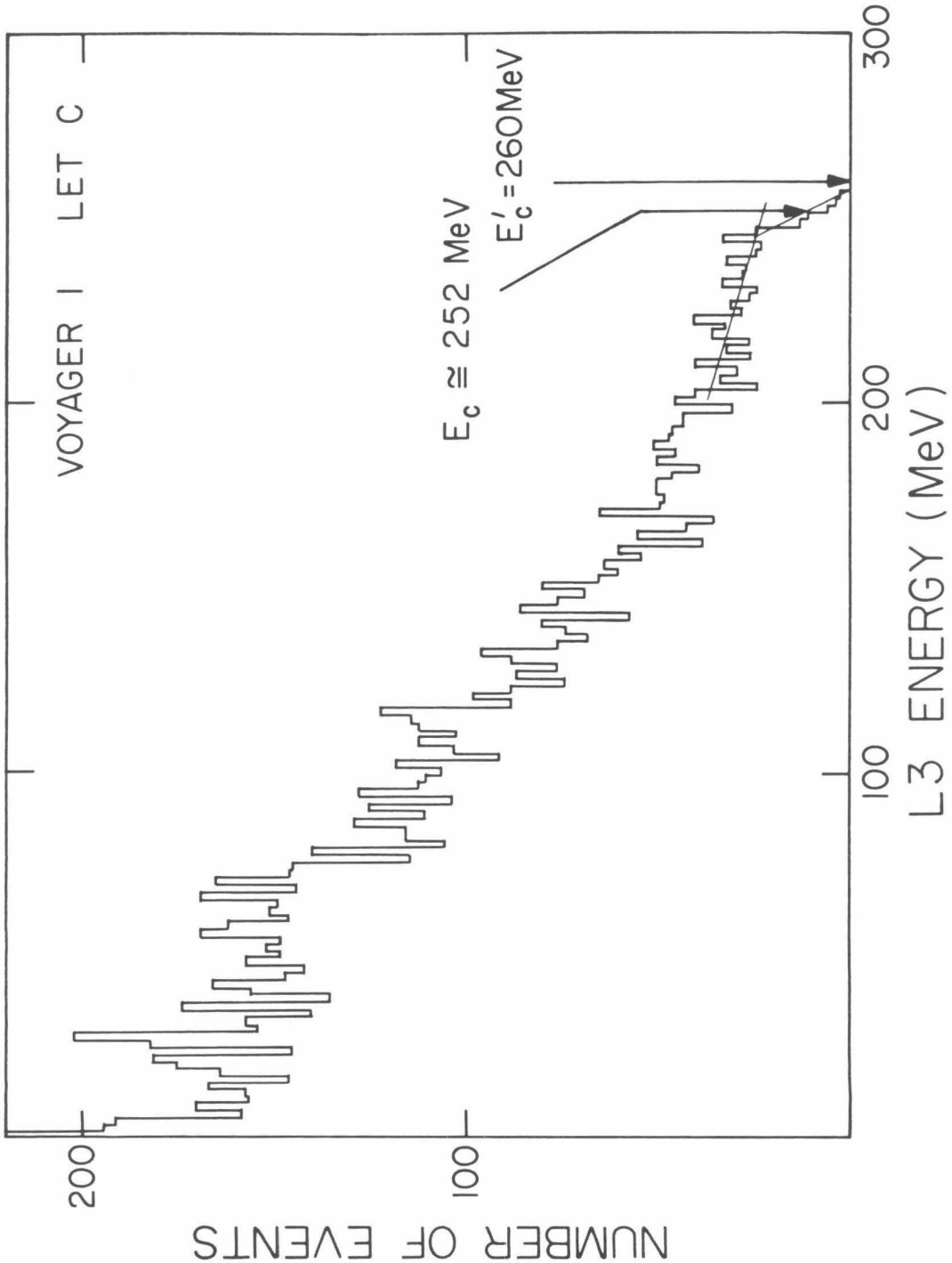
VOYAGER I LET C
$E_c \cong 252$ MeV
$E'_c = 260$MeV
NUMBER OF EVENTS
200
100
100
200
300
L3 ENERGY (MeV)

previous section. For every event, a charge measurement Z1 was calculated by numerically solving:

$$T_{L1} = R(E_{L1}+E_{L2}+E_{L3}, Z1, M) - R(E_{L2}+E_{L3}, Z1, M)$$

where T_{L1} is the mean pathlength for the appropriate L1 detector, $R(E, Z, M)$ is the range in silicon of a nucleus with energy E, nuclear charge Z1, and mass M. For the purpose of solving the above equation, the mass, M, was approximated by the following continuous function of Z1:

$$M \equiv \begin{cases} 2(Z1) & \text{for } Z1 \leq 20.0 \\ 40.0 + 4.772(Z1-20.0) & \text{for } 20.0 \leq Z1 < 21.0 \\ 2.132(Z1) & \text{for } Z1 \geq 21.0 \end{cases}$$

(This approximation is accurate for most of the abundant isotopes from carbon through iron —the small errors which are incurred for some of the rarer isotopes produce predictable shifts in the calculated charge measurement which are negligible for this study.)

Similarly, for three detector events (where the L3 detector was triggered) a second charge measurement Z2 was calculated by solving:

$$T_{L2} = R(E_{L2}+E_{L3}, Z2, M) - R(E_{L3}, Z2, M).$$

The generalized range–energy function, R, was taken to be of the semi–empirical form used by Heckman et. al. (1960) to summarize their measurements of the range of heavy ions in nuclear emulsion:

$$R(E,M,Z) = \left(\frac{M}{Z^2}\right)R_p\left(\frac{E}{M}\right) + MZ^{\frac{2}{3}}C\left(\frac{137\beta}{Z}\right).$$

The first term in the expression is the particle range as scaled from the proton range–energy relation, R_p, of Janni (1966). The second term corrects for charge–pickup which becomes significant in the LETs energy range for high Z nuclei such as iron. The function C, appropriate for silicon detectors, was obtained from the Voyager 2 flight data as follows:

(1) The 'L1 versus L2+L3" and 'L2 versus L3" energy loss tracks of neon, magnesium, silicon, and iron were derived from the Voyager 2 flight data using an iterative technique like that described earlier for the oxygen tracks.

(2) Guided by the results of Heckman et. al. (1960) the function C was parameterized as:

$$C(x) = A_1A_2\left[\exp\left(-\frac{x}{A_3} - \frac{x^2}{A_6}\right) - 1.0\right]$$

$$+ A_1\left\{A_4 - A_5\ln\left[1.0 + \exp\left(-\frac{x-A_4}{A_5}\right)\right]\right\}.$$

(3) The parameters A_i were adjusted using a computer program to get the best agreement between the Ne, Mg, Si and Fe tracks obtained from the flight data and the corresponding track locations calculated using the above generalized range–energy relation and the L1 and L2 detector mean pathlengths. The resulting fits were not perfect and it was necessary to weight the Fe data more heavily to obtain an adequate fit for Fe at the expense of Ne, Mg and Si. The adopted

function C is plotted in Figure 3.5.

The results of the charge calculations are illustrated in Figure 3.6, a scatter plot of the charge measurement Z1 versus total energy, $E_{L1}+E_{L2}+E_{L3}$, for a typical LET. The calculated charge is adequately independent of energy, except near threshold. A similar result was seen for the other LETs and on plots of Z2 versus energy. (The unusual clump of events seen in Figure 3.6 at the energy threshold near Z1=28 is due to a background effect which will be discussed later.)

3.4 Two Parameter ($\frac{dE}{dx}$–E) Analysis

The selection of PHA events for use in the "two parameter" abundance and flux measurements for nuclei of C, O, Ne, Mg, Si and Fe (presented in Section 4.4) was made as follows:

(1) The events were sorted according to their Z1 charge measurement using charge boundaries (listed in Table 3.2) chosen to lie at about ± 2.5 sigma from the mean value of Z1 for each element, thus excluding a negligible fraction of "good" events.

(2) For each element, the events were then sorted by their total energy measurement, $E_{L1}+E_{L2}+E_{L3}$, into bins corresponding to incident kinetic energy/nucleon intervals (listed in Table 4.4) that were chosen to be within the energy response range of all the LETs used. The total energy ($E_{L1}+E_{L2}+E_{L3}$) interval corresponding to a given incident kinetic energy/nucleon interval was calculated using the mean nuclear mass for each element (averaged over the isotope fractions given by Cameron 1973) and a small correction for ionization energy loss in the

Figure 3.5

The adopted range–energy extension function, C(x). (The values of the parameters A1 through A6 which define this function are 3.2209, 2.0040, 0.92383, 1.1242, 0.28267, 0.98002, respectively -- see text.)

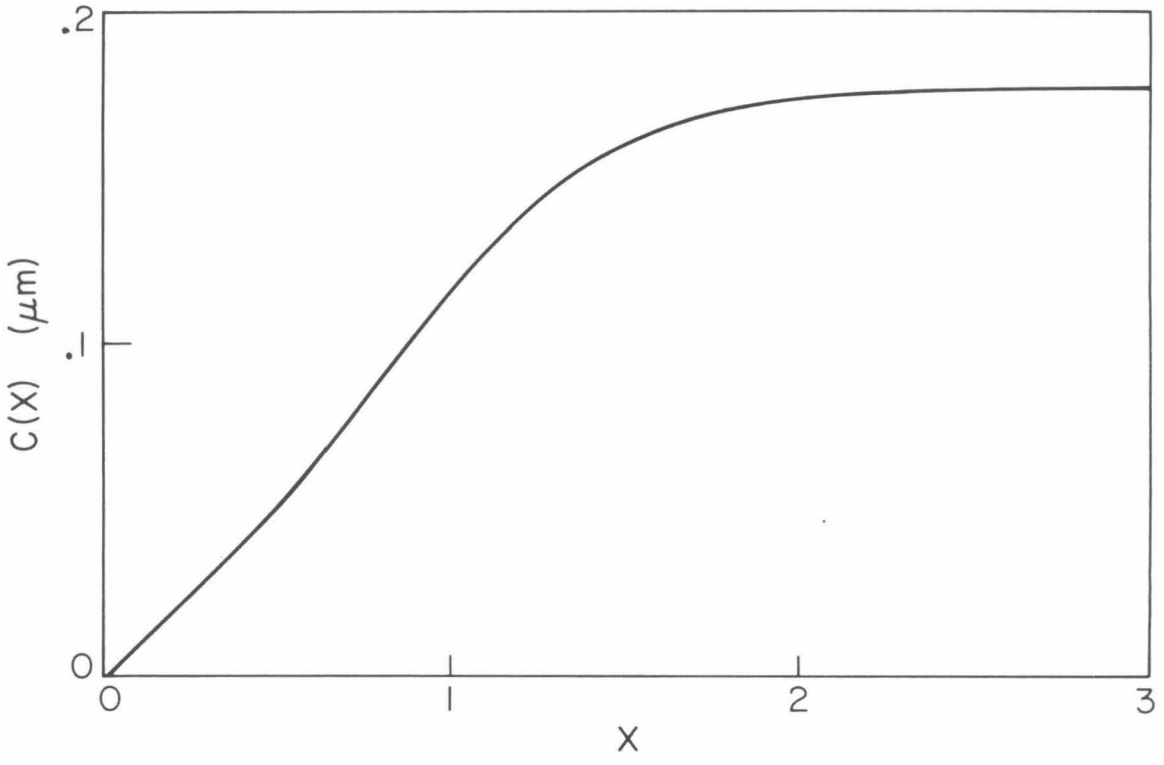
.2
.1
0
C(X) (μm)
0
1
2
3
X

Figure 3.6

A scatter plot of the charge measurement Z1 versus energy ($E_{L1}+E_{L2}+E_{L3}$) for PHA events obtained with LET B of **Voyager 2** during the period September 1977 to May 1978. (To prevent plot saturation, only every tenth event is plotted for $Z1 < 9$. PHA events with $E_{L2} < 2$ MeV or $Z1 < 4$ are primarily due to background effects that will be discussed in section 3.5.2 and are not included in this plot.)

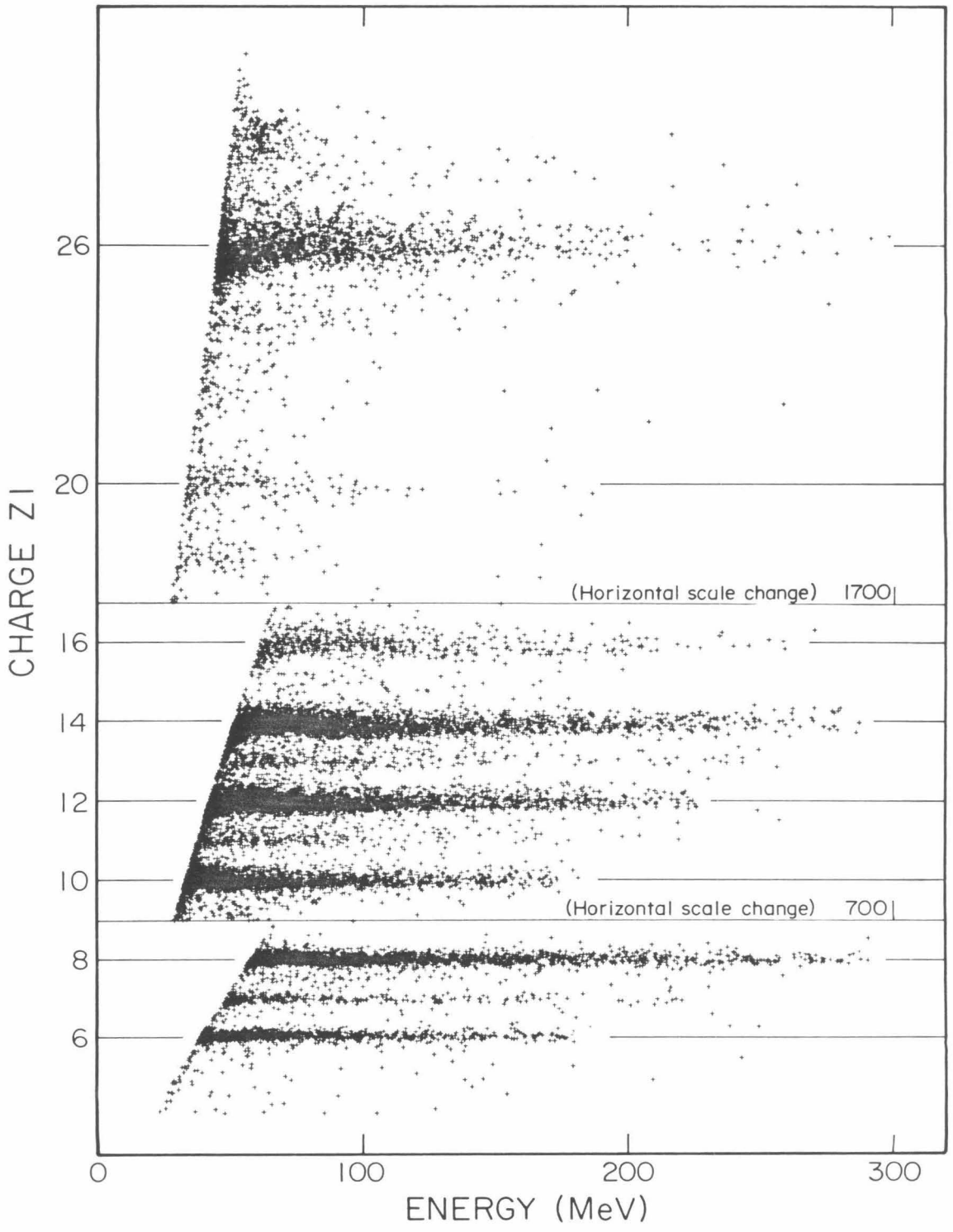
26
20
16
14
12
10
8
6
CHARGE Z I
(Horizontal scale change) 1700
(Horizontal scale change) 700
0
100
200
300
ENERGY (MeV)

TABLE 3.2

Charge Boundaries for

Two Parameter (Z1) Analysis

Z	Element	Lower Boundary	Upper Boundary
6	C	5.78	6.27
8	O	7.67	8.36
10	Ne	9.63	10.42
12	Mg	11.49	12.50
14	Si	13.35	14.53
26	Fe	- (see Appendix B)	-

thin Al entrance windows. The term "energy/nucleon", as used here and throughout this work, actually refers to energy per proton mass unit. Since, for nuclei of H through Ni the difference between the number of nucleons and the mass in proton mass units is less than 1 percent, this error in terminology in negligible.

The two parameter analysis of iron nuclei required special attention (described in Appendix B) due to the background mechanism which caused the unusual clump of events seen in Figure 3.6 near Z1=28.

3.5 Three Parameter ($\frac{dE}{dx}-\frac{dE}{dx}-E$) Analysis for $Z \geq 3$ Nuclei

The selection of PHA events for use in the low background abundance measurements for nuclei of lithium through nickel (presented in Section 4.3) was made as follows:

(1) For each PHA event the charge measurements Z1 and Z2 were checked for consistency as described in Section 3.5.1 below.

(2) PHA events with consistent charge measurements were sorted into element bins using the average of Z1 and Z2, and the charge boundaries discussed in Section 3.5.1 below (and listed in Table 3.3).

(3) PHA events in each of the element bins from carbon through nickel were then counted if the total energy measurements, $E_{L1}+E_{L2}+E_{L3}$, were within energy intervals (calculated as described in Section 3.3) corresponding to incident energies from 8.7 to 15 MeV/nucleon.

(4) For PHA events in the element bins from lithium through oxygen, a second count was obtained for the incident energy interval 5.9–9.3 MeV/nucleon. The total energy boundaries for Li, Be and B were calculated using the nuclear masses of ^{7}Li, ^{9}Be and ^{11}B respectively.

The 8.7–15 MeV/nucleon interval is optimum for the elements carbon through nickel in the sense that this is the three detector response interval common to these elements in all the LETs used. Likewise, 5.9–9.3 MeV/nucleon is optimum for the elements lithium through oxygen.

Three parameter analysis for iron required special attention as discussed in Section 3.5.2 and in Appendix B.

3.5.1 The Charge Consistency Check

Figure 3.7 shows a plot of Z1 versus Z2 for a sample of events from LET C of Voyager 1. The events with consistent Z1 and Z2 charge measurements fall in clumps along the diagonal, while other events fall in off–diagonal locations that are characteristic of various "background" effects to be discussed below. An expanded view of the events along the diagonal in Figure 3.7 is shown in Figure 3.8, a plot of (Z1–Z2) versus (Z1+Z2)/2. The lines indicate the consistency requirement used:

$$|Z1-Z2| < .0164(Z1+Z2) \quad \text{for } (Z1+Z2)/2 > 5.5\,,$$
$$< .180 \quad \text{for } (Z1+Z2)/2 \leq 5.5\,.$$

Figure 3.7

A scatter plot of the charge measurements Z1 and Z2 for PHA events obtained with LET C of Voyager 1 during the period September 1977 to May 1978. (To prevent plot saturation, only every tenth event is plotted in the region where Z1 and Z2 are both less than 9.)

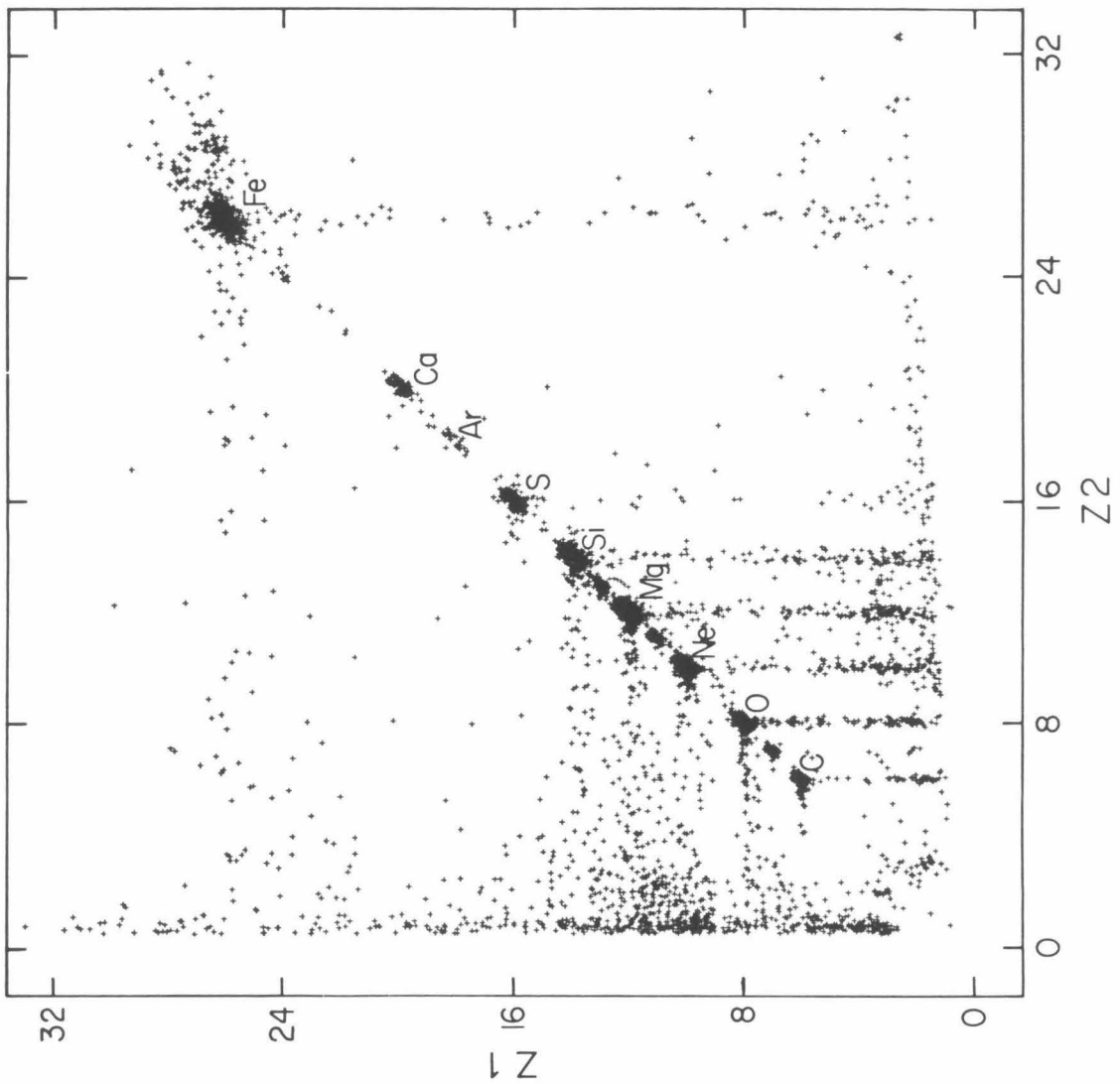
Fe
Ca
Ar
S
Si
Mg
Ne
O
C
0
8
16
24
32
Z2
Z1

Figure 3.8

A scatter plot of (Z1−Z2) versus (Z1+Z2)/2 for the same PHA events as in Figure 3.7. The lines indicate the consistency requirement used.

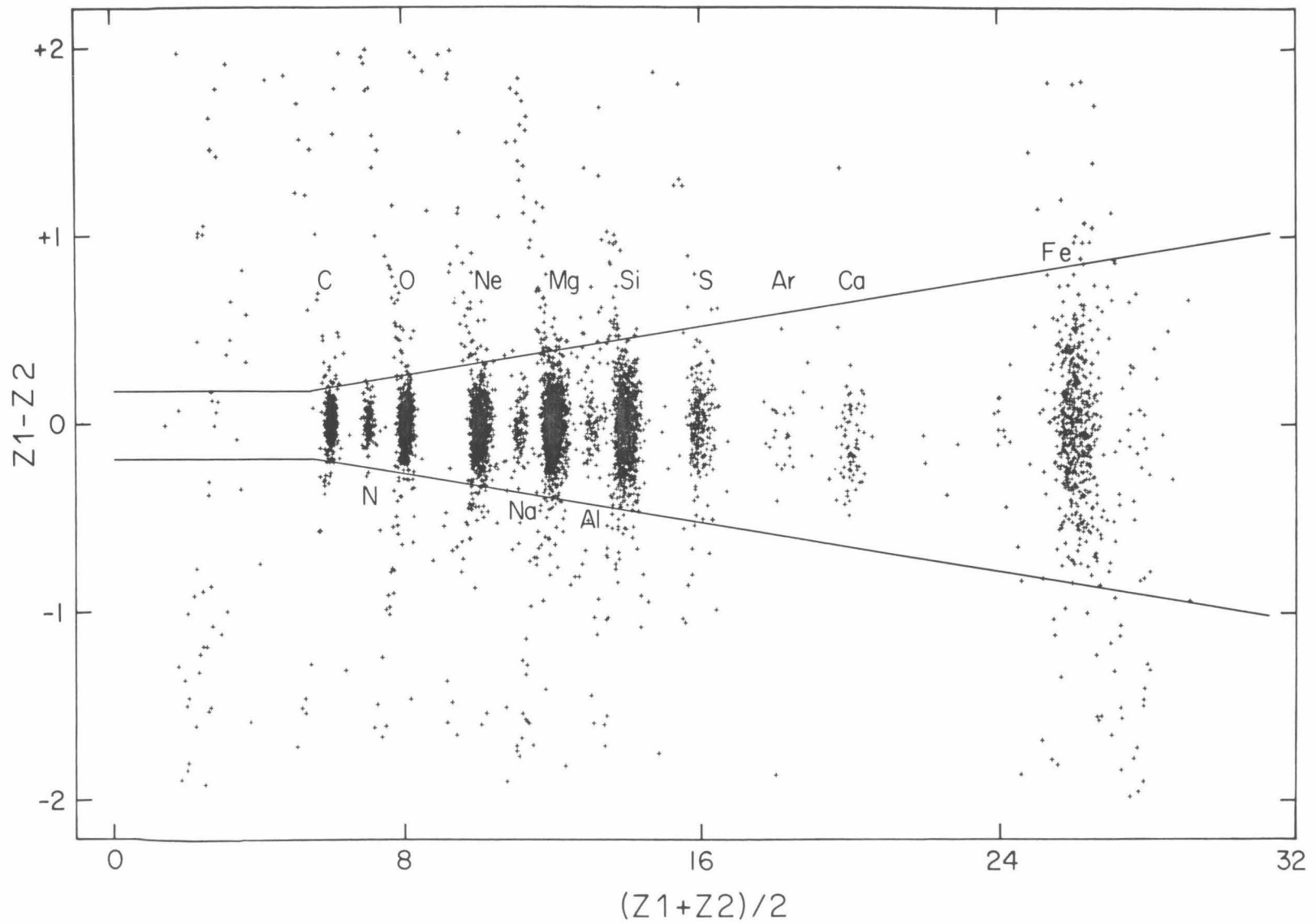
+2
+1
0
-1
-2
Z1-Z2
C
O
Ne
Mg
Si
S
Ar
Ca
Fe
N
Na
Al
0
8
16
24
32
(Z1+Z2)/2

In order to eliminate only a negligible fraction of "good" events this requirement was chosen to cut the distribution of (Z1−Z2) at about ± 3 sigma for each element from carbon through nickel. The quality of the resulting data is shown in Figure 3.9, a (Z1+Z2)/2 histogram of the charge consistent events with energies from 8.7 to 15 MeV/nucleon acquired with the LETs on both Voyagers during the seven largest solar energetic particle events observed in the September 1977 to May 1978 time period. The rms charge resolution ranges from 0.08 units at carbon to 0.27 units at iron. The charge boundaries used to sort the events into various element bins were chosen by inspection of Figure 3.9 and are indicated by arrows. Due to spillover from the iron peak, abundances of Co and Mn were not obtained. Portions of the charge scale (near Co and Mn) that were not included in any other element bin are indicated by shading between the arrows of figure 3.9.

The effect of the consistency check is shown by the comparison of Figure 3.9 with Figure 3.10, a Z1 histogram of all of the PHA events from the same time periods and telescopes as in Figure 3.9. Table 3.3 compares the number of PHA events obtained for each element with and without the consistency check. This comparison indicates that, in the 8.7−15 MeV/nucleon energy interval, two and three parameter analysis yield similar (within 3 percent) abundances for the major elements (such as C, O, Ne, Mg, and Si), but that three parameter analysis is necessary to reduce the background for the rarer elements (such as N, Na, Al, and Cr) which have more abundant neighboring elements of higher Z.

Figure 3.9

A histogram of (Z1+Z2)/2 for charge consistent PHA events corresponding to nuclei with incident energies from 8.7 to 15 MeV/nucleon. The histogram includes PHA events from all the LETs used on both Voyager spacecraft, summed over the seven major flare events in the September 1977 to May 1978 period. The data above oxygen and below carbon are replotted with an expanded vertical scale. The arrows indicate the charge boundaries used to count PHA events corresponding to the different elements. (The cross-hatched regions of the charge scale are discussed in the text.)

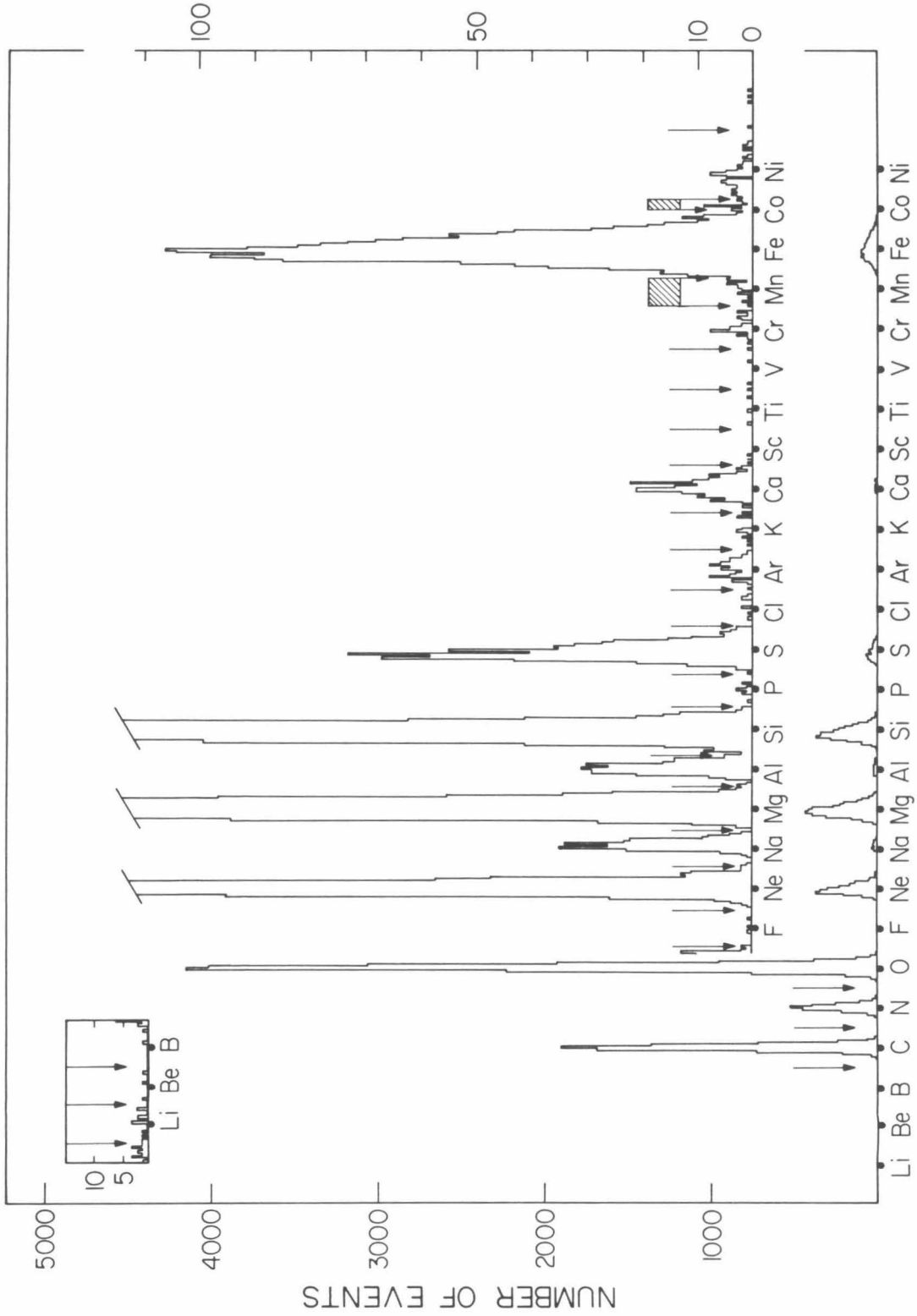
NUMBER OF EVENTS
5000
4000
3000
2000
1000
10
5
Li Be B
100
50
10
0
Li Be B C N O F Ne Na Mg Al Si P S Cl Ar K Ca Sc Ti V Cr Mn Fe Co Ni
F Ne Na Mg Al Si P S Cl Ar K Ca Sc Ti V Cr Mn Fe Co Ni

Figure 3.10

A histogram of the Z1 charge measurement, including PHA events summed over the same time periods and LET telescopes as in Figure 3.9. The effect of the charge consistency check may be seen by the comparison of this histogram, to the histogram of Figure 3.9.

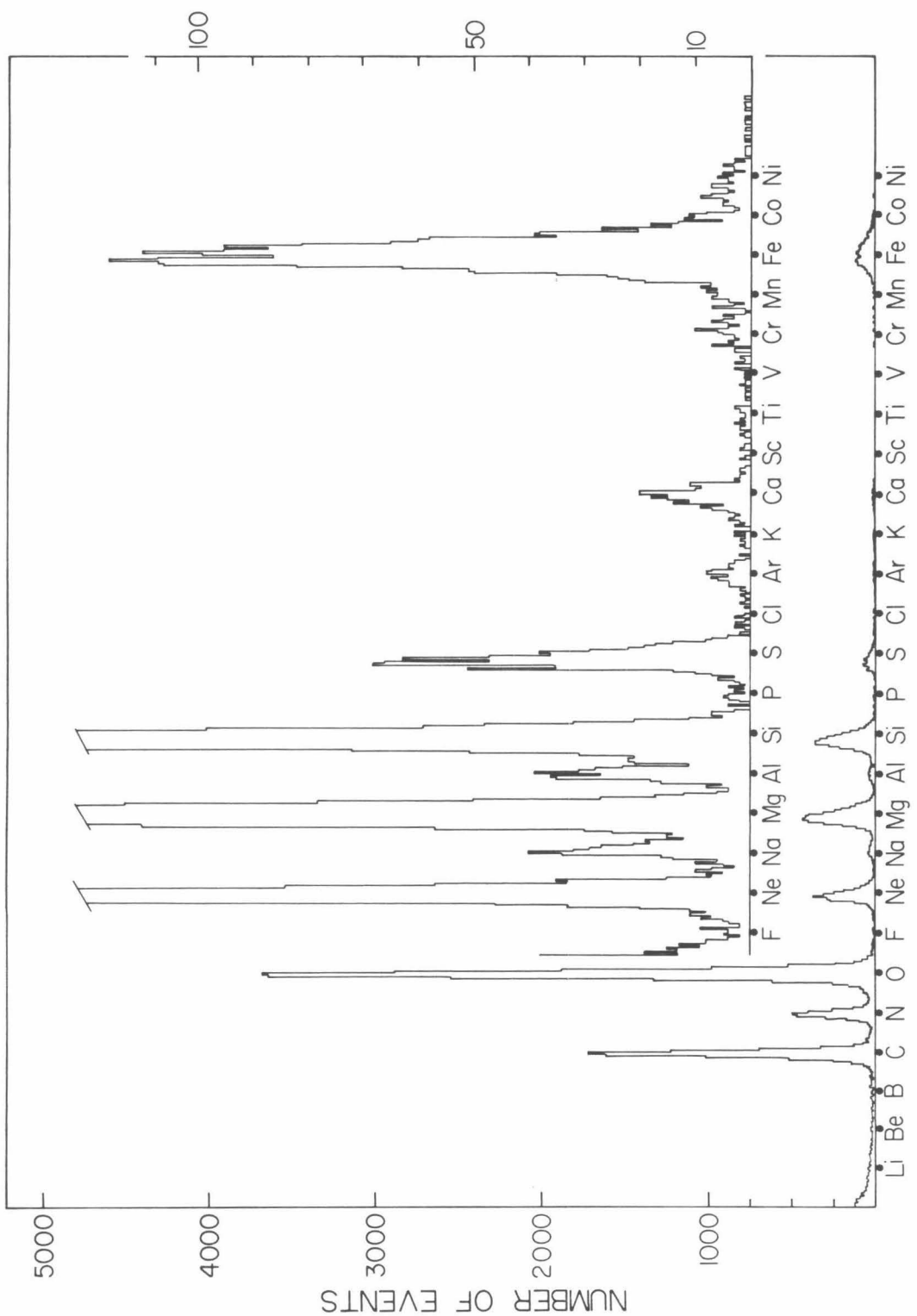
NUMBER OF EVENTS
5000
4000
3000
2000
1000
100
50
10
Li Be B C N O F Ne Na Mg Al Si P S Cl Ar K Ca Sc Ti V Cr Mn Fe Co Ni
F Ne Na Mg Al Si P S Cl Ar K Ca Sc Ti V Cr Mn Fe Co Ni

TABLE 3.3

The Effect of the Charge Consistency Check

Z	Element	Charge Range	PHA Event Count		Rejected Fraction
			without check	with check	
3	Li	2.5 - 3.5	838	14	0.983 ± 0.004
4	Be	3.5 - 4.5	413	3	0.993 ± 0.004
5	B	4.5 - 5.5	384	2	0.995 ± 0.004
6	C	5.5 - 6.5	8058	7026	0.128 ± 0.004
7	N	6.5 - 7.5	2729	2096	0.232 ± 0.008
8	O	7.5 - 8.65	19323	17929	0.072 ± 0.002
9	F	8.65 - 9.5	107	4	0.963 ± 0.018
10	Ne	9.5 - 10.65	2257	2050	0.092 ± 0.006
11	Na	10.65 - 11.5	308	195	0.367 ± 0.027
12	Mg	11.5 - 12.6	3564	3299	0.074 ± 0.004
13	Al	12.6 - 13.4	328	237	0.277 ± 0.025
14	Si	13.4 - 14.6	3003	2842	0.054 ± 0.004
15	P	14.6 - 15.4	37	10	0.730 ± 0.073
16	S	15.4 - 16.6	613	578	0.057 ± 0.009
17	Cl	16.6 - 17.5	17	10	0.412 ± 0.119
18	Ar	17.5 - 18.5	68	61	0.103 ± 0.037
19	K	18.5 - 19.4	23	13	0.435 ± 0.103
20	Ca	19.4 - 20.6	201	181	0.100 ± 0.021
21	Sc	20.6 - 21.5	13	3	0.769 ± 0.117
22	Ti	21.5 - 22.5	25	4	0.840 ± 0.073
23	V	22.5 - 23.5	19	3	0.842 ± 0.084
24	Cr	23.5 - 24.6	80	38	0.525 ± 0.056
26	Fe	25.25 - 27.0	1879	1570	0.164 ± 0.009
28	Ni	27.2 - 29.0	115	82	0.287 ± 0.042

3.5.2 Background

Most of the events eliminated by the consistency check are due to incomplete charge collection near the edge of the active areas of detectors L1 and L2. Edge effects in L1 produce the events with deficient Z1 charge measurements, but normal Z2 measurements, that are observed in Figure 3.7 in bands extending downward from the clumps along the diagonal. Edge effects in L2 result in the bands extending leftward from the clumps. (These bands are poorly defined and curve downward because both the Z1 and Z2 charge measurements depend on the L2 pulse height.) The number of events in these bands indicates that the area of the "edge" of L1 or L2 is roughly independent of nuclear species and is about 6 percent of the fully active area. Edge effects are effectively removed by the consistency check since the probability for a heavy nucleus to masquerade as a lighter one by hitting the edge of both L1 and L2 is small.

The band of events in Figure 3.7 which are near Z2=1 are likely due to the accidental coincidence of a low energy heavy nucleus which stops in L1 and a proton which penetrates L1 and L2, and stops in L3. The smear of events near (Z1 , Z2 = 3) may be caused by either electronic pileup of protons and alphas or by nuclear interactions of these particles in the LET detectors or nearby material.

In addition to the above background effects there is an unusual one (to be discussed in detail in Appendix B) which resulted in the clump of events near (Z1=26 , Z2=28). These events have L1 and L3 pulse heights which are appropriate for iron nuclei, but have L2 pulse

heights which are too large by about 10 percent. This effect caused a disproportionately large fraction of iron nuclei to be rejected by the consistency check (see Table 3.3), and required a correction of about 20 percent to the 8.7–15 MeV/nucleon iron abundances as discussed in Appendix B.

3.6 Three Parameter ($\frac{dE}{dx} - \frac{dE}{dx} - E$) Analysis for Helium Nuclei

The helium abundance and flux measurements presented in this work are based on three detector PHA events selected as follows:

(1) Helium PHA events were selected from the LET $Z < 3$ events using a "slant" threshold on the L2 and L3 pulse heights:

$$\frac{P_{L2}}{35} + \frac{P_{L3}}{47} > 1 .$$

A sample of the selected events is shown in Figure 3.11(a), a scatter plot of L2 energy versus L3 energy.

(2) For each event two mass measurements were calculated and required to be consistent (as described below). The rejected events of the sample shown in Figure 3.11a are replotted in panel (b), while the accepted events are shown in panel (c). Some of the rejected events lie on the L2 versus L3 helium track and are due to edge effects in L1. The number of these events indicates that for He nuclei the area of the edge of L1 is effectively 6 percent of the fully active area of L1. This is the same percentage as found for the $Z \geq 3$ nuclei, suggesting again that the edge effects are independent of Z and that their rejection by the consistency check does not introduce a

Figure 3.11

Scatter plots of the energy deposited in detector L2 versus the energy deposited in L3 for a sample of Z< 3 PHA events obtained with LET C of Voyager 1. Panel (a) shows candidate He PHA events selected using a "slant" threshold (indicated by the sloping line) to discriminate against proton PHA events (which fall below the line and are not shown). The candidate He PHA events which did not pass the mass consistency check (see text) are plotted in panel (b), while the accepted events are shown in panel (c). (Note that the scatter plots do not show the effects of discrete PHA channel numbers -- a pseudo-random number with uniform distribution between 0.0 and 1.0 was added to each pulse height channel number before conversion to energy units; see later text.)

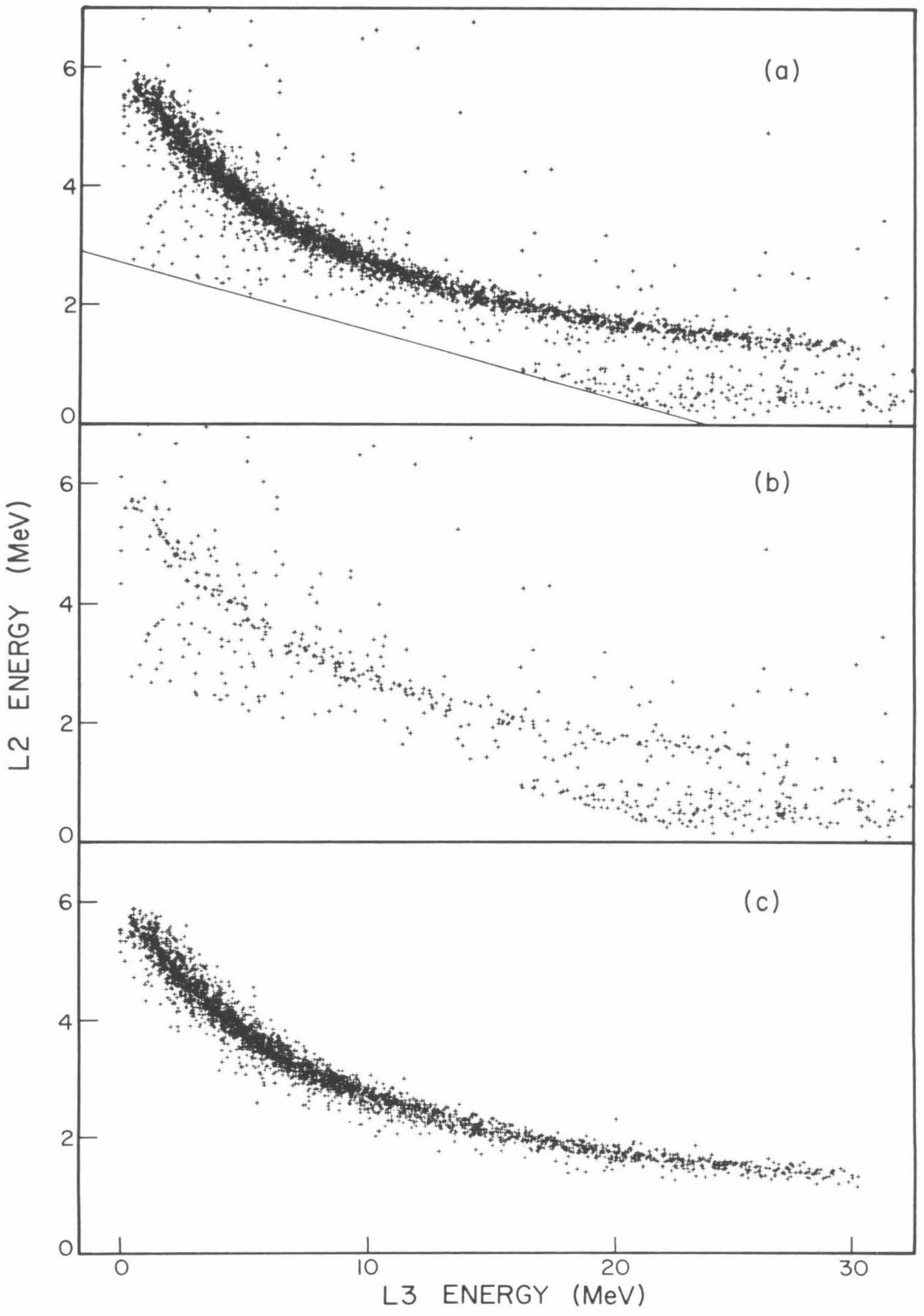
(a)
(b)
(c)
L2 ENERGY (MeV)
L3 ENERGY (MeV)
0
2
4
6
0
10
20
30

Z-dependent bias. The rejected events which lie below the track may be caused by front incident protons which undergo nuclear interaction in L3 or by the accidental coincidence of a particle in L1 with a side incident proton in L2 and L3.

(3) Events with average mass measurement in the interval 3 to 5 amu were sorted into various energy bins by their total energy measurement, $E_{L1}+E_{L2}+E_{L3}$. The energy bins were chosen to be within the response range of all the LETs used and correspond (as discussed in Section 3.4) to the incident energy/nucleon intervals listed in Table 4.4.

The two mass measurements, M1 and M2, were calculated by solving:

$$T_{L1} = R(E_{L1}+E_{L2}+E_{L3}, M1) - R(E_{L2}+E_{L3}, M1)$$

and

$$T_{L2} = R(E_{L2}+E_{L3}, M2) - R(E_{L3}, M2) .$$

T_{L1} and T_{L2} are the mean pathlengths for the appropriate L1 and L2 detectors. E_{L1} , E_{L2} and E_{L3} are the energies deposited in detectors L1, L2 and L3. $R(E, M)$ is the range in silicon of a nucleus with nuclear charge $Z = 2$, and mass M, as scaled from the ^{4}He range-energy relation R_{He} of Vidor (1975) as follows:

$$R(E, M) = \left(\frac{M}{M_{He}}\right) R_{He}\left(\frac{E \cdot M_{He}}{M}\right) ,$$

where M_{He} is the mass of the ^{4}He nucleus.

In order to properly account for the effects of finite PHA channel widths, a psuedo-random number with uniform distribution from 0.0 to 1.0 was added to each L1, L2 and L3 pulse height channel number before the conversion to energies E_{L1} , E_{L2} and E_{L3}. Since the channel widths are small (about 70 KeV for detectors L1 and L2, and 500 KeV for L3) the approximation of a uniform distribution of energy measurements over each pulse height channel is accurate. The main effect of the random number addition is to produce continuous, rather than discrete, distributions for the mass measurments M1 and M2.

The means of the M1 and M2 ^{4}He mass distributions were found to vary from LET to LET, and as a function of total energy and time for a given LET, by less than about 0.2 amu. The means were typically within 0.2 amu of the ^{4}He nuclear mass ($\approx$ 4 amu) suggesting that systematic errors in the energy measurements E_{L1} and E_{L2} were less than about 2 percent for energies near 6 MeV, while systematic errors in the E_{L3} energy measurements were less than about 3 percent near 30 MeV. However, since 0.2 amu is a significant fraction of the helium mass resolution ($\approx$ 0.3 amu) achieved for individual LETs, the mass measurements M1 and M2 were adjusted (to obtain $M1_{adj}$ and $M2_{adj}$) by the addition of correction factors (listed in Table 3.4) chosen for each LET to shift the mean masses to 4 amu.

The mass consistency requirement:

$$\left| M1_{adj} - M2_{adj} \right| < 1.0$$

was chosen to cut the $(M1_{adj} - M2_{adj})$ distributions at about $\pm$ (3 sigma

TABLE 3.4

LET Helium Mass Correction Factors

	ΔM1	ΔM2
Voyager 1		
LET A	0.216	0.211
LET B	-	-
LET C	0.197	0.138
LET D	0.123	0.110
Voyager 2		
LET A	0.047	0.004
LET B	0.209	-0.050
LET C	0.102	-0.058
LET D	-0.007	-0.045

+ .25 amu) in order to reject only a negligible fraction of good events. The mass resolution achieved is illustrated in Figure 3.12 which shows two $(M1_{adj}+M2_{adj})/2$ histograms of mass consistent PHA events from the LETs on both Voyagers. Histogram (a) is for the flare event of September 9, 1977, while histogram (b) is for the small ^{3}He rich event of October 13, 1977. Since no ^{3}He peak was seen in the mass histograms for any of the large flare events studied in this paper, the mass selection interval 3 to 5 amu was chosen to include essentially all good ^{4}He events, with negligible ^{3}He contamination.

In one of the major flare events studied (the April 29, 1978 event) the He mass resolution was degraded due to high count rates. In this case, the consistency check was relaxed to $|M1_{adj} - M2_{adj}| < 2.0$ and the mass selection interval was increased to 2–5 amu to prevent the rejection of ^{4}He PHA events which were apparently affected by baseline shifts in the L1 pulse height analyzers.

3.7 Fluence and Relative Abundance Measurements

3.7.1 Definitions and Terminology

The "differential flux" $\frac{dJ_Z}{dE}$ of nuclei with nuclear charge Z is defined, as a function of energy/nucleon E, direction Ω, location r, and time t, by:

$$\frac{dJ_z}{dE}(E,\Omega,r,t) \equiv N/(dA \cdot d\Omega \cdot dt \cdot dE)$$

$$\text{particles}/(\text{cm}^2 \text{ sr sec MeV/nucleon})$$

Figure 3.12

Helium mass histograms, summed over mass consistent PHA events from the LETs on both Voyager spacecraft. Histogram (a) is for the flare event of September 9, 1977; (b) is for a small ^{3}He-rich event of October 13, 1977.

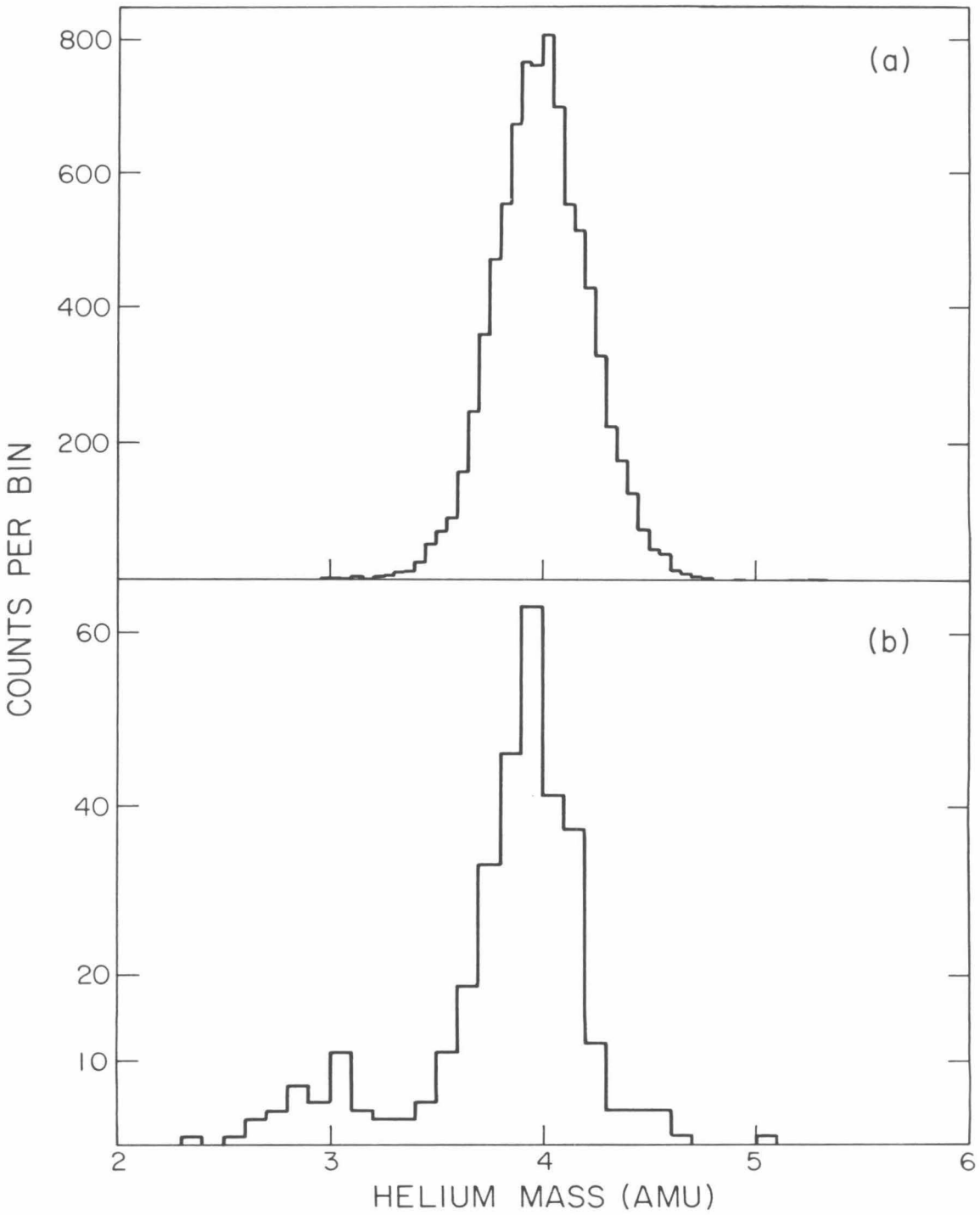
800
600
400
200
(a)
60
40
20
10
(b)
COUNTS PER BIN
2
3
4
5
6
HELIUM MASS (AMU)

where, in the time interval dt (sec) containing t, N is the number of nuclei which (a) cross a surface area dA (cm^2) that is oriented normal to Ω, (b) have trajectories within the solid angle $d\Omega$ (sr) centered on Ω, and (c) have kinetic energies in the range dE about E (MeV/nucleon).

The "integral flux" J_z is defined as the integral with respect to energy/nucleon of the differential flux, and therefore refers to the flux contained within some specified energy/nucleon interval.

The integration with respect to time of a flux yields a "fluence".

The SEP "relative abundance" of two different nuclear species is defined here as the ratio of their differential fluxes at common values of E, Ω, r and t.

Generally, measurements of SEP flux, fluence, and relative abundances are averaged over some range of energies, incidence angles and times and are performed at a particular location in the heliosphere. The averaging techniques employed in the fluence and relative abundance measurements presented in this thesis are described below.

3.7.2 Fluence Measurements

For each spacecraft, the integral flux $J_{Z,i,j}$ of nuclei, with nuclear charge Z, in energy interval i, was calculated for each three-hour interval j by averaging the fluxes measured in each LET k as follows:

$$J_{Z,i,j} = \left(\frac{1}{K}\right)\sum_{k}\left(\frac{N_{Z,i,j,k}}{NPHA_{j,k}}\right)\left(\frac{C_{j,k}}{T_{j,k}}\right)(LT_{j,k}\cdot G_k)^{-1}\ .$$

$$\text{particles}/(\text{cm}^2\cdot\text{sr}\cdot\text{sec}) \qquad (3.2)$$

The terms are explained below:

- K is the number (either 3 or 4) of LETs used; LET B on Voyager 1 and, at times, LET C on Voyager 2 were excluded due to the problems discussed in Appendix B.

- $N_{Z,i,j,k}$ is the number of PHA events (selected by two or three parameter analysis as discussed in previous sections) for element Z , energy interval i , three-hour interval j , and LET k .

- $NPHA_{j,k}$ is the total number of PHA events read out from the appropriate ($Z<3$ or $Z\geq 3$) event buffer for LET k during the three-hour interval j .

- $C_{j,k}$ is the number of $Z<3$ or $Z\geq 3$ counts recorded by the rate accumulator for LET k during interval j .

- $T_{j,k}$ is the length of time (in seconds) during which the counts $C_{j,k}$ were accumulated. (This time was often less than three hours since the spacecraft were not continuously monitored.)

- $LT_{j,k}$ is a small correction for dead time of the rate accumulator. Laboratory measurements (Gehrels, private communication, 1980) of the high count rate response of the

LET electronics indicate that:

$$LT_{j,k} = (1 - T1 \cdot R1_{j,k})(1 - T2 \cdot R2_{j,k})$$

where $R1_{j,k}$ and $R4_{j,k}$ are the count rates for detectors L1 and L4, with effective dead times per count of T1 = 18 μsec and T4 = 20 μsec respectively.

- G_k is the geometry factor (in cm^2 steradian) for LET k (from Gehrels 1980).

For each spacecraft, the integral fluence measurement $W_{Z,i,t}$, summed over a flare period t, including three-hour intervals indexed by the subscript j, was calculated using:

$$W_{Z,i,t} = \sum_j J_{Z,i,j} \cdot \Delta T \quad \text{particles}/(cm^2 \cdot sr)$$

where ΔT = 10800 seconds (3 hours) and the subscript i still indicates the energy/nucleon interval. Since the spacecraft were not continuously monitored, some three-hour intervals were necessarily excluded from the sum. For each flare event a rough estimate (included in Tables 4.2 through 4.7) of the missing fluence was made by interpolating the counting rate for $Z \geq 3$ nuclei through data gaps.

The statistical uncertainty in the flux and fluence measurements is dominated by the uncertainty in the number of PHA events ($N_{Z,i,j,k}$) obtained for a particular element and energy bin. $N_{Z,i,j,k}$ is always much smaller than either the total number of PHA events ($NPHA_{j,k}$) or the number of rate scalar counts ($C_{j,k}$). Thus, the

statistical uncertainty was estimated using the right hand side of equation (3.2) with $N_{Z,i,j,k}$ replaced by $(N_{Z,i,j,k})^{\frac{1}{2}}$.

3.7.3 Relative Abundance Measurements

Two different types of relative abundance measurements were made for each flare event: "flux weighted" and "PHA event weighted". The flux weighted relative abundance measurement $\langle A_{Z1,Z2,i} \rangle_{F,t}$ of nuclear species Z1 and Z2, for the common energy/nucleon interval i, and time period t, is defined as the ratio of fluences:

$$\langle A_{Z1,Z2,i} \rangle_{F,t} \equiv W_{Z1,i,t} / W_{Z2,i,t} .$$

The PHA event weighted relative abundance measurement $A_{Z1,Z2,i\ P,t}$ may be defined for nuclear species Z1 and Z2 which are pulse height analyzed with the same priority (i.e. Z1,Z2< 3 or Z1,Z2 ≥ 3), as the ratio of PHA event counts:

$$\langle A_{Z1,Z2,i} \rangle_{P,t} \equiv N_{Z1,i,t} / N_{Z2,i,t} .$$

If the true relative abundance of the two nuclear species is constant during the averaging time, t, then $\langle A \rangle_F$ and $\langle A \rangle_P$ will be the same within statistical error. However, if the true relative abundance varies during t and if the flux is high enough to saturate the telemetry rate for PHA events, then the two measurements may be systematically different. In the next chapter the time variation of relative abundances during individual flare events will be examined, and "flux" and "PHA event" weighted measurements will be compared.

It is important to note that for a flare event in which the PHA event telemetry saturates, the flux weighted abundance measurements will generally have larger statistical uncertainties than the corresponding PHA event weighted measurements. This is because a flux weighted measurement may depend primarily on a disproportionately small number of PHA events acquired during the time of peak flux, while "PHA event weighting" makes full use of PHA events acquired throughout the averaging time period, giving each event equal statistical weight. Since PHA event weighting produces smaller statistical uncertainty, it was desirable to extend the technique to obtain relative abundances of nuclei which are not pulse height analyzed with equal probability. In particular, the PHA event weighted abundance measurement $\langle A_{He,Z,i} \rangle_{P,t}$ of helium relative to element Z (≥ 3) for a common energy/nucleon interval i, and a time period t, was defined separately for each spacecraft by :

$$\langle A_{He,Z,i} \rangle_{P,t} \equiv 1.06 \cdot \exp\left[\sum_j w_j \cdot \ln\left(\frac{N_{He,i,j}}{N_{Z,i,j}} \cdot \frac{P_{Z,j}}{P_{He,j}} \right) \Big/ \sum_j w_j \right] ,$$

where:

- $N_{He,i,j}$ and $N_{Z,i,j}$ are the numbers of PHA events for helium and element Z acquired during a time subinterval j (of length chosen to be six hours) and summed over the LETs used.

- $P_{He,j}$ and $P_{Z,j}$ are the pulse height analysis probabilities for $Z < 3$ and $Z \geq 3$ nuclei respectively:

$$P_{He,j} \equiv NPHA_{(Z<3),j} \Big/ C_{(Z<3),j} ,$$

$$P_{Z,j} \equiv NPHA_{(Z\geq 3),j} \,/\, C_{(Z\geq 3),j} \,,$$

where NPHA and C are the numbers of PHA events and rate scalar counts (for $Z<3$ or $Z\geq 3$ nuclei) obtained during time j, and summed over the LETs used.

- w_j is a weighting factor chosen to minimize an estimate σ_p of the statistical uncertainty in $A_{He,Z,i\ P,t}$:

$$w_j = \left(\frac{1}{N_{He,i,j}} + \frac{1}{N_{Z,i,j}} \right)^{-1} ,$$

$$\sigma_p = \left(\sum_j w_j \right)^{-\frac{1}{2}} \cdot \langle A_{He,Z,i} \rangle_{P,t} \ .$$

- The factor of 1.06 accounts for the 6 percent difference between the effective geometry factor for He nuclei (which were counted by three parameter $\frac{dE}{dx}-\frac{dE}{dx}-E$ analysis) and the effective geometry factor for the higher Z nuclei (which for this measurement where counted using two parameter $\frac{dE}{dx}-E$ analysis).

- The logarithmic average was used to obtain the desirable property: $\langle A_{He,Z} \rangle_P = 1 / \langle A_{Z,He} \rangle_P$.

Chapter 4

Observations

4.1 Overview

The seven largest solar energetic particle (SEP) events in the September 1977 to May 1978 period are selected for study. The time development of each event is examined in order to select an optimum averaging time period for SEP relative abundance measurements. Abundance measurements of nuclei from He (Z=2) through Ni (Z=28) are presented for each flare event and are compared to other reported measurements which are available for four of the seven flare events. Fluence measurements are presented for the more abundant elements (He, C, O, Ne, Mg, Si, and Fe+Ni) in several energy bins from 3 to 30 MeV/nucleon. The possible systematic errors in the presented measurements are estimated.

4.2 Energetic Particle Event Selection

Figure 4.1 shows the hourly averaged flux of $Z > 3$ nuclei with energies above about 3 MeV/nucleon, as measured by the LETs on Voyager 1 during the period September 1977 through May 1978. The seven largest energetic particle events (labeled i through vii) were selected for study because of the statistical accuracy available for $Z \geq 3$ abundance measurements. Optical, radio and/or X-ray data (Coffey 1977, 1978) indicate that for each of the first four events a large solar flare occurred within a few hours before the arrival of relativistic electrons (as measured by the Voyager High Energy Telescopes). The last

Figure 4.1

The hourly averaged flux of $Z \geq 3$ nuclei measured with the LETs on Voyager 1. The energy threshold for detection varies from about 3 MeV/nucleon for carbon nuclei, to 5 MeV/nucleon for iron nuclei. The seven largest energetic particle events are labeled i through vii. (The quantization of the flux measurement at low levels corresponds to the detection of a small integer number of nuclei.)

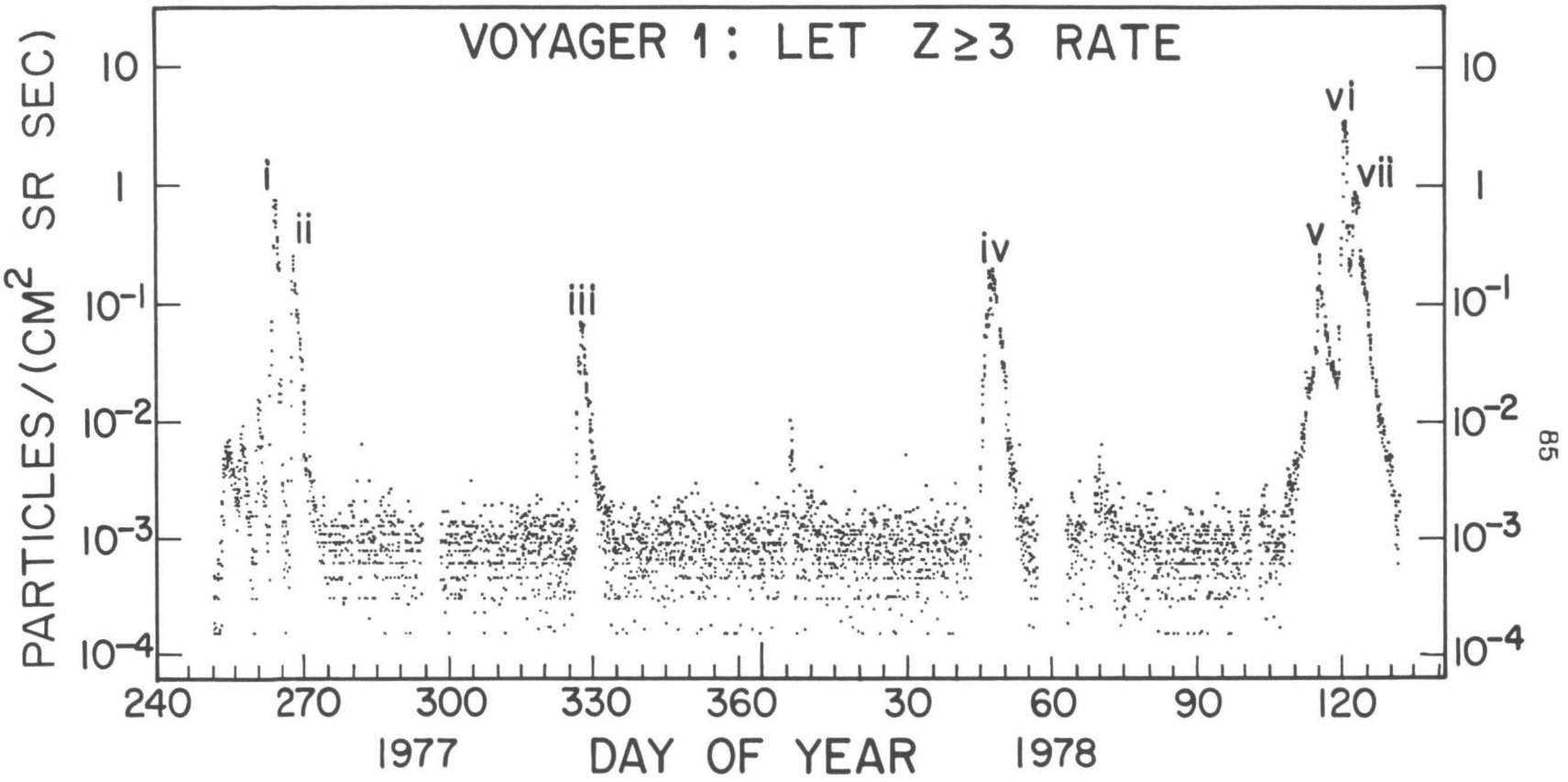
VOYAGER 1: LET Z≥3 RATE
PARTICLES/(CM² SR SEC)
10
1
10⁻¹
10⁻²
10⁻³
10⁻⁴
i
ii
iii
iv
v
vi
vii
240
270
300
330
360
30
60
90
120
1977
DAY OF YEAR
1978

three events were not well separated, but were part of a general intensity increase accompanied by several large solar flares.

The selected energetic particle events are large: The peak flux of protons (> 20 MeV) observed in the events ranges from about 20 to 500 particles/($cm^2 \cdot sr \cdot sec$) placing all seven events in the upper 5 percent of the size distribution for energetic particle events recorded near the time of the previous solar maximum, 1967 through 1969 (Svestka 1976). The first three of the seven events were observed by neutron monitors at ground level (Coffey 1977, 1978).

A compilation of references to some recent energetic particle observations of the first four events may be found in Wibberenz (1979). The importance, location on the sun, and time of maximum for the large optical flares preceding energetic particle events i, iii and iv are respectively: 3B, N08W57, 1977 September 19 10:38 UT; 2B, N24W40, 1977 November 22 10:05 UT; and 2N, N15W20, 1978 February 13 1:43 UT (Coffey 1977, 1978). Energetic particle event ii probably originated in a flare which occurred just beyond the west limb in the same active region which produced the flare of 1977 September 19. (Type II and III radio emissions were observed at about 5:55 UT of 1977 September 24; Coffey 1978)

4.3 Energetic Particle Event Time Profiles

The time structure of the seven selected energetic particle events is displayed in Figures 4.2 through 4.6. Shown separately for each Voyager spacecraft are: (1) counting rates corresponding to protons

Figures 4.2 through 4.6

Energetic particle event time profiles. Various counting rates (labeled LA1, BSP, and Z≥ 3), element ratios (C/O, Ne/O, Mg/O, Si/O and [Fe+Ni]/O), and the oxygen spectral index (γ_{oxygen}) are averaged in successive three hour intervals and are plotted separately for Voyager 1 (—,●) and Voyager 2 (.....,o). The counting rates LA1, BSP, and Z≥ 3 correspond respectively to protons above about 0.5 MeV, protons above 20 MeV, and Z≥ 3 nuclei above an energy threshold which varies from about 3 MeV/nucleon for carbon to 5 MeV/nucleon for iron. The element ratios are for the common interval 5–15 MeV/nucleon, except in the case of the He/O ratio where the energy range is 4.0–7.8 MeV/nucleon. The oxygen spectral index was computed from the ratio of oxygen PHA events obtained in the 4.0–6.1 and 6.1–15 MeV/nucleon energy intervals. (The cross–hatched boxes are discussed in the text.)

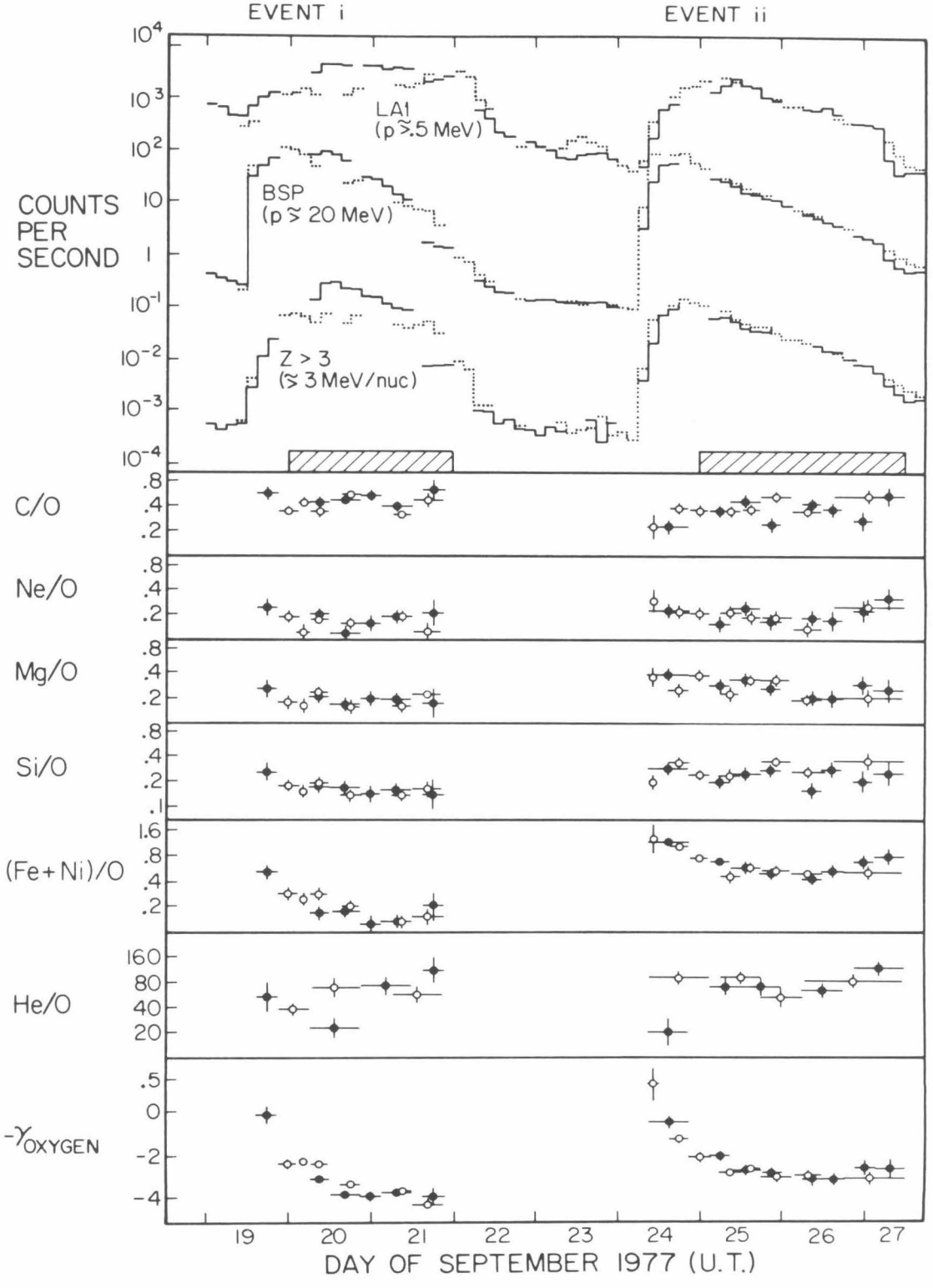
EVENT i
EVENT ii
COUNTS PER SECOND
LA1 (p ≳ 5 MeV)
BSP (p ≳ 20 MeV)
Z > 3 (≳ 3 MeV/nuc)
C/O
Ne/O
Mg/O
Si/O
(Fe+Ni)/O
He/O
-γ OXYGEN
DAY OF SEPTEMBER 1977 (U.T.)

Figure 4.2

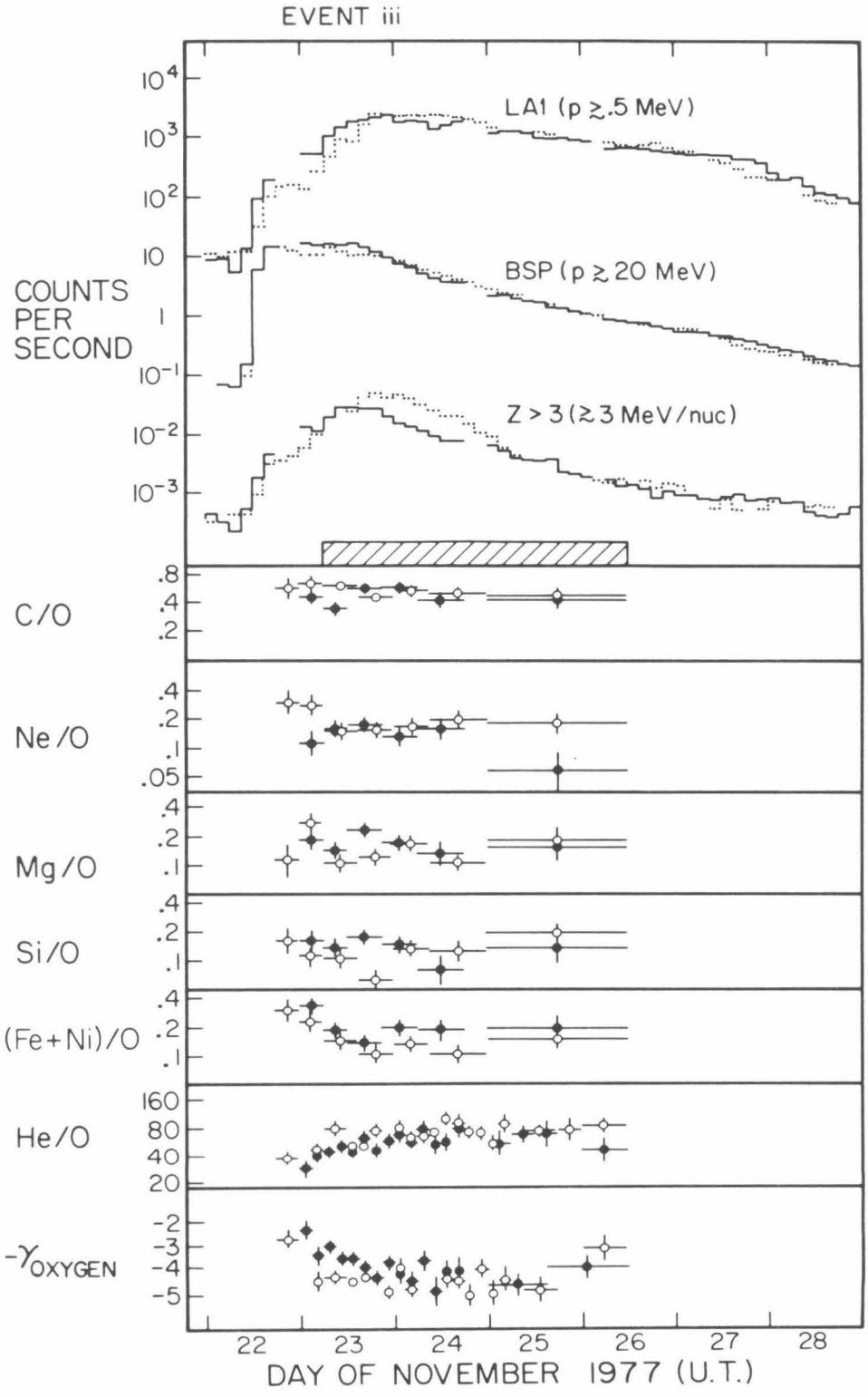
EVENT iii
LA1 (p ≳.5 MeV)
BSP (p ≳ 20 MeV)
Z > 3 (≳3 MeV/nuc)
COUNTS PER SECOND
C/O
Ne/O
Mg/O
Si/O
(Fe+Ni)/O
He/O
-γOXYGEN
DAY OF NOVEMBER 1977 (U.T.)

Figure 4.3

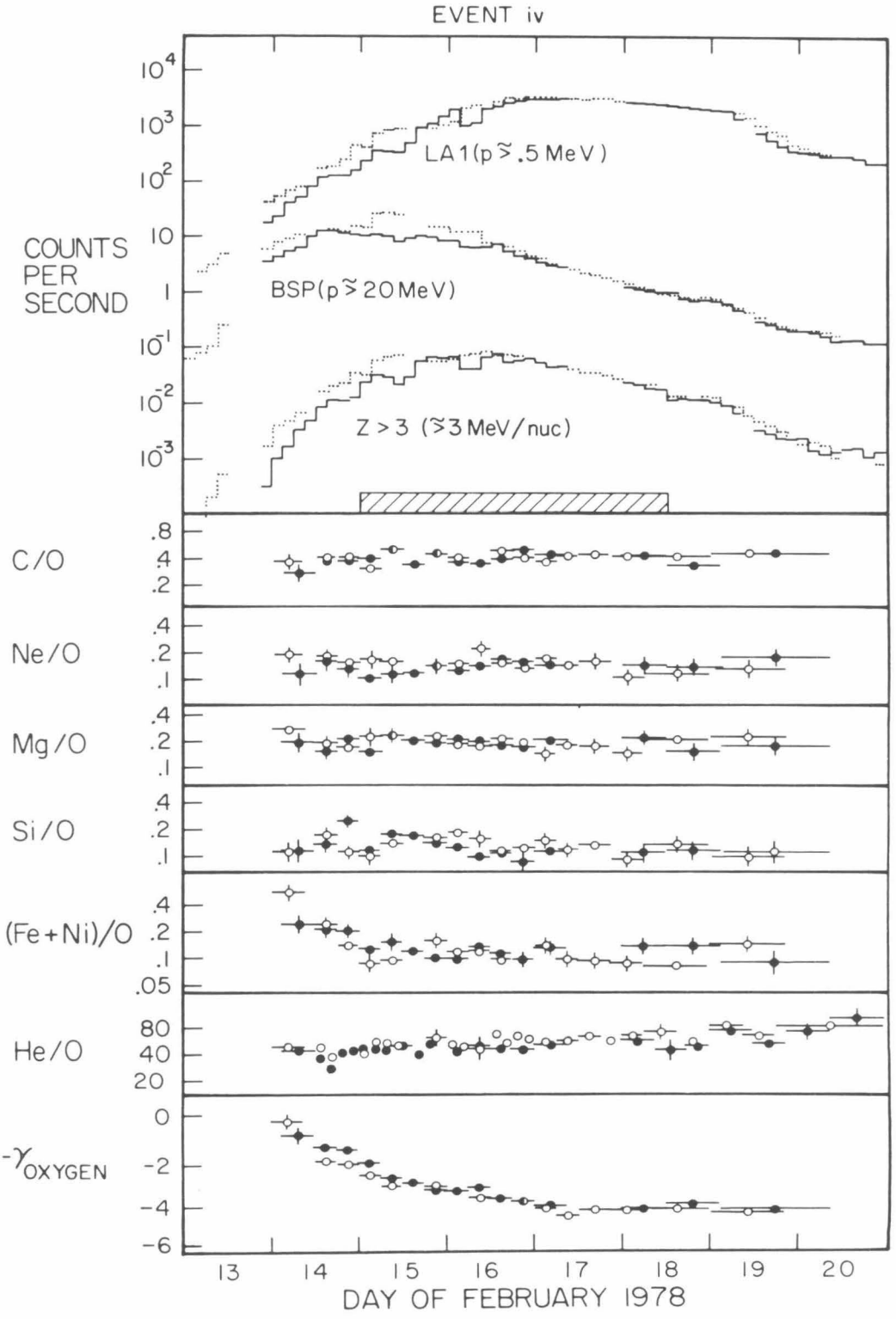
EVENT iv
COUNTS PER SECOND
LA1(p≳.5 MeV)
BSP(p≳20 MeV)
Z>3 (≳3 MeV/nuc)
C/O
Ne/O
Mg/O
Si/O
(Fe+Ni)/O
He/O
-γOXYGEN
DAY OF FEBRUARY 1978

Figure 4.4

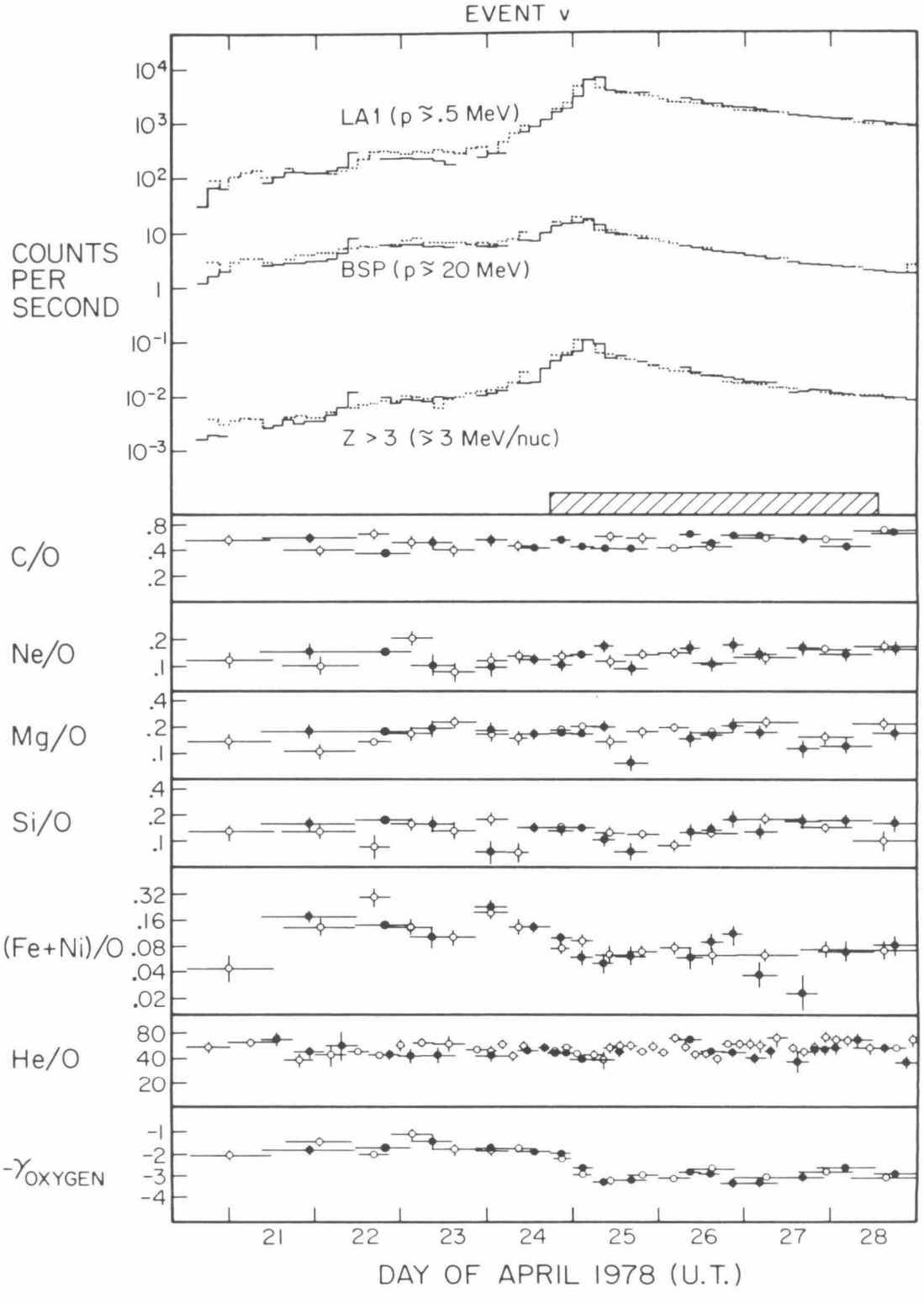
EVENT v
LA1 (p ≳.5 MeV)
BSP (p ≳ 20 MeV)
Z > 3 (≳ 3 MeV/nuc)
COUNTS PER SECOND
C/O
Ne/O
Mg/O
Si/O
(Fe+Ni)/O
He/O
-γOXYGEN
DAY OF APRIL 1978 (U.T.)

Figure 4.5

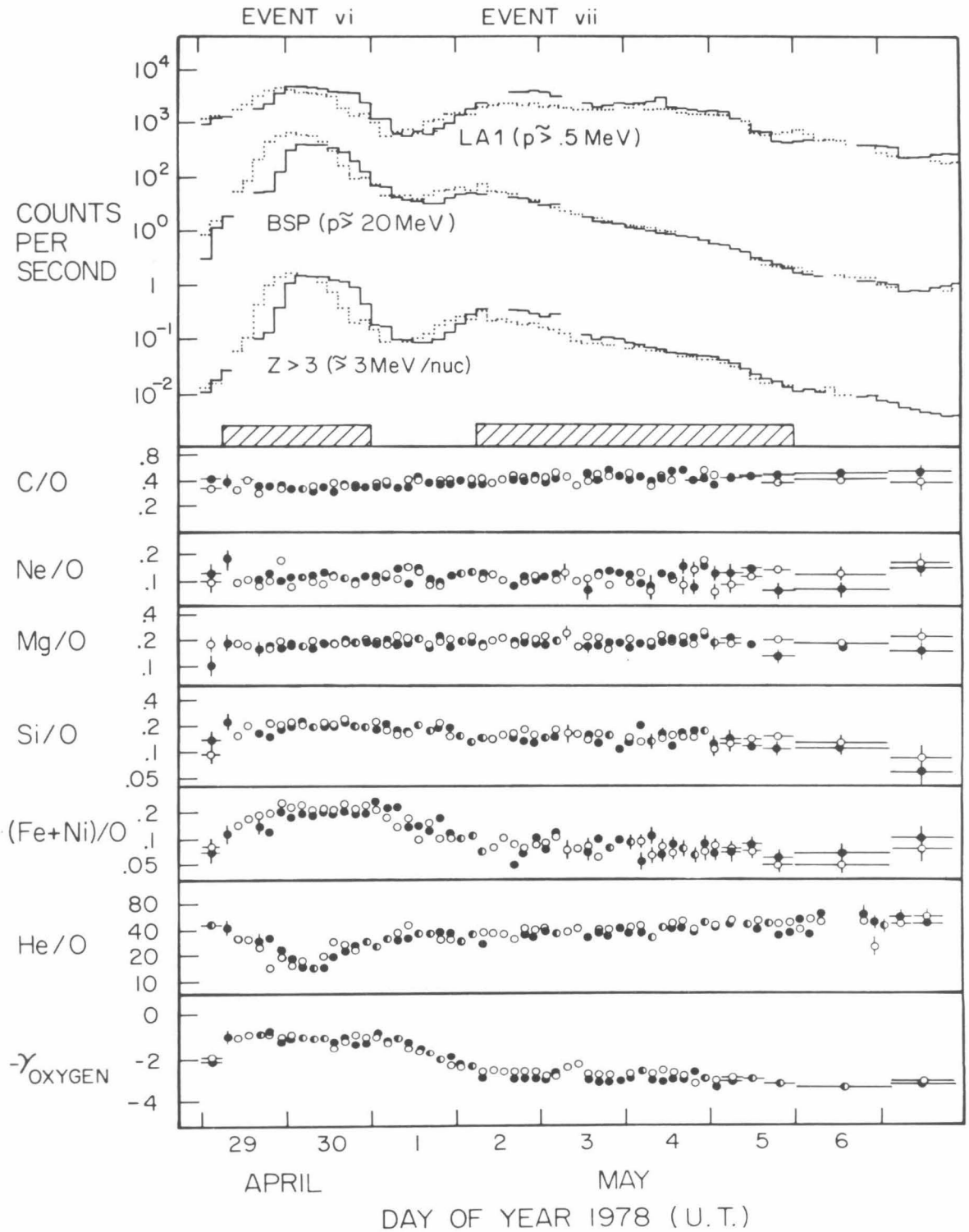
EVENT vi
EVENT vii
COUNTS PER SECOND
LA1 (p≳.5 MeV)
BSP (p≳20 MeV)
Z>3 (≳3 MeV/nuc)
C/O
Ne/O
Mg/O
Si/O
(Fe+Ni)/O
He/O
-γ OXYGEN
29
30
1
2
3
4
5
6
APRIL
MAY
DAY OF YEAR 1978 (U.T.)

Figure 4.6

above 0.5 MeV, protons above 20 MeV, and $Z \geq 3$ nuclei above about 3 MeV/nucleon, (2) the abundance ratios C/O, Ne/O, Mg/O, Si/O and (Fe+Ni)/O measured over the energy range 5.0–15.0 MeV/nucleon, (3) the He/O ratio measured for the 4.0–7.8 MeV/nucleon energy interval, and (4) the spectral index γ (assuming $dJ/dE \propto E^{-\gamma}$) of oxygen, obtained from the ratio of oxygen PHA events in the 6.1–15.0 and 4.0–6.1 MeV/nucleon energy intervals. The main features of these plots are summarized below.

(1) Generally, there is good agreement between the Voyager 1 and 2 measurements of abundance ratios and the oxygen spectral index. Thus, for the relative abundance results presented later we combined the data from Voyagers 1 and 2 (improving statistical accuracy and averaging over any small spatial inhomogeneities which may exist between the spacecraft).

(2) The (Fe+Ni)/O ratio decreased by a factor of three to five during the first 12 to 24 hours of each of the energetic particle events which showed velocity dispersion. Velocity dispersion was identified in the first four events (Figures 4.2 through 4.4) by the earlier arrival of protons above 20 MeV relative to protons above 0.5 MeV and by a softening of the oxygen spectra early in the events. Time variations associated with velocity dispersion were also seen for the He/O ratio, which increased during the 1977 November 22 and 1978 February 14 events.

(3) In contrast to (2), systematic time variations were not apparent for the C/O, Ne/O, Mg/O and Si/O ratios, which were constant within about ± 30 percent throughout each of the energetic particle events.

(4) The last three events showed more complex time structure than the first four well-separated events. It is interesting to note that the 1978 April 29 event showed no velocity dispersion, had a symmetrical intensity rise and fall, and occurred at Voyager 2 six hours earlier than at Voyager 1. Since Voyager 2 was located about 1/8 AU sunward of Voyager 1, these features suggest that the energetic particles were trapped in a structure which was moving radially away from the sun at about 800-1000 km/sec.

Abundance time variations, such as in (2) above, which are associated with velocity dispersion have been seen at somewhat lower energies by a number of experimenters (see, e.g., Van Allen, Venketarangan and Venkatesan 1974; O'Gallagher et. al. 1976; Scholer et. al. 1978; von Rosenvinge and Reames 1979) and are thought to be a propagation effect in which nuclei with the same velocity, but different charge to mass ratios, diffuse from the sun to the spacecraft at different rates. O'Gallagher et. al. (1976) studied the arrival time distributions of H, He, C, O, and Fe nuclei (0.5 to 5 MeV/nucleon) in one flare event which showed particularly regular intensity versus time profiles and concluded that the H through O nuclei were almost fully stripped but that the Fe nuclei had retained about 16± 5 of their 26 electrons (charge state of 10 ± 5). Although direct charge state measurements at these energies are not available

for comparison, these results are consistent with measurements at lower energies by Sciambi et. al. 1977 and Gloeckler et. al. 1976 who found mean charge states of 5.8 for carbon, 6.3 for oxygen (averaging over nine flares, for energies 15–600 KeV/nucleon), and 11.6 for iron (from a single event, for energies 8–250 Kev/nucleon).

The significance of the observed abundance time variations will be further discussed in the next chapter. Here we consider the effect of the time variations on time averaged abundance measurements for individual flare events. Abundance time variations have been studied recently by Scholer et. al. (1978) using a relatively standard propagation model which incorporates rigidity dependent diffusion, convection and adiabatic deceleration. The results are in qualitative agreement with the observed time dependence of the (Fe+Ni)/O ratio, and suggest that the ratio observed later in an event, after the initial decrease of the (Fe+Ni)/O ratio, approximates the injection ratio at the sun. This was taken into account in the selection of averaging time intervals (indicated by the shaded boxes of Figures 4.2 through 4.6) for the abundance measurements presented in the next section.

For the four flare events which showed velocity dispersion (events i, ii, iii, and iv) the selected averaging periods exclude times early in the events when the Fe/O ratio was decreasing. For the other three events which show more complex time structure the averaging time periods were selected differently. The averaging time for event v was chosen to include the period late in the event when the Fe/O ratio was roughly constant. The averaging time for event vi includes essentially

the whole event. For event vii, the averaging period was selected to avoid contamination by event vi.

The sensitivity of the abundance measurements to the choice of averaging time period was checked by comparing Fe/O measurements averaged over the selected time periods to the corresponding measurements averaged over entire flare events. For those four flare events with the largest Fe/O time variations, the results are listed in Table 4.1. In addition, the two averaging techniques "flux" and "PHA event" weighting (discussed in Section 3.7) are compared. For the Fe/O relative abundance measurement, the effects of averaging technique and time period selection are seen to be comparable in size to the statistical errors, but are small compared with the flare to flare differences.

4.4 Relative Abundances

Abundance results for each of the seven energetic particle events are presented in Tables 4.2 and 4.3. The main results are the relative abundances of the elements carbon through nickel which are based entirely on three detector PHA events (see Section 3.5 and Appendix B) and were obtained for a single common velocity interval corresponding to the interval 8.7–15.0 MeV/nucleon. The He/Si ratios are for the LET response interval 4.6–7.8 MeV/nucleon which is common to He and Si, and were obtained using three detector helium PHA events (see Section 3.6) and two detector silicon PHA events (see Section 3.4). All of the abundances are "PHA event" averaged (see Section 3.7.2) over time periods chosen as discussed above.

Table 4.1

Fe/O Abundance Ratio

(8.7-15 MeV/Nucleon)

	Solar Energetic Particle Event			
	1977 Sep. 19	1977 Sep. 24	1977 Nov. 22	1978 Feb. 13
Full Event				
Flux Weighted	0.28±0.05	0.78±0.06	0.31±0.04	0.12±0.01
PHA Event Weighted	0.33±0.04	0.78±0.05	0.35±0.04	0.13±0.01
Partial Event (onset excluded)				
Flux Weighted	0.24±0.04	0.67±0.07	0.26±0.05	0.10±0.01
PHA Event Weighted	0.29±0.04	0.67±0.06	0.30±0.05	0.11±0.01

TABLE 4.2

Numbers of Nuclei Detected and Abundances Relative to Silicon, 8.7-15 MeV/nucleon

Z	Element	1977 Sep. 20 0000 UT to Sep. 22 0000 UT	1977 Sep. 25 0000 UT to Sep. 27 1200 UT	1977 Nov. 23 0600 UT to Nov. 26 1200 UT	1978 Feb. 15 0000 UT to Feb. 18 0600 UT	1978 Apr. 24 1800 UT to Apr. 28 1200 UT	1978 Apr. 29 0600 UT to May 1 0000 UT	1978 May 2 0600 UT to May 6 0000 UT
6	C	151 3.02 ±0.49[+]	134 1.20 ±0.15	72 2.12 ±0.44	519 3.58 ±0.34	658 4.39 ±0.40	3727 1.96 ±0.06	1765 3.90 ±0.20
7	N	35 0.70 ±0.15	42 0.37 ±0.07	22 0.65 ±0.18	133 0.92 ±0.11	152 1.01 ±0.12	1230 0.65 ±0.02	482 1.06 ±0.07
8	O	285 5.70 ±0.87	347 3.10 ±0.34	179 5.26 ±0.98	1113 7.68 ±0.68	1252 8.35 ±0.72	10956 5.77 ±0.14	3797 8.38 ±0.42
9	F	0 <0.04	0 <0.02	0 <0.05	0 <0.013	0 <0.012	3 <0.003[§]	1 <0.007[§]
10	Ne	49 0.98 ±0.20	87 0.78 ±0.11	30 0.88 ±0.22	162 1.12 ±0.13	156 1.04 ±0.12	1153 0.61 ±0.02	413 0.91 ±0.06
11	Na	2 $0.040^{+0.053}_{-0.026}$	10 $0.09^{+0.04}_{-0.03}$	2 $0.06^{+0.08}_{-0.04}$	13 $0.090^{+0.032}_{-0.025}$	13 $0.087^{+0.031}_{-0.024}$	112 0.059±0.006	43 0.095±0.015
12	Mg	49 0.98 ±0.20	97 0.87 ±0.12	30 0.88 ±0.22	236 1.63 ±0.17	222 1.48 ±0.16	1956 1.03 ±0.03	709 1.57 ±0.09
13	Al	5 $0.10^{+0.07}_{-0.05}$	12 $0.11^{+0.04}_{-0.03}$	4 $0.12^{+0.09}_{-0.06}$	9 $0.06^{+0.03}_{-0.02}$	21 0.14 ±0.03	139 0.073±0.006	47 0.104±0.016
14	Si	50 ≡1.0	112 ≡1.0	34 ≡1.0	145 ≡1.0	150 ≡1.0	1898 ≡1.0	453 ≡1.0
15	P	0 <0.04	1 <0.03[§]	0 <0.05	1 <0.023[§]	1 <0.022[§]	7 <0.006[§]	0 <0.004
16	S	6 $0.12^{+0.07}_{-0.05}$	27 0.24 ±0.05	14 $0.41^{+0.14}_{-0.11}$	31 0.21 ±0.04	36 0.24 ±0.05	401 0.21 ±0.01	63 0.14 ±0.02
17	Cl	2 <0.09[§]	0 <0.02	0 <0.05	0 <0.013	2 <0.031[§]	6 <0.005[§]	0 <0.004
18	Ar	3 $0.06^{+0.06}_{-0.03}$	6 $0.054^{+0.032}_{-0.021}$	2 $0.06^{+0.08}_{-0.04}$	6 $0.041^{+0.025}_{-0.017}$	1 $0.007^{+0.015}_{-0.006}$	37 0.019±0.003	6 $0.013^{+0.008}_{-0.005}$
19	K	0 <0.04	1 <0.03[§]	0 <0.05	1 <0.023[§]	0 <0.012	10 <0.008[§]	1 <0.007[§]
20	Ca	7 $0.14^{+0.08}_{-0.05}$	25 0.22 ±0.05	4 $0.12^{+0.09}_{-0.06}$	13 $0.090^{+0.032}_{-0.025}$	10 $0.067^{+0.029}_{-0.021}$	106 0.056±0.006	16 $0.035^{+0.011}_{-0.009}$
21	Sc	0 <0.04	1 <0.03[§]	0 <0.05	0 <0.013	0 <0.012	2 <0.002[§]	0 <0.004
22	Ti	0 <0.04	0 <0.02	0 <0.05	0 <0.013	0 <0.012	4 <0.004[§]	0 <0.004
23	V	1 <0.07[§]	0 <0.02	0 <0.05	0 <0.013	0 <0.012	2 <0.002[§]	0 <0.004
24	Cr	0 0.04	2 $0.018^{+0.024}_{-0.012}$	1 $0.029^{+0.068}_{-0.025}$	4 $0.028^{+0.022}_{-0.013}$	3 $0.020^{+0.020}_{-0.011}$	21 0.011±0.002	7 $0.015^{+0.008}_{-0.006}$
26	Fe	82 1.64 ±0.29	233 2.08 ±0.24	53 1.56 ±0.34	121 0.83 ±0.10	90 0.60 ±0.08	1073 0.57 ±0.02	170 0.38 ±0.03
28	Ni	6 $0.12^{+0.07}_{-0.05}$	15 $0.13^{+0.04}_{-0.03}$	2 $0.06^{+0.08}_{-0.04}$	4 $0.028^{+0.022}_{-0.013}$	5 $0.033^{+0.023}_{-0.015}$	45 0.024±0.004	5 $0.011^{+0.008}_{-0.005}$

NOTES: (+) The ($\pm 1\sigma$) uncertainties include the effect of counting statistics only.
(§) 84% confidence upper limits only are quoted for these elements since possible background contributions have not been assessed.

TABLE 4.3

Abundance Results for He; Abundance Upper Limits for Li, Be, and B

	Solar Energetic Particle Event*						
	(i)	(ii)	(iii)	(iv)	(v)	(vi)	(vii)
4.6-7.8 MeV/nuc							
He/Si	468 ± 60†	433 ± 45	565 ± 49	384 ± 15	386 ± 19	97#	240 ± 6
5.9-9.3 MeV/nuc							
Li/O	<0.006§	<0.007	<0.003	<0.0011	<0.0008	<0.0050	<0.0016
Be/O	<0.0024	<0.005	<0.003	<0.0006	<0.0019	<0.0005	<0.0004
B/O	<0.0024	<0.003	<0.003	<0.0006	<0.0014	<0.0004	<0.0004

NOTES: (*) The events correspond to the time periods listed in Table 4.2.
(†) The (±1σ) uncertainties include the effect of counting statistics only.
(§) 84% confidence upper limits.
(#) The statistical error is much smaller than the possible error from other sources -- see Section 4.4.1.

For most elements the abundances are normalized to silicon to facilitate comparison to solar abundances measured by other means. However, the elements Li, Be, and B have very low abundances in the sun and their presence in our data would indicate spallation of energetic C, N and O nuclei. Thus, the Li, Be and B abundance upper limits are referenced to O and are based entirely on three parameter analysis in the LET response interval 5.4–9.3 MeV/nucleon which is common to the elements Li through O (see Section 3.5).

The listed ($\pm 1\sigma$) uncertainties include only the effect of counting statistics, which is generally large compared to the possible systematic errors (discussed below). Eighty–four percent confidence upper limits are quoted if no counts were obtained for an element or if the element showed no clear peak in the charge histogram, Figure 3.9.

4.4.1 Systematic Error

The main sources of systematic error in the relative abundance measurements of C through Ni (8.7–15.0 MeV/nucleon; Table 4.2) are:

(1) Energy threshold errors. The actual energy threshold may differ slightly from 8.7 MeV/nucleon, and more importantly, may vary with nuclear charge Z as a result of (a) possible systematic errors in the energy calibration of the LET detectors and/or (b) deviations of the thickness of the thin Al windows from the 3 μm value specified by the manufacturer. The variation of the threshold with Z would arise since, near the 8.7 MeV/nucleon threshold, nuclei with different Z

deposit their energy in different proportions among the Al entrance window and the detectors L1, L2 and L3.

The size of the possible systematic error in the energy calibration of the LET detectors was checked in two different ways during the data analysis and was found to be about 2 percent for the L1 and L2 detectors (see Section 3.6) and about 3 percent for the L3 detectors (see Sections 3.3 and 3.6). As a result of the manner in which energy is distributed among the detectors by incident nuclei near the 8.7 MeV/nucleon threshold, a possible variation of the threshold with Z is most sensitive to a relative calibration error between the L3 energy and the average of L1 and L2 energies. This relative error was conservatively taken to be 5 percent, and the resulting Z-dependent shift of the 8.7 MeV/nucleon energy threshold was calculated for each element, carbon through nickel. Assuming typical energy spectra, $dJ/dE \propto E^{-3}$ (see Section 4.5), the energy threshold shifts yield an error of about $0.5 \cdot |Z1-Z2|$ percent in the relative abundance of elements with nuclear charge Z1 and Z2. For adjacent elements this error is very small, and is only about 10 percent for the most widely separated elements carbon and nickel. Such possible errors are much smaller than the observed flare-to-flare variation (e.g. the Ni/C ratio measurements range over a factor of ten; see Table 4.2) and are usually smaller than the statistical error.

The effect of possible Al window thickness errors is also small. For example, in order to induce a Z-dependence in the relative abundance measurements of about $0.5 \cdot |Z1-Z2|$ (again, for energy spectra $dJ/dE \propto E^{-3}$) a window would have to be twice as thick as the

specified 3 μm.

(2) Charge assignment error and the "iron" problem for Cr and Ni. For the elements with clear charge peaks in the charge histogram, Figure 3.9, the biases introduced by the data selection and charge assignment techniques are negligible (see Section 3.5), with the possible exception of the iron group nuclei. The background effect discussed in Appendix B necessitated corrections of about 20 percent to the iron abundances. The same background effect probably also occurs for Cr and Ni nuclei, however corrections were not applied for these elements. The error thus induced (about 20 percent) is probably comparable in size, but opposite in sign, to that produced by spillover of Fe nuclei into the Cr and Ni peaks. Therefore a rough estimate of the systematic uncertainty in the the abundances of Cr and Ni relative to Fe is ± 20 percent.

The main systematic error in the He/Si ratios (4.6–7.8 MeV/nucleon; Table 4.3) results from the possible energy threshold errors discussed above. A 5 percent relative error in energy calibration between detectors L3 and L1+L2, together with E^{-3} energy spectra, gives an error of 11 percent in the He/Si ratio. The He/Si measurement in event vi may have an additional systematic error (on the order of 20 percent) due to the high count rate degradation of He mass resolution mentioned in Section 3.6. Note that this possible additional error is still small compared to the factor of three dip in the He/Si ratio during event vi (see Figure 4.6). Since both the possible systematic error and the time variation of the He/Si ratio in event vi are much larger than the statistical error, the statistical error is not

quoted in Table 4.3 and the reader is referred to this discussion.

4.4.2 Comparison to Other Reported Observations

The abundance results of Tables 4.2 and 4.3 have been compared to other reported observations -- McGuire, von Rosenvinge and McDonald (1979) for flare events i, ii, iii, and iv, and Dietrich and Simpson (1978) for event ii. For most of the elements (namely He, C, N, O, Ne, Na, Mg, Al, Si, S, Ar, Ca, and Fe) the various measurements generally agree within statistical errors. The largest non-statistical difference occurs for the Fe/O ratio in event ii -- we obtained $Fe/O = 0.70 \pm 0.06$, while McGuire, von Rosenvinge and McDonald (1979) found $(Fe+Ni)/O = 1.17 \pm 0.11$. This difference may be due to McGuire et. al. including the event onset period in their averaging time.

However, our results do not support the high abundances of the rare elements B, F and Cr reported by Dietrich and Simpson (1978) for event ii. Their finite results are significantly higher than our upper limits for B and F and our finite value for Cr (as reported earlier in Cook et. al. 1979). The discrepancies may result from the fact that Dietrich and Simpson's results were obtained at energies above 25 MeV/nucleon, while our data are for the lower energy interval 8.7-15 MeV/nucleon. However, the B, F and Cr results of Dietrich and Simpson (1978) are based on only a few PHA events, so there is concern about contamination from the more abundant elements C, O, Ne and Fe.

Dietrich and Simpson (1978) compared their SEP abundances to "solar system" abundances which were a mixture of results from different sources and concluded that (a) the enhancement of even-Z nuclei increased monotonically with Z and that (b) the rare nuclei (B, F, Na, Al and Cr) were additionally enhanced due to fragmentation of heavier nuclei in traversing ≈ 0.6 g/cm^2 of solar atmospheric material (see Figure 1.3). We disagree with both conclusions. The over-enhancement of Na and Al, as well as the monotonicity of the enhancement of even-Z nuclei disappears if the SEP abundances are compared to a consistent set of abundances based only on solar spectroscopy (see Cook et. al. 1979, McGuire, von Rosenvinge and McDonald 1979, and Chapter 5 of this thesis). For event ii, our abundances for Na, Al and Cr and upper limits for B and F are consistent with negligible matter traversal and with the upper limit of 0.06 gm/cm^2 reported by McGuire, von Rosenvinge and McDonald (1979).

4.5 Fluence Measurements and Energy Spectra

Fluence measurements of He, C, O, Ne, Mg, Si and Fe nuclei for several energy/nucleon bins are presented in Tables 4.4 through 4.10; one table for each energetic particle event. The fluence measurements were integrated (as described in Section 3.7) over time periods chosen to include entire energetic particle events, and are averaged over Voyagers 1 and 2. Table 4.11 lists the fluences measured for the entire time period from September 1977 to May 1978.

TABLE 4.4

Fluence Measurements for the Flare Period: 1977 September 19 1200 UT to 1977 September 22 1500 UT

HE	ENERGY	3.0-3.3	3.3-3.6	3.6-4.0	4.0-5.0	5.0-6.1	6.1-7.8	(MeV/Nucleon)			
	COUNTS*	49	26	39	60	47	31				
	FLUENCE†	1.24E 05	4.50E 04	8.24E 04	1.15E 05	1.02E 05	6.08E 04	$(cm^2 \cdot sr)^{-1}$			
	+-	2.59E 04	1.41E 04	1.89E 04	2.19E 04	2.35E 04	1.87E 04				
C	ENERGY	4.0-4.5	4.5-5.0	5.0-5.5	5.5-6.1	6.1-7.1	7.1-7.8	7.8-8.7	8.7-10.6	10.6-12.7	12.7-15.0
	COUNTS	290	279	153	114	158	80	69	106	45	31
	FLUENCE	6.54E 02	7.00E 02	3.90E 02	2.71E 02	3.88E 02	1.77E 02	1.89E 02	2.39E 02	1.02E 02	5.25E 01
	+-	5.00E 01	5.36E 01	4.13E 01	3.24E 01	4.02E 01	2.43E 01	2.92E 01	3.10E 01	2.25E 01	1.19E 01
O	ENERGY	4.0-4.5	4.5-5.0	5.0-5.5	5.5-6.1	6.1-7.1	7.1-7.8	7.8-8.7	8.7-10.6	10.6-12.7	12.7-15.0
	COUNTS	638	495	390	323	367	182	154	165	99	63
	FLUENCE	1.56E 03	1.18E 03	9.46E 02	7.93E 02	8.81E 02	4.26E 02	3.39E 02	3.80E 02	2.03E 02	1.35E 02
	+-	7.83E 01	6.87E 01	6.28E 01	5.76E 01	6.38E 01	4.23E 01	3.61E 01	4.06E 01	2.76E 01	2.51E 01
NE	ENERGY	4.5-5.0	5.0-5.5	5.5-6.1	6.1-7.1	7.1-7.8	7.8-8.7	8.7-10.6	10.6-12.7	12.7-15.0	15.0-18.7
	COUNTS	59	64	58	61	19	24	34	19	10	4
	FLUENCE	1.35E 02	1.47E 02	1.54E 02	1.61E 02	3.81E 01	4.72E 01	7.77E 01	3.36E 01	1.00E 01	1.88E 01
	+-	2.36E 01	2.35E 01	2.81E 01	2.60E 01	1.09E 01	1.20E 01	1.91E 01	1.12E 01	3.31E 00	1.31E 01
MG	ENERGY	4.5-5.0	5.0-5.5	5.5-6.1	6.1-7.1	7.1-7.8	7.8-8.7	8.7-10.6	10.6-12.7	12.7-15.0	15.0-20.0
	COUNTS	74	68	61	84	33	21	37	13	16	12
	FLUENCE	1.84E 02	1.69E 02	1.65E 02	2.31E 02	7.55E 01	4.65E 01	7.15E 01	2.22E 01	3.51E 01	2.03E 01
	+-	2.71E 01	2.61E 01	2.78E 01	3.35E 01	1.65E 01	1.39E 01	1.72E 01	9.35E 00	1.41E 01	7.91E 00
SI	ENERGY	4.6-5.0	5.0-5.5	5.5-6.1	6.1-7.1	7.1-7.8	7.8-8.7	8.7-10.6	10.6-12.7	12.7-15.0	15.0-20.0
	COUNTS	51	48	43	71	29	26	31	21	7	11
	FLUENCE	1.13E 02	1.15E 02	9.50E 01	1.34E 02	6.63E 01	6.26E 01	7.50E 01	4.53E 01	1.48E 01	1.56E 01
	+-	2.20E 01	2.24E 01	1.93E 01	2.08E 01	1.56E 01	1.63E 01	1.78E 01	1.46E 01	6.90E 00	6.60E 00
FE§	ENERGY	5.0-5.5	5.5-6.1	6.1-7.1	7.1-7.8	7.8-8.7	8.7-10.6	10.6-12.7	12.7-15.0	15.0-20.0	20.0-29.0
	COUNTS	60	47	72	28	34	51	37	28	37	33
	FLUENCE	1.35E 02	9.46E 01	1.55E 02	6.46E 01	1.02E 02	9.44E 01	6.53E 01	6.30E 01	5.02E 01	3.64E 01
	+-	2.52E 01	1.70E 01	2.46E 01	1.61E 01	2.35E 01	1.89E 01	1.54E 01	1.70E 01	1.32E 01	7.74E 00

NOTES: (*) Counts are summed over Voyagers 1 and 2.
(†) Fluences are averaged over Voyagers 1 and 2. The fluence missing due to data gaps is estimated to be about 35 percent of the quoted fluence.
(§) Includes nickel.

TABLE 4.5

Fluence Measurements for the Flare Period: 1977 September 24 0600 UT to 1977 September 27 1500 UT

HE	ENERGY	3.0-3.3	3.3-3.6	3.6-4.0	4.0-5.0	5.0-6.1	6.1-7.8	(MeV/Nucleon)			
	COUNTS*	64	62	67	124	90	96				
	FLUENCE†	3.59E 04	3.59E 04	5.04E 04	7.60E 04	5.71E 04	7.14E 04	$(cm^2 \cdot sr)^{-1}$			
	+-	6.72E 03	6.95E 03	9.62E 03	9.49E 03	8.74E 03	1.03E 04				
C	ENERGY	4.0-4.5	4.5-5.0	5.0-5.5	5.5-6.1	6.1-7.1	7.1-7.8	7.8-8.7	8.7-10.6	10.6-12.7	12.7-15.0
	COUNTS	200	183	118	126	138	56	61	75	70	43
	FLUENCE	2.41E 02	2.20E 02	1.50E 02	1.57E 02	1.88E 02	6.41E 01	7.63E 01	1.07E 02	1.09E 02	6.46E 01
	+-	2.10E 01	2.09E 01	1.81E 01	1.71E 01	1.99E 01	9.75E 00	1.17E 01	1.62E 01	1.66E 01	1.28E 01
O	ENERGY	4.0-4.5	4.5-5.0	5.0-5.5	5.5-6.1	6.1-7.1	7.1-7.8	7.8-8.7	8.7-10.6	10.6-12.7	12.7-15.0
	COUNTS	468	341	266	322	346	192	166	241	165	112
	FLUENCE	5.64E 02	4.47E 02	3.16E 02	3.88E 02	4.57E 02	2.76E 02	2.12E 02	3.26E 02	2.68E 02	2.00E 02
	+-	3.27E 01	3.13E 01	2.44E 01	2.65E 01	3.04E 01	2.47E 01	1.99E 01	2.58E 01	2.62E 01	2.33E 01
NE	ENERGY	4.5-5.0	5.0-5.5	5.5-6.1	6.1-7.1	7.1-7.8	7.8-8.7	8.7-10.6	10.6-12.7	12.7-15.0	15.0-18.7
	COUNTS	67	44	53	72	35	32	49	51	24	24
	FLUENCE	8.49E 01	5.57E 01	6.09E 01	9.12E 01	5.20E 01	4.68E 01	6.37E 01	7.67E 01	3.03E 01	5.14E 01
	+-	1.36E 01	1.06E 01	1.05E 01	1.22E 01	1.22E 01	9.94E 00	1.12E 01	1.40E 01	7.86E 00	1.34E 01
MG	ENERGY	4.5-5.0	5.0-5.5	5.5-6.1	6.1-7.1	7.1-7.8	7.8-8.7	8.7-10.6	10.6-12.7	12.7-15.0	15.0-20.0
	COUNTS	85	64	64	109	58	56	72	46	37	53
	FLUENCE	1.05E 02	9.14E 01	7.80E 01	1.74E 02	8.25E 01	7.96E 01	1.10E 02	6.65E 01	5.26E 01	6.69E 01
	+-	1.39E 01	1.42E 01	1.17E 01	2.10E 01	1.35E 01	1.31E 01	1.61E 01	1.17E 01	9.83E 00	1.10E 01
SI	ENERGY	4.6-5.0	5.0-5.5	5.5-6.1	6.1-7.1	7.1-7.8	7.8-8.7	8.7-10.6	10.6-12.7	12.7-15.0	15.0-20.0
	COUNTS	49	58	63	83	39	55	72	54	43	57
	FLUENCE	7.14E 01	7.66E 01	8.46E 01	1.08E 02	5.65E 01	7.95E 01	1.24E 02	1.03E 02	6.33E 01	9.36E 01
	+-	1.34E 01	1.43E 01	1.39E 01	1.46E 01	1.18E 01	1.36E 01	1.85E 01	1.85E 01	1.28E 01	1.48E 01
FE§	ENERGY	5.0-5.5	5.5-6.1	6.1-7.1	7.1-7.8	7.8-8.7	8.7-10.6	10.6-12.7	12.7-15.0	15.0-20.0	20.0-29.0
	COUNTS	154	160	225	104	130	198	140	107	161	135
	FLUENCE	2.55E 02	2.39E 02	3.34E 02	1.59E 02	2.16E 02	3.01E 02	2.12E 02	1.76E 02	2.59E 02	1.99E 02
	+-	2.57E 01	2.36E 01	2.75E 01	1.98E 01	2.38E 01	2.62E 01	2.19E 01	2.07E 01	2.54E 01	2.06E 01

NOTES: (*) Counts are summed over Voyagers 1 and 2.
(+) Fluences are averaged over Voyagers 1 and 2. The fluence missing due to data gaps is estimated to be about 34 percent of the quoted fluence.
(§) Includes nickel.

TABLE 4.6

Fluence Measurements for the Flare Period: 1977 November 22 1200 UT to 1977 November 27 0300 UT

HE	ENERGY	3.0-3.3	3.3-3.6	3.6-4.0	4.0-5.0	5.0-6.1	6.1-7.8	(MeV/Nucleon)			
	COUNTS*	1336	979	864	1272	524	354				
	FLUENCE†	5.48E 04	4.59E 04	3.75E 04	5.87E 04	2.43E 04	1.56E 04	$(cm^2 \cdot sr)^{-1}$			
	+-	2.08E 03	1.95E 03	1.68E 03	2.22E 03	1.46E 03	1.19E 03				
C	ENERGY	4.0-4.5	4.5-5.0	5.0-5.5	5.5-6.1	6.1-7.1	7.1-7.8	7.8-8.7	8.7-10.6	10.6-12.7	12.7-15.0
	COUNTS	587	404	264	161	174	83	49	51	30	20
	FLUENCE	3.04E 02	2.19E 02	1.31E 02	8.14E 01	9.25E 01	4.19E 01	2.50E 01	2.92E 01	1.94E 01	1.02E 01
	+-	1.41E 01	1.58E 01	8.32E 00	6.60E 00	8.06E 00	4.71E 00	3.67E 00	5.41E 00	4.95E 00	2.32E 00
O	ENERGY	4.0-4.5	4.5-5.0	5.0-5.5	5.5-6.1	6.1-7.1	7.1-7.8	7.8-8.7	8.7-10.6	10.6-12.7	12.7-15.0
	COUNTS	1100	677	465	345	344	134	126	134	71	46
	FLUENCE	5.66E 02	3.50E 02	2.41E 02	1.72E 02	1.80E 02	7.08E 01	6.85E 01	8.08E 01	3.43E 01	2.39E 01
	+-	1.89E 01	1.51E 01	1.28E 01	9.94E 00	1.03E 01	6.77E 00	7.18E 00	9.41E 00	4.17E 00	3.69E 00
NE	ENERGY	4.5-5.0	5.0-5.5	5.5-6.1	6.1-7.1	7.1-7.8	7.8-8.7	8.7-10.6	10.6-12.7	12.7-15.0	15.0-18.7
	COUNTS	119	66	59	63	18	15	20	15	11	7
	FLUENCE	6.36E 01	3.43E 01	3.06E 01	3.23E 01	7.86E 00	6.51E 00	9.24E 00	7.12E 00	5.92E 00	3.63E 00
	+-	6.90E 00	4.40E 00	4.78E 00	4.17E 00	1.92E 00	1.73E 00	2.13E 00	1.91E 00	1.81E 00	1.42E 00
MG	ENERGY	4.5-5.0	5.0-5.5	5.5-6.1	6.1-7.1	7.1-7.8	7.8-8.7	8.7-10.6	10.6-12.7	12.7-15.0	15.0-20.0
	COUNTS	100	51	57	56	37	13	21	13	8	9
	FLUENCE	5.28E 01	2.98E 01	2.75E 01	2.75E 01	2.88E 01	6.66E 00	1.02E 01	7.14E 00	4.37E 00	4.69E 00
	+-	6.42E 00	6.04E 00	3.71E 00	3.75E 00	1.16E 01	1.88E 00	2.28E 00	2.06E 00	1.56E 00	1.60E 00
SI	ENERGY	4.6-5.0	5.0-5.5	5.5-6.1	6.1-7.1	7.1-7.8	7.8-8.7	8.7-10.6	10.6-12.7	12.7-15.0	15.0-20.0
	COUNTS	48	39	38	46	24	18	31	11	6	7
	FLUENCE	3.12E 01	1.91E 01	2.24E 01	2.67E 01	1.27E 01	8.55E 00	1.91E 01	5.33E 00	2.51E 00	3.52E 00
	+-	6.94E 00	3.12E 00	4.99E 00	5.88E 00	2.72E 00	2.06E 00	4.90E 00	1.62E 00	1.05E 00	1.36E 00
FE§	ENERGY	5.0-5.5	5.5-6.1	6.1-7.1	7.1-7.8	7.8-8.7	8.7-10.6	10.6-12.7	12.7-15.0	15.0-20.0	20.0-29.0
	COUNTS	33	45	40	25	23	42	31	21	21	22
	FLUENCE	2.37E 01	2.32E 01	1.98E 01	1.31E 01	1.13E 01	2.09E 01	1.48E 01	1.08E 01	9.90E 00	1.14E 01
	+-	6.66E 00	3.53E 00	3.17E 00	2.69E 00	2.42E 00	3.30E 00	2.75E 00	2.41E 00	2.20E 00	2.47E 00

NOTES: (*) Counts are summed over Voyagers 1 and 2.

(†) Fluences are averaged over Voyagers 1 and 2. The fluence missing due to data gaps is estimated to be about 5 percent of the quoted fluence.

(§) Includes nickel.

TABLE 4.7

Fluence Measurements for the Flare Period: 1978 February 13 2100 UT to 1978 February 21 0900 UT

HE	ENERGY	3.0-3.3	3.3-3.6	3.6-4.0	4.0-5.0	5.0-6.1	6.1-7.8	(MeV/Nucleon)			
	COUNTS*	2204	1887	2120	4052	3159	3470				
	FLUENCE†	1.27E 05	1.20E 05	1.28E 05	1.96E 05	1.32E 05	1.04E 05	$(cm^2 \cdot sr)^{-1}$			
	+-	5.72E 03	7.78E 03	9.36E 03	6.55E 03	6.01E 03	3.71E 03				
C	ENERGY	4.0-4.5	4.5-5.0	5.0-5.5	5.5-6.1	6.1-7.1	7.1-7.8	7.8-8.7	8.7-10.6	10.6-12.7	12.7-15.0
	COUNTS	1271	1008	748	664	764	333	355	409	245	135
	FLUENCE	9.39E 02	7.02E 02	5.09E 02	4.63E 02	5.14E 02	2.19E 02	2.81E 02	2.64E 02	1.59E 02	7.63E 01
	+-	4.75E 01	3.26E 01	2.37E 01	2.21E 01	2.35E 01	1.55E 01	3.57E 01	1.52E 01	1.15E 01	7.08E 00
O	ENERGY	4.0-4.5	4.5-5.0	5.0-5.5	5.5-6.1	6.1-7.1	7.1-7.8	7.8-8.7	8.7-10.6	10.6-12.7	12.7-15.0
	COUNTS	2929	2154	1729	1649	1708	817	744	910	527	301
	FLUENCE	2.07E 03	1.51E 03	1.25E 03	1.15E 03	1.23E 03	6.48E 02	5.09E 02	5.90E 02	4.08E 02	1.83E 02
	+-	5.17E 01	4.94E 01	5.56E 01	3.61E 01	4.97E 01	4.62E 01	2.62E 01	2.42E 01	4.08E 01	1.18E 01
NE	ENERGY	4.5-5.0	5.0-5.5	5.5-6.1	6.1-7.1	7.1-7.8	7.8-8.7	8.7-10.6	10.6-12.7	12.7-15.0	15.0-18.7
	COUNTS	300	246	249	263	156	102	130	78	45	46
	FLUENCE	2.18E 02	1.84E 02	1.62E 02	1.68E 02	1.09E 02	6.98E 01	8.37E 01	5.57E 01	3.18E 01	2.71E 01
	+-	1.90E 01	1.58E 01	1.11E 01	1.15E 01	1.02E 01	7.82E 00	8.22E 00	7.62E 00	5.66E 00	4.78E 00
MG	ENERGY	4.5-5.0	5.0-5.5	5.5-6.1	6.1-7.1	7.1-7.8	7.8-8.7	8.7-10.6	10.6-12.7	12.7-15.0	15.0-20.0
	COUNTS	475	319	311	360	181	142	207	102	59	63
	FLUENCE	3.19E 02	2.22E 02	2.12E 02	2.60E 02	1.19E 02	9.81E 01	1.57E 02	6.45E 01	4.03E 01	3.96E 01
	+-	1.59E 01	1.64E 01	1.51E 01	1.73E 01	1.01E 01	9.44E 00	1.74E 01	7.21E 00	6.09E 00	6.06E 00
SI	ENERGY	4.6-5.0	5.0-5.5	5.5-6.1	6.1-7.1	7.1-7.8	7.8-8.7	8.7-10.6	10.6-12.7	12.7-15.0	15.0-20.0
	COUNTS	267	219	234	266	110	89	126	81	41	38
	FLUENCE	1.85E 02	1.42E 02	1.66E 02	2.08E 02	7.14E 01	5.94E 01	1.31E 02	4.91E 01	2.07E 01	2.54E 01
	+-	1.29E 01	1.02E 01	1.47E 01	2.87E 01	7.42E 00	6.76E 00	3.34E 01	6.37E 00	3.44E 00	5.26E 00
FE§	ENERGY	5.0-5.5	5.5-6.1	6.1-7.1	7.1-7.8	7.8-8.7	8.7-10.6	10.6-12.7	12.7-15.0	15.0-20.0	20.0-29.0
	COUNTS	223	184	242	99	99	143	70	51	41	26
	FLUENCE	1.49E 02	1.23E 02	1.58E 02	6.30E 01	6.19E 01	1.20E 02	3.71E 01	2.71E 01	2.27E 01	1.39E 01
	+-	1.12E 01	1.30E 01	1.15E 01	6.79E 00	6.77E 00	3.08E 01	4.73E 00	4.29E 00	4.03E 00	3.13E 00

NOTES: (*) Counts are summed over Voyagers 1 and 2.
(†) Fluences are averaged over Voyagers 1 and 2. The fluence missing due to data gaps is estimated to be about 11 percent of the quoted fluence.
(§) Includes nickel.

TABLE 4.8

Fluence Measurements for the Flare Period: 1978 April 24 0000 UT to 1978 April 29 0300 UT

HE	ENERGY	3.0-3.3	3.3-3.6	3.6-4.0	4.0-5.0	5.0-6.1	6.1-7.8	(MeV/Nucleon)			
	COUNTS*	1337	1111	1219	2121	1412	1186				
	FLUENCE†	7.50E 04	6.54E 04	6.83E 04	1.22E 05	8.15E 04	6.27E 04	$(cm^2 \cdot sr)^{-1}$			
	+-	3.56E 03	3.01E 03	3.21E 03	4.59E 03	3.64E 03	2.73E 03				
C	ENERGY	4.0-4.5	4.5-5.0	5.0-5.5	5.5-6.1	6.1-7.1	7.1-7.8	7.8-8.7	8.7-10.6	10.6-12.7	12.7-15.0
	COUNTS	876	755	550	501	593	301	288	445	246	164
	FLUENCE	6.85E 02	5.60E 02	4.11E 02	3.96E 02	4.35E 02	2.28E 02	2.12E 02	3.13E 02	1.66E 02	1.09E 02
	+-	3.16E 01	2.60E 01	2.28E 01	2.58E 01	2.32E 01	1.68E 01	1.45E 01	1.68E 01	1.17E 01	9.48E 00
O	ENERGY	4.0-4.5	4.5-5.0	5.0-5.5	5.5-6.1	6.1-7.1	7.1-7.8	7.8-8.7	8.7-10.6	10.6-12.7	12.7-15.0
	COUNTS	1847	1427	1098	1096	1237	635	581	799	499	357
	FLUENCE	1.39E 03	1.06E 03	8.10E 02	8.46E 02	8.80E 02	4.67E 02	4.35E 02	5.84E 02	3.54E 02	2.64E 02
	+-	4.17E 01	3.59E 01	3.07E 01	3.42E 01	2.93E 01	2.23E 01	2.47E 01	2.75E 01	1.80E 01	1.86E 01
NE	ENERGY	4.5-5.0	5.0-5.5	5.5-6.1	6.1-7.1	7.1-7.8	7.8-8.7	8.7-10.6	10.6-12.7	12.7-15.0	15.0-18.7
	COUNTS	176	139	136	164	80	78	96	57	58	47
	FLUENCE	1.24E 02	9.52E 01	9.90E 01	1.18E 02	6.54E 01	5.90E 01	7.04E 01	4.89E 01	5.16E 01	4.02E 01
	+-	1.04E 01	8.55E 00	9.73E 00	1.21E 01	1.12E 01	8.14E 00	1.04E 01	1.03E 01	1.00E 01	1.02E 01
MG	ENERGY	4.5-5.0	5.0-5.5	5.5-6.1	6.1-7.1	7.1-7.8	7.8-8.7	8.7-10.6	10.6-12.7	12.7-15.0	15.0-20.0
	COUNTS	257	197	155	215	117	107	146	79	58	60
	FLUENCE	1.98E 02	1.36E 02	1.20E 02	1.49E 02	1.01E 02	8.32E 01	1.07E 02	5.42E 01	4.83E 01	3.81E 01
	+-	1.56E 01	1.05E 01	1.10E 01	1.11E 01	1.40E 01	9.64E 00	9.96E 00	6.61E 00	1.05E 01	5.21E 00
SI	ENERGY	4.6-5.0	5.0-5.5	5.5-6.1	6.1-7.1	7.1-7.8	7.8-8.7	8.7-10.6	10.6-12.7	12.7-15.0	15.0-20.0
	COUNTS	150	171	112	164	84	76	106	60	33	53
	FLUENCE	1.22E 02	1.25E 02	8.32E 01	1.16E 02	6.01E 01	5.40E 01	6.91E 01	4.05E 01	2.24E 01	3.65E 01
	+-	1.21E 01	1.07E 01	9.70E 00	1.01E 01	7.27E 00	6.63E 00	7.38E 00	5.82E 00	4.19E 00	5.42E 00
FE§	ENERGY	5.0-5.5	5.5-6.1	6.1-7.1	7.1-7.8	7.8-8.7	8.7-10.6	10.6-12.7	12.7-15.0	15.0-20.0	20.0-29.0
	COUNTS	102	72	87	48	50	76	47	29	26	9
	FLUENCE	7.19E 01	5.36E 01	6.10E 01	3.73E 01	3.40E 01	5.39E 01	3.61E 01	1.92E 01	1.52E 01	7.72E 00
	+-	9.02E 00	6.82E 00	7.22E 00	5.89E 00	5.22E 00	7.11E 00	6.85E 00	3.89E 00	3.05E 00	2.89E 00

NOTES: (*) Counts are summed over Voyagers 1 and 2.
(†) Fluences are averaged over Voyagers 1 and 2. The fluence missing due to data gaps is estimated to be about 14 percent of the quoted fluence.
(§) Includes nickel.

TABLE 4.9

Fluence Measurements for the Flare Period: 1978 April 29 0600 UT to 1978 May 1 0000 UT

HE	ENERGY	3.0-3.3	3.3-3.6	3.6-4.0	4.0-5.0	5.0-6.1	6.1-7.8	(MeV/Nucleon)			
	COUNTS*	353	315	392	933	853	1064				
	FLUENCE†	8.69E 04	8.00E 04	1.07E 05	2.32E 05	2.10E 05	2.52E 05	$(cm^2 \cdot sr)^{-1}$			
	+-	6.30E 03	5.90E 03	7.38E 03	1.03E 04	9.39E 03	1.02E 04				
C	ENERGY	4.0-4.5	4.5-5.0	5.0-5.5	5.5-6.1	6.1-7.1	7.1-7.8	7.8-8.7	8.7-10.6	10.6-12.7	12.7-15.0
	COUNTS	776	853	686	807	1274	831	965	1597	1453	996
	FLUENCE	1.63E 03	1.81E 03	1.45E 03	1.76E 03	2.87E 03	1.86E 03	2.17E 03	3.45E 03	3.11E 03	2.24E 03
	+-	6.83E 01	7.24E 01	6.55E 01	7.20E 01	9.60E 01	7.84E 01	8.49E 01	1.04E 02	9.91E 01	8.58E 01
O	ENERGY	4.0-4.5	4.5-5.0	5.0-5.5	5.5-6.1	6.1-7.1	7.1-7.8	7.8-8.7	8.7-10.6	10.6-12.7	12.7-15.0
	COUNTS	2380	2311	2229	2696	3969	2469	2759	4820	3992	2813
	FLUENCE	5.30E 03	5.10E 03	4.87E 03	6.00E 03	8.73E 03	5.46E 03	6.36E 03	1.08E 04	8.85E 03	6.41E 03
	+-	1.32E 02	1.27E 02	1.23E 02	1.37E 02	1.64E 02	1.30E 02	1.46E 02	1.88E 02	1.70E 02	1.46E 02
NE	ENERGY	4.5-5.0	5.0-5.5	5.5-6.1	6.1-7.1	7.1-7.8	7.8-8.7	8.7-10.6	10.6-12.7	12.7-15.0	15.0-18.7
	COUNTS	229	242	303	421	247	328	504	432	304	264
	FLUENCE	5.06E 02	5.45E 02	6.44E 02	9.56E 02	5.83E 02	7.80E 02	1.18E 03	9.80E 02	6.80E 02	5.58E 02
	+-	4.04E 01	4.36E 01	4.30E 01	5.67E 01	4.65E 01	5.30E 01	6.48E 01	5.66E 01	4.81E 01	4.12E 01
MG	ENERGY	4.5-5.0	5.0-5.5	5.5-6.1	6.1-7.1	7.1-7.8	7.8-8.7	8.7-10.6	10.6-12.7	12.7-15.0	15.0-20.0
	COUNTS	450	409	452	759	428	542	896	695	532	644
	FLUENCE	9.60E 02	8.99E 02	9.96E 02	1.69E 03	9.71E 02	1.21E 03	2.06E 03	1.59E 03	1.17E 03	1.49E 03
	+-	5.25E 01	5.37E 01	5.77E 01	7.27E 01	5.66E 01	6.17E 01	8.43E 01	7.45E 01	5.94E 01	7.14E 01
SI	ENERGY	4.6-5.0	5.0-5.5	5.5-6.1	6.1-7.1	7.1-7.8	7.8-8.7	8.7-10.6	10.6-12.7	12.7-15.0	15.0-20.0
	COUNTS	466	522	598	912	591	604	925	644	440	443
	FLUENCE	1.06E 03	1.15E 03	1.35E 03	2.10E 03	1.37E 03	1.36E 03	2.13E 03	1.48E 03	9.69E 02	9.72E 02
	+-	5.89E 01	5.91E 01	6.68E 01	8.28E 01	6.73E 01	6.67E 01	8.43E 01	6.92E 01	5.47E 01	5.82E 01
FE§	ENERGY	5.0-5.5	5.5-6.1	6.1-7.1	7.1-7.8	7.8-8.7	8.7-10.6	10.6-12.7	12.7-15.0	15.0-20.0	20.0-29.0
	COUNTS	917	880	1081	579	523	721	360	154	124	42
	FLUENCE	2.17E 03	1.98E 03	2.54E 03	1.39E 03	1.17E 03	1.58E 03	8.28E 02	3.63E 02	2.11E 02	8.13E 01
	+-	8.60E 01	7.99E 01	9.24E 01	6.98E 01	6.18E 01	7.14E 01	5.46E 01	3.83E 01	2.16E 01	1.45E 01

NOTES: (*) Counts are summed over Voyagers 1 and 2.
(†) Fluences are averaged over Voyagers 1 and 2. The fluence missing due to data gaps is estimated to be about 0.5 percent of the quoted fluence.
(§) Includes nickel.

TABLE 4.10

Fluence Measurements for the Flare Period: 1978 May 2 0600 UT to 1978 May 7 1800 UT

HE	ENERGY	3.0-3.3	3.3-3.6	3.6-4.0	4.0-5.0	5.0-6.1	6.1-7.8	(MeV/Nucleon)			
	COUNTS*	2358	1932	2143	3900	2717	2431				
	FLUENCE†	1.41E 05	1.24E 05	1.39E 05	2.59E 05	1.86E 05	1.76E 05	$(cm^2 \cdot sr)^{-1}$			
	+-	4.64E 03	4.38E 03	4.88E 03	6.38E 03	5.61E 03	5.48E 03				
C	ENERGY	4.0-4.5	4.5-5.0	5.0-5.5	5.5-6.1	6.1-7.1	7.1-7.8	7.8-8.7	8.7-10.6	10.6-12.7	12.7-15.0
	COUNTS	2126	1980	1424	1390	1742	883	805	1069	594	298
	FLUENCE	1.66E 03	1.58E 03	1.09E 03	1.08E 03	1.38E 03	6.98E 02	6.38E 02	8.47E 02	4.83E 02	2.38E 02
	+-	3.99E 01	3.93E 01	3.18E 01	3.19E 01	3.65E 01	2.60E 01	2.45E 01	2.85E 01	2.18E 01	1.52E 01
O	ENERGY	4.0-4.5	4.5-5.0	5.0-5.5	5.5-6.1	6.1-7.1	7.1-7.8	7.8-8.7	8.7-10.6	10.6-12.7	12.7-15.0
	COUNTS	5341	4212	3474	3531	3977	1889	1851	2307	1189	630
	FLUENCE	4.11E 03	3.33E 03	2.75E 03	2.78E 03	3.16E 03	1.50E 03	1.45E 03	1.82E 03	9.37E 02	4.96E 02
	+-	6.18E 01	5.69E 01	5.15E 01	5.15E 01	5.52E 01	3.79E 01	3.74E 01	4.14E 01	2.97E 01	2.14E 01
NE	ENERGY	4.5-5.0	5.0-5.5	5.5-6.1	6.1-7.1	7.1-7.8	7.8-8.7	8.7-10.6	10.6-12.7	12.7-15.0	15.0-18.7
	COUNTS	481	352	388	459	232	195	249	143	62	50
	FLUENCE	3.69E 02	2.65E 02	3.05E 02	3.68E 02	1.86E 02	1.53E 02	1.89E 02	1.15E 02	4.80E 01	4.08E 01
	+-	1.85E 01	1.55E 01	1.69E 01	1.87E 01	1.36E 01	1.23E 01	1.28E 01	1.05E 01	6.61E 00	6.41E 00
MG	ENERGY	4.5-5.0	5.0-5.5	5.5-6.1	6.1-7.1	7.1-7.8	7.8-8.7	8.7-10.6	10.6-12.7	12.7-15.0	15.0-20.0
	COUNTS	761	665	597	828	410	345	432	233	120	89
	FLUENCE	6.05E 02	5.28E 02	4.65E 02	6.57E 02	3.23E 02	2.73E 02	3.48E 02	1.85E 02	9.86E 01	6.79E 01
	+-	2.40E 01	2.26E 01	2.09E 01	2.51E 01	1.76E 01	1.62E 01	1.83E 01	1.32E 01	1.01E 01	7.62E 00
SI	ENERGY	4.6-5.0	5.0-5.5	5.5-6.1	6.1-7.1	7.1-7.8	7.8-8.7	8.7-10.6	10.6-12.7	12.7-15.0	15.0-20.0
	COUNTS	567	541	508	593	342	293	293	134	73	59
	FLUENCE	4.63E 02	4.30E 02	4.07E 02	4.73E 02	2.75E 02	2.44E 02	2.27E 02	1.07E 02	6.12E 01	4.14E 01
	+-	2.15E 01	2.03E 01	1.99E 01	2.12E 01	1.63E 01	1.58E 01	1.43E 01	1.01E 01	7.87E 00	5.65E 00
FE§	ENERGY	5.0-5.5	5.5-6.1	6.1-7.1	7.1-7.8	7.8-8.7	8.7-10.6	10.6-12.7	12.7-15.0	15.0-20.0	20.0-29.0
	COUNTS	362	300	348	142	109	116	61	29	17	3
	FLUENCE	2.74E 02	2.37E 02	2.86E 02	1.14E 02	8.87E 01	9.12E 01	4.80E 01	2.32E 01	1.35E 01	2.22E 00
	+-	1.55E 01	1.49E 01	1.69E 01	1.05E 01	9.03E 00	9.24E 00	6.71E 00	4.53E 00	3.39E 00	1.33E 00

NOTES: (*) Counts are summed over Voyagers 1 and 2.
(†) Fluences are averaged over Voyagers 1 and 2. The fluence missing due to data gaps is estimated to be about 20 percent of the quoted fluence.
(§) Includes nickel.

TABLE 4.11

Fluence Measurements for the Entire Period: 1977 September 19 1200 UT to 1978 May 7 1800 UT

HE	ENERGY	3.0-3.3	3.3-3.6	3.6-4.0	4.0-5.0	5.0-6.1	6.1-7.8	(MeV/Nucleon)			
	COUNTS*	18222	13821	14364	24147	15981	15395				
	FLUENCE†	6.82E 05	5.47E 05	6.51E 05	1.11E 06	8.23E 05	7.85E 05	$(cm^2 \cdot sr)^{-1}$			
	+-	2.86E 04	1.92E 04	2.49E 04	2.75E 04	2.79E 04	2.44E 04				
C	ENERGY	4.0-4.5	4.5-5.0	5.0-5.5	5.5-6.1	6.1-7.1	7.1-7.8	7.8-8.7	8.7-10.6	10.6-12.7	12.7-15.0
	COUNTS	7074	6351	4634	4480	5796	3133	3227	4695	3402	2151
	FLUENCE	6.77E 03	6.39E 03	4.61E 03	4.71E 03	6.53E 03	3.68E 03	4.03E 03	5.90E 03	4.64E 03	3.10E 03
	+-	1.15E 02	1.12E 02	9.42E 01	9.61E 01	1.19E 02	9.14E 01	1.03E 02	1.18E 02	1.08E 02	9.10E 01
O	ENERGY	4.0-4.5	4.5-5.0	5.0-5.5	5.5-6.1	6.1-7.1	7.1-7.8	7.8-8.7	8.7-10.6	10.6-12.7	12.7-15.0
	COUNTS	17050	13677	11552	12137	14653	7899	8030	11986	8407	5623
	FLUENCE	1.72E 04	1.44E 04	1.25E 04	1.37E 04	1.73E 04	9.92E 03	1.05E 04	1.64E 04	1.23E 04	8.58E 03
	+-	1.86E 02	1.74E 02	1.65E 02	1.71E 02	1.99E 02	1.56E 02	1.64E 02	2.05E 02	1.85E 02	1.56E 02
NE	ENERGY	4.5-5.0	5.0-5.5	5.5-6.1	6.1-7.1	7.1-7.8	7.8-8.7	8.7-10.6	10.6-12.7	12.7-15.0	15.0-18.7
	COUNTS	1664	1379	1464	1838	960	955	1396	967	628	550
	FLUENCE	1.66E 03	1.48E 03	1.60E 03	2.12E 03	1.16E 03	1.28E 03	1.89E 03	1.43E 03	9.35E 02	8.12E 02
	+-	5.78E 01	5.71E 01	5.81E 01	6.97E 01	5.42E 01	5.85E 01	7.23E 01	6.23E 01	5.13E 01	4.77E 01
MG	ENERGY	4.5-5.0	5.0-5.5	5.5-6.1	6.1-7.1	7.1-7.8	7.8-8.7	8.7-10.6	10.6-12.7	12.7-15.0	15.0-20.0
	COUNTS	2580	2114	2053	2953	1581	1512	2245	1500	1040	1157
	FLUENCE	2.68E 03	2.31E 03	2.32E 03	3.57E 03	1.92E 03	2.00E 03	3.16E 03	2.20E 03	1.59E 03	1.87E 03
	+-	7.07E 01	6.97E 01	7.28E 01	9.07E 01	6.75E 01	6.90E 01	9.29E 01	7.88E 01	6.46E 01	7.42E 01
SI	ENERGY	4.6-5.0	5.0-5.5	5.5-6.1	6.1-7.1	7.1-7.8	7.8-8.7	8.7-10.6	10.6-12.7	12.7-15.0	15.0-20.0
	COUNTS	1942	1945	1924	2626	1486	1437	1972	1241	794	828
	FLUENCE	2.29E 03	2.30E 03	2.43E 03	3.51E 03	2.10E 03	2.05E 03	3.04E 03	1.98E 03	1.25E 03	1.29E 03
	+-	7.18E 01	7.17E 01	7.70E 01	9.58E 01	7.36E 01	7.32E 01	9.68E 01	7.50E 01	5.80E 01	6.18E 01
FE§	ENERGY	5.0-5.5	5.5-6.1	6.1-7.1	7.1-7.8	7.8-8.7	8.7-10.6	10.6-12.7	12.7-15.0	15.0-20.0	20.0-29.0
	COUNTS	2249	2059	2526	1255	1166	1624	920	519	519	328
	FLUENCE	3.35E 03	3.00E 03	3.85E 03	1.99E 03	1.82E 03	2.46E 03	1.36E 03	7.43E 02	6.44E 02	3.85E 02
	+-	9.68E 01	8.87E 01	1.03E 02	7.63E 01	7.21E 01	8.63E 01	6.29E 01	4.78E 01	3.72E 01	2.72E 01

NOTES: (*) Counts are summed over Voyagers 1 and 2.
(+) Fluences are averaged over Voyagers 1 and 2. The fluence missing due to data gaps is estimated to be about 9 percent of the quoted fluence.
(§) Includes nickel.

The fluence measurements presented here are intended to serve several purposes. In Chapter 5 they will be used to examine the energy/nucleon dependence of SEP composition in the 5 to 15 MeV/nucleon interval. In addition, the fluence measurements should eventually be combined with forthcoming results from the Voyager Low Energy Charged Particle Experiment and the Voyager High Energy Telescopes to study SEP composition over a wide energy range from below 1 to above 100 MeV/nucleon. Finally, the fluence measurements presented here are important to a number of astrophysical problems which are not addressed in this thesis, including the study of the effects of SEPs on lunar rocks and soil (see, e.g., Price et. al. 1974) and the consideration of flaring stars as possible injectors of energetic particles into the galactic cosmic ray accelerator (see, e.g., Montmerle 1979).

In anticipation of the discussion in Chapter 5, the fluence measurements of the elements C, O, Ne, Mg, Si, and Fe+Ni in each flare event were fit by power law functions of the form $A \cdot (E/7.5)^{-\gamma}$ by minimizing the function:

$$\chi^2(A,\gamma) = \frac{1}{4}\sum_{i=1}^{6}\left[W_i - \int_{E_i}^{E_{i+1}} A \cdot (E/7.5)^{-\gamma} dE \right]^2 / \sigma_i^2 \quad (4.1)$$

where W_i and σ_i are the fluence and its statistical error for energy/nucleon bin i having lower and upper energy/nucleon boundaries E_i and E_{i+1} respectively. The same six energy/nucleon bins in the interval 5–15 MeV/nucleon were used for each element. The fluence measurements for these energy/nucleon bins and the best fit power law functions are plotted in Figure 4.7. The best fit spectral

Figure 4.7

Energy spectra of the elements C, O, Ne, Mg, Si, and Fe+Ni for the flare events i through vii. Also shown are best fit power law functions of the form $A(E/7.5)^{-\gamma}$, where E is kinetic energy per nucleon. (χ^2 is defined in the text.)

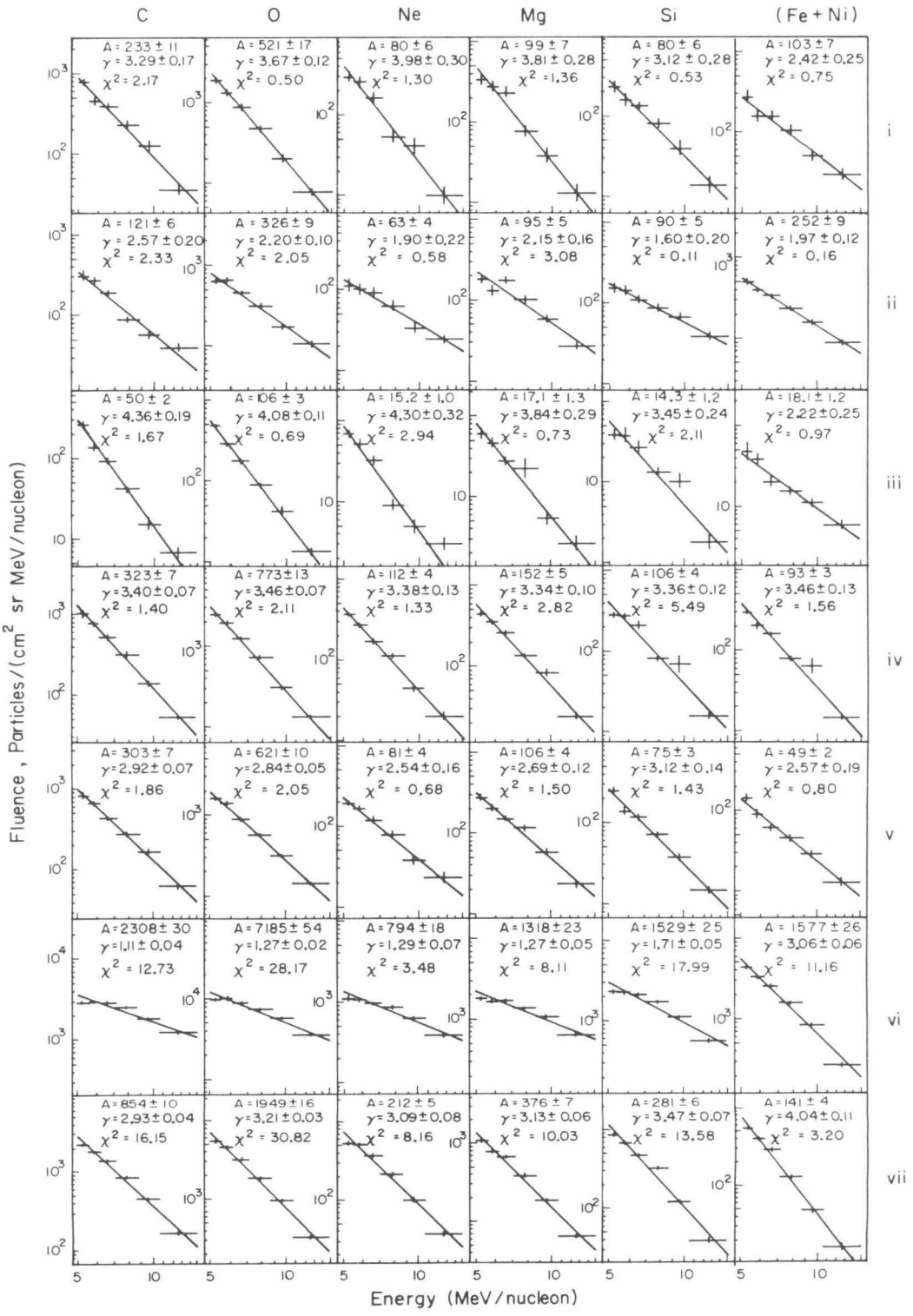
C
O
Ne
Mg
Si
(Fe+Ni)
i
ii
iii
iv
v
vi
vii
A = 233 ± 11
γ = 3.29 ± 0.17
χ² = 2.17
A = 521 ± 17
γ = 3.67 ± 0.12
χ² = 0.50
A = 80 ± 6
γ = 3.98 ± 0.30
χ² = 1.30
A = 99 ± 7
γ = 3.81 ± 0.28
χ² = 1.36
A = 80 ± 6
γ = 3.12 ± 0.28
χ² = 0.53
A = 103 ± 7
γ = 2.42 ± 0.25
χ² = 0.75
A = 121 ± 6
γ = 2.57 ± 0.20
χ² = 2.33
A = 326 ± 9
γ = 2.20 ± 0.10
χ² = 2.05
A = 63 ± 4
γ = 1.90 ± 0.22
χ² = 0.58
A = 95 ± 5
γ = 2.15 ± 0.16
χ² = 3.08
A = 90 ± 5
γ = 1.60 ± 0.20
χ² = 0.11
A = 252 ± 9
γ = 1.97 ± 0.12
χ² = 0.16
A = 50 ± 2
γ = 4.36 ± 0.19
χ² = 1.67
A = 106 ± 3
γ = 4.08 ± 0.11
χ² = 0.69
A = 15.2 ± 1.0
γ = 4.30 ± 0.32
χ² = 2.94
A = 17.1 ± 1.3
γ = 3.84 ± 0.29
χ² = 0.73
A = 14.3 ± 1.2
γ = 3.45 ± 0.24
χ² = 2.11
A = 18.1 ± 1.2
γ = 2.22 ± 0.25
χ² = 0.97
A = 323 ± 7
γ = 3.40 ± 0.07
χ² = 1.40
A = 773 ± 13
γ = 3.46 ± 0.07
χ² = 2.11
A = 112 ± 4
γ = 3.38 ± 0.13
χ² = 1.33
A = 152 ± 5
γ = 3.34 ± 0.10
χ² = 2.82
A = 106 ± 4
γ = 3.36 ± 0.12
χ² = 5.49
A = 93 ± 3
γ = 3.46 ± 0.13
χ² = 1.56
A = 303 ± 7
γ = 2.92 ± 0.07
χ² = 1.86
A = 621 ± 10
γ = 2.84 ± 0.05
χ² = 2.05
A = 81 ± 4
γ = 2.54 ± 0.16
χ² = 0.68
A = 106 ± 4
γ = 2.69 ± 0.12
χ² = 1.50
A = 75 ± 3
γ = 3.12 ± 0.14
χ² = 1.43
A = 49 ± 2
γ = 2.57 ± 0.19
χ² = 0.80
A = 2308 ± 30
γ = 1.11 ± 0.04
χ² = 12.73
A = 7185 ± 54
γ = 1.27 ± 0.02
χ² = 28.17
A = 794 ± 18
γ = 1.29 ± 0.07
χ² = 3.48
A = 1318 ± 23
γ = 1.27 ± 0.05
χ² = 8.11
A = 1529 ± 25
γ = 1.71 ± 0.05
χ² = 17.99
A = 1577 ± 26
γ = 3.06 ± 0.06
χ² = 11.16
A = 854 ± 10
γ = 2.93 ± 0.04
χ² = 16.15
A = 1949 ± 16
γ = 3.21 ± 0.03
χ² = 30.82
A = 212 ± 5
γ = 3.09 ± 0.08
χ² = 8.16
A = 376 ± 7
γ = 3.13 ± 0.06
χ² = 10.03
A = 281 ± 6
γ = 3.47 ± 0.07
χ² = 13.58
A = 141 ± 4
γ = 4.04 ± 0.11
χ² = 3.20
Fluence , Particles/(cm² sr MeV/nucleon)
Energy (MeV/nucleon)

indices are summarized in Table 4.12.

The normalizing energy, 7.5 MeV/nucleon, was chosen such that A and γ were roughly independent fitting parameters, allowing the statistical uncertainty in A to be estimated by:

$$\sigma_A = A \cdot \left[\sum_{i=1}^{6} \left(\frac{W_i}{\sigma_i} \right)^2 \right]^{-\frac{1}{2}}$$

The statistical uncertainty in γ was estimated (as described by Bevington 1969, p. 243) as that increment to the best fit value of γ which increased χ^2 by 0.25 from its minimum value.

Note that the above spectral indices are derived from fluence measurements which are integrated over entire SEP events, rather than over the time periods selected in Section 4.3 to exclude event onset times. Due to the softening of energy spectra which occurs throughout some events (see, e.g., the oxygen spectral index in Figure 4.4) the spectral index measurement for a given element typically does depend somewhat on the choice of averaging time period. However, in the discussion in Chapter 5 we will be interested only in the differences between the energy spectra of the different elements. These differences were found to be insensitive to whether or not the event onset times were included in the averaging time periods.

4.5.1 Systematic Error

The relative systematic errors between fluence measurements for the different elements and energy bins are dominated by LET detector energy calibration errors (except in the case of He in event vi,

TABLE 4.12

Spectral Index, γ (assuming $dJ/dE \sim E^{-\gamma}$)‡

Z	Element	Solar Energetic Particle Event* (i)	(ii)	(iii)	(iv)	(v)	(vi)#	(vii)#
6	C	3.29±0.17†	2.57±0.20	4.36±0.19	3.40±0.07	2.92±0.07	1.11±0.04	2.93±0.04
8	O	3.67±0.12	2.20±0.10	4.08±0.11	3.46±0.07	2.84±0.05	1.27±0.02	3.21±0.03
10	Ne	3.98±0.30	1.90±0.22	4.30±0.32	3.38±0.13	2.54±0.16	1.29±0.07	3.09±0.08
12	Mg	3.81±0.28	2.15±0.16	3.84±0.29	3.34±0.10	2.69±0.12	1.27±0.05	3.13±0.06
14	Si	3.12±0.28	1.60±0.20	3.45±0.24	3.36±0.12	3.12±0.14	1.71±0.05	3.47±0.07
26	Fe§	2.42±0.25	1.97±0.12	2.22±0.25	3.46±0.13	2.57±0.19	3.06±0.06	4.04±0.11

NOTES: (‡) Spectral indices were obtained by least squares fits using six energy bins in the interval 5-15 MeV/nucleon; see text.
(*) The events correspond to the time periods of Tables 4.4 through 4.10 respectively.
(#) Spectra were not well fit by a power law function; γ increased with energy.
(†) The ($\pm 1\sigma$) uncertainties include the effect of particle counting statistics only.
(§) Includes nickel.

as indicated later in this section and in Section 4.4.1) The effect of such possible errors on relative abundance measurements (in particular, for the 8.7–15 MeV/nucleon interval) was discussed in section 4.4.1, and found to be small; about $0.5 \cdot |Z1-Z2|$ percent for the relative abundance of elements with nuclear charge Z1 and Z2. Here we consider the effect of possible energy calibration errors on the spectral index γ. The possible error in γ was estimated by (1) calculating the shift of energy thresholds (E_i, see above section) induced by a 5 percent relative error between the L3 and L1+L2 energy measurements and (2) using the shifted E_i in expression 4.1 to recompute γ. The average percentage changes in γ for the elements C, O, Ne, Mg, Si, and Fe were about 7, 4, 1.6, 1.2, 0.5 and −1.0 respectively. While these possible errors are small relative to many of the observed differences in spectral index among the different elements (see Table 4.12), they are sometimes comparable to the statistical errors and therefore are taken into account in the spectral index comparisons of the next chapter.

The main sources of possible absolute error in the fluence measurements of Tables 4.4 through 4.11 are discussed below:

(1) Geometry factor. The uncertainty in the absolute LET geometry factors is estimated as 6 percent since the area of the "edge" of detectors L1 and L2 was found to be about 6 percent of their active areas (see Sections 3.5.2 and 3.6).

(2) Energy calibration. Conservatively estimating the absolute error of particle energy measurement at 5 percent and assuming a typically steep energy spectrum ($dJ/dE \propto E^{-3}$) gives a fluence error of 15 percent.

(3) Data gaps. The fluence missing due to data gaps was estimated for each flare event and ranges from 0.5 to 35 percent of the measured fluence. Thus, the error in the uncorrected fluence measurements (i.e. those listed in Tables 4.4 through 4.11) due to data gaps is $\leq$ 35 percent. Since the gaps were generally short (about 3 to 12 hours) and the flux was typically a fairly smooth function of time, the estimates of missing fluence are probably accurate to better than about $\pm$ 50 percent. Thus, if the fluence measurements were corrected for the missing fluence, the residual uncertainty due to data gaps would range from about 0 to 20 percent for the different flare events.

(4) Anisotropy. The fluence measurements of Tables 4.4–4.11 may differ from omni–directional fluence measurements as the result of particle anisotropy. For each flare event, the size of such possible differences was estimated by comparing (a) fluence measurements averaged over all four Voyager 1 LETs to (b) fluence measurements averaged over only Voyager 1 LETs A and C, which, pointing in opposite directions, measure the omni–directional component of the fluence. The differences between the fluence measurements (a) and (b) ranged from about 0 to 20 percent with a typical value of about 10 percent.

(5) High count rates. Possible systematic error due to high

counting rates only occurs for He in event vi, where as mentioned earlier, the mass resolution was somewhat degraded. Although for event vi, the He mass consistency check was relaxed and dead time corrections were applied, the residual systematic error in the He fluence measurements may be on the order of 20 percent.

Combining the above error estimates gives an absolute error for the fluence measurements of Tables 4.4 through 4.11 in the range of about 15 to 50 percent, depending mainly on the data gaps.

Chapter 5

Discussion

5.1 Overview

With the goal of understanding the relationship between SEP elemental composition and the composition of the sun, this chapter discusses the systematics of the SEP observations presented in Chapter 4. As discussed in the Introduction, we will (a) examine the time and velocity (energy/nucleon) dependence of the SEP composition in the individual flare events, (b) select for further study those flare events which have SEP composition that is approximately independent of energy/nucleon, (c) compare the selected SEP composition results from flare to flare, and (d) compare the selected SEP composition results to solar abundance measurements from other sources: spectroscopy of the photosphere and corona, and solar wind measurements.

An overview of our SEP abundance results and their relationship to other solar abundance measurements is shown in Figure 5.1, a plot of the SEP abundance measurements (from Tables 4.2 and 4.3) for all seven flare events, along with abundances for the photosphere, corona and solar wind. Although the SEP composition is seen to vary from flare to flare, the average SEP abundances, when normalized to silicon, are similar to abundances from the other sources for all the elements shown except C, N, and O, where the SEP values are persistently low relative to the photosphere. For oxygen, the SEP abundances are similar to the solar wind and active coronal region

Figure 5.1

Elemental abundances relative to silicon. References: (*) Meyer and Reeves (1977), (†) Bame et. al. (1975), (§) Parkinson et. al. (1977).

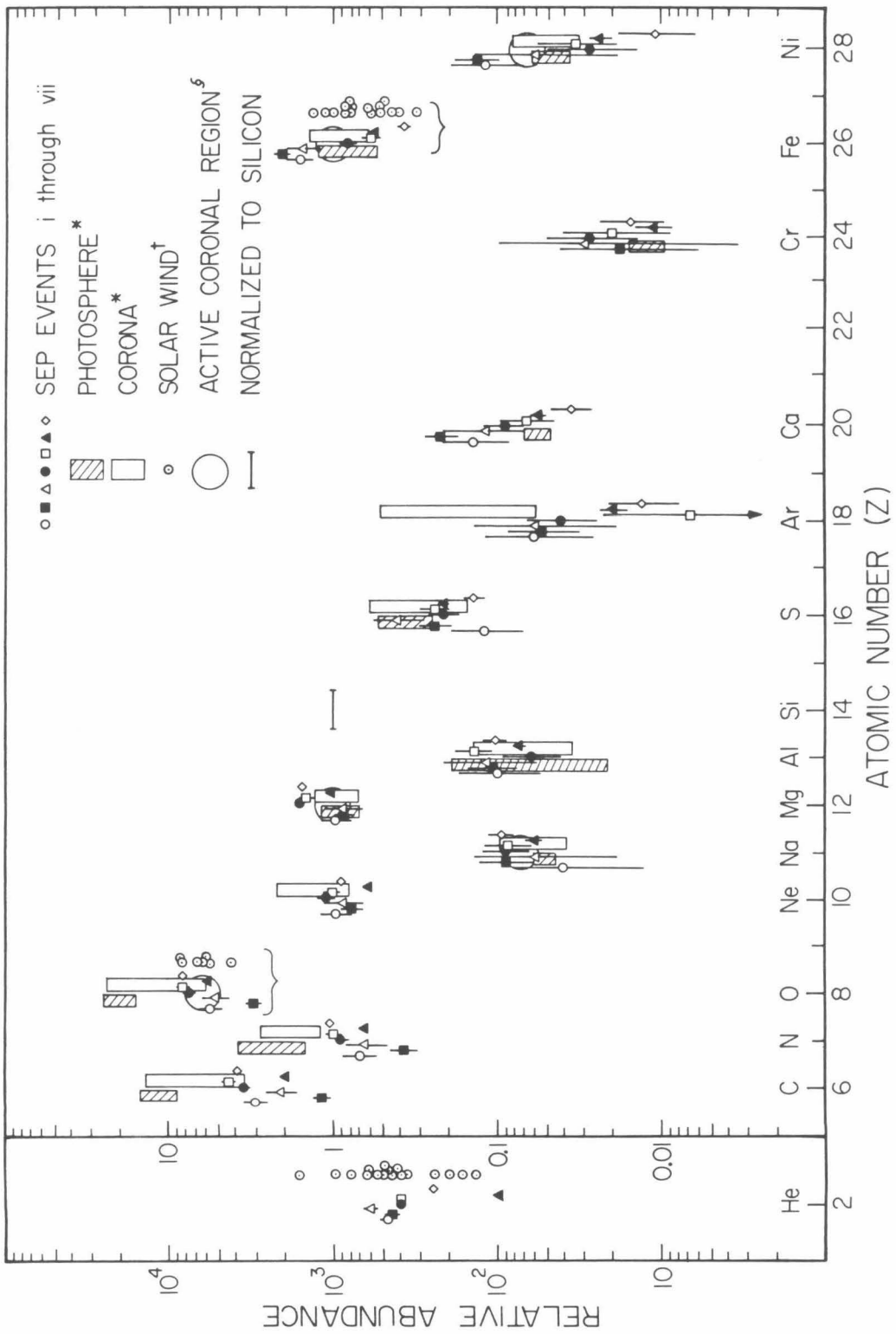
SEP EVENTS i through vii
PHOTOSPHERE*
CORONA*
SOLAR WIND†
ACTIVE CORONAL REGION§
NORMALIZED TO SILICON
RELATIVE ABUNDANCE
ATOMIC NUMBER (Z)
He C N O Ne Na Mg Al Si S Ar Ca Cr Fe Ni
2 6 8 10 12 14 16 18 20 22 24 26 28
10 1 0.1 0.01
10^4 10^3 10^2 10

values.

In the following discussion of the time and velocity dependence of SEP abundances in individual flare events, we are particularly interested in whether or not there is an indication of SEP acceleration and/or propagation bias which may account for the persistent differences seen between SEP elemental composition and the results of photospheric spectroscopy.

5.2 Time and Velocity Dependence of SEP Abundances for Individual Flare Events

The time development of the seven SEP events was discussed (in Section 4.3) in connection with the selection of averaging time periods for the SEP abundance measurements for each flare event. Clear evidence for systematic abundance time variations was seen for the Fe/O ratio (5–15 MeV/nucleon), which decreased by a factor of three to five in each of the four flare events that showed velocity dispersion in the particle arrival times. In two of these four events the He/O ratio (4.0–7.8 MeV/nucleon) increased with time. However, the key point for the discussion in this chapter is that systematic time variations among the elements C, O, Ne, Mg and Si were found to be relatively small — less than about ± 30 percent in the 5–15 MeV/nucleon interval. Thus, propagation effects which would result in abundance time variations do not appear to account for the persistent difference — a factor of three to five — between the SEP and photospheric abundances of C and O relative to Mg and Si.

The velocity (or energy/nucleon) dependence of the SEP abundance ratios provides a more critical test for possible acceleration/propagation biases. This dependence may be derived from Figure 4.7 which shows, for each flare event, the measured energy/nucleon spectra for each of the elements C, O, Ne, Mg, Si and Fe+Ni. Over the relatively narrow energy interval from 5 to 15 MeV/nucleon, the comparison of the spectral indices (slopes of the power law fits) suffices to accurately determine the energy/nucleon dependence of the relative abundances. In Figure 5.2, such comparisons are made for each flare event. Despite the variation of the spectral indices from flare to flare, the spectral indices of C, O, Ne and Mg are roughly equal in a given flare event. However, the spectral index of Fe+Ni is often significantly different from those of C, O, Ne and Mg. The spectral indices of Si show some significant differences with those of C, O, Ne and Mg, with a tendency in the direction of the Fe+Ni spectral indices.

The relation between the SEP spectral index and relative abundance measurements is explored in Figure 5.3. For every element pair in the set of elements (C, O, Ne, Mg, Si and Fe+Ni) for which spectral indices were measured, the "relative abundance" is plotted versus the difference in spectral index measurements. Here, "relative abundance" refers to the relative abundance at 7.5 MeV/nucleon, that is, the ratio of the "A" parameters of Figure 4.7. Also plotted are horizontal solid and dashed lines which indicate respectively the photospheric relative abundance measurements and their estimated uncertainties. A number of interesting features are apparent in

Figure 5.2

Spectral indices for the elements C, O, Ne, Mg, Si and Fe+Ni in flare events i through vii. The ($\pm$ 1σ) error bars include the effect of counting statistics only. ($\overline{\gamma}$ and χ^2 are defined later in Section 5.3)

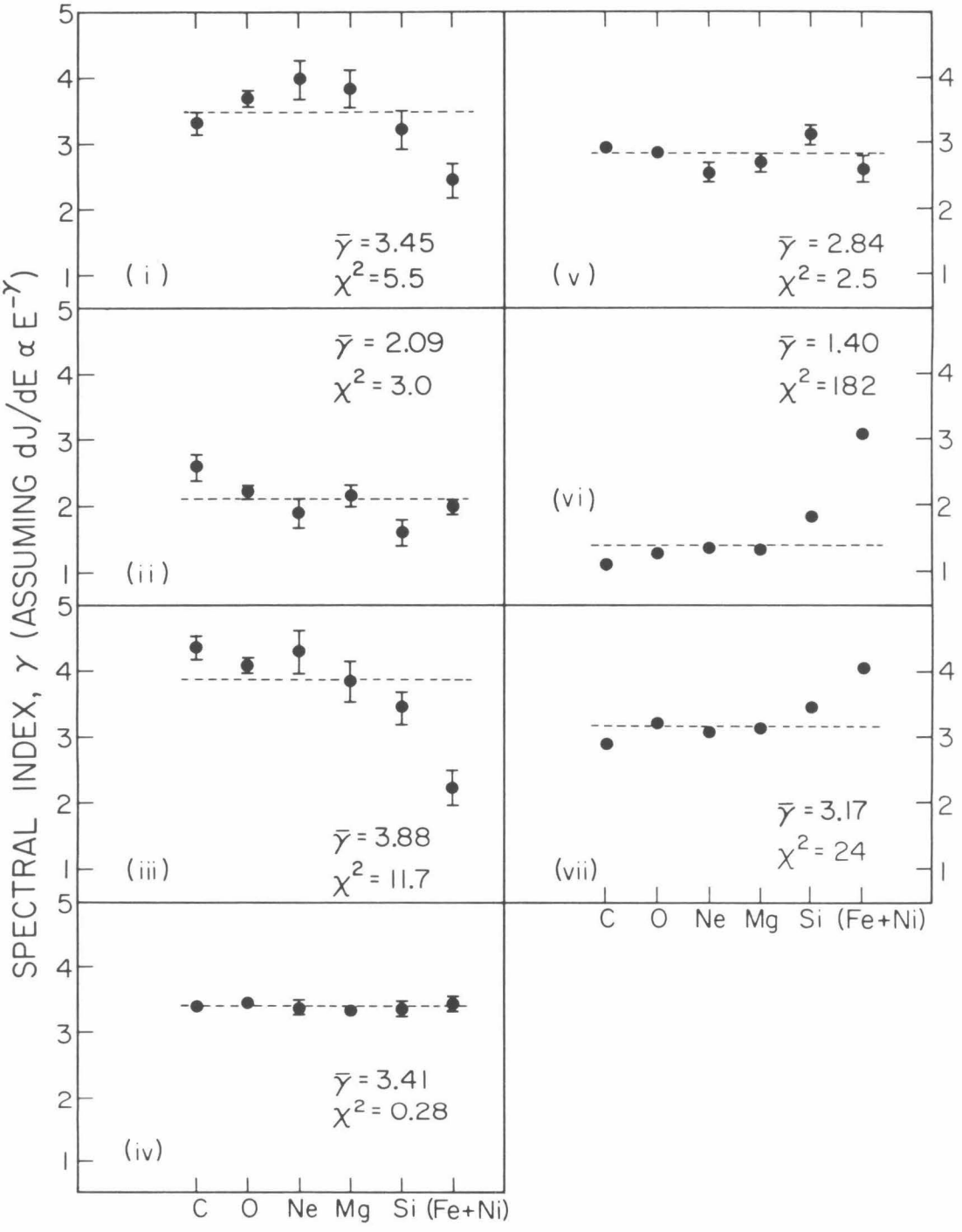
SPECTRAL INDEX, γ (ASSUMING dJ/dE ∝ E^-γ)
(i)
γ̄ = 3.45
χ² = 5.5
(ii)
γ̄ = 2.09
χ² = 3.0
(iii)
γ̄ = 3.88
χ² = 11.7
(iv)
γ̄ = 3.41
χ² = 0.28
(v)
γ̄ = 2.84
χ² = 2.5
(vi)
γ̄ = 1.40
χ² = 182
(vii)
γ̄ = 3.17
χ² = 24
C O Ne Mg Si (Fe+Ni)

Figure 5.3

Relative SEP abundance plotted versus the difference in spectral index $(\gamma_x - \gamma_y)$ **for the various element pairs among the elements** C, O, Ne, Mg, Si, and Fe+Ni. The $(\pm 1\sigma)$ error bars include the effect of particle counting statistics and, in the case of $(\gamma_x - \gamma_y)$, a contribution due to possible systematic error (see Section 4.5.1). The horizontal solid and dashed lines indicate respectively the photospheric abundance results and their estimated uncertainties (from Meyer and Reeves 1977).

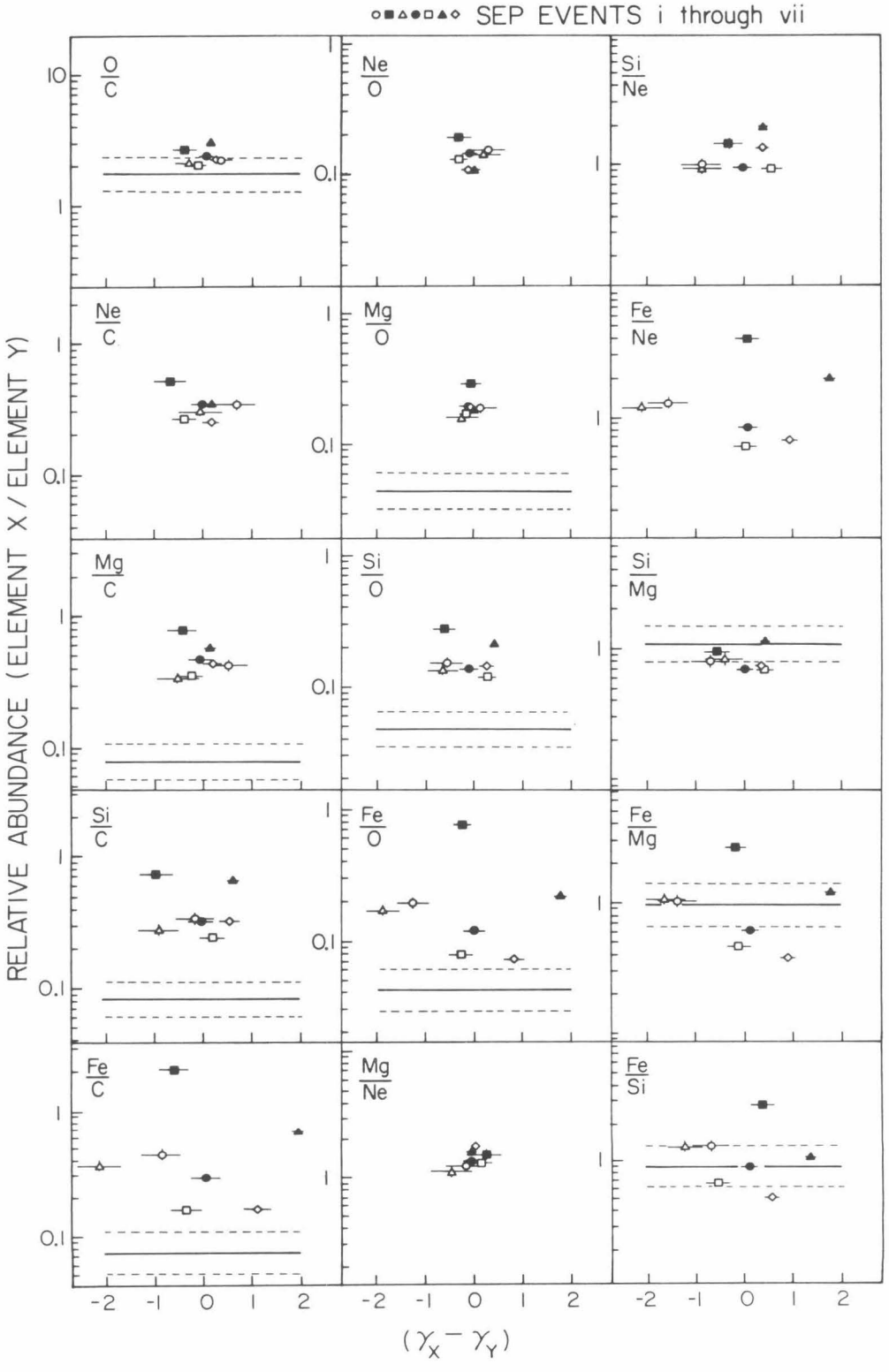
○■△●□▲◇ SEP EVENTS i through vii
O/C
Ne/O
Si/Ne
Ne/C
Mg/O
Fe/Ne
Mg/C
Si/O
Si/Mg
Si/C
Fe/O
Fe/Mg
Fe/C
Mg/Ne
Fe/Si
RELATIVE ABUNDANCE (ELEMENT X / ELEMENT Y)
(γX − γY)

Figure 5.3:

(1) The average value of $\delta\gamma \equiv \gamma_x - \gamma_y$ is approximately zero for each element pair [x,y]. Thus, averaged over all seven flare events, the SEP relative abundances would be nearly independent of velocity (or energy/nucleon). This contrasts with the results of Crawford et. al. (1975) which suggested that in SEPs the heavier elements are always increasingly enhanced at lower energies. On the other hand, our result is consistent with the measurements of Mason, Hovestadt and Gloeckler (1979) which indicate that SEP composition at energies near 1 MeV/nucleon is nearly identical to that measured above 10 MeV/nucleon. The different conclusions of Crawford et. al. (1975) regarding the energy dependence of SEP composition may just be the result of a different flare sample. However, Mason, Hovestadt and Gloeckler (1979) have suggested that the low energy heavy element enhancements reported by Crawford et. al. (1975), which were obtained mainly in low altitude rocket flights, may have been caused by the earth's magnetic field. (Also, see the review of recent spacecraft observations by Mewaldt 1980).

(2) There is essentially no correlation between $\delta\gamma$ and relative abundance for any element pair. A correlation would be expected if the relative abundances were constant at some energy/nucleon E_0 that was not too far removed from the observation range, 5–15 MeV/nucleon, since in this case the relative abundance at 7.5 MeV/nucleon would be proportional to $(E_0/7.5)^{\delta\gamma}$. For element pairs (like [Fe,X], where X = C, O, Ne, Mg or Si) which show a large flare-to-flare abundance variation, the lack of correlation between

$\delta\gamma$ and relative abundance indicates that there is no nearby energy/nucleon at which the relative abundances tend to be constant from flare to flare. This also contrasts with the results of Crawford et. al. (1975) which suggested that the range of flare-to-flare variation of the SEP Fe/O ratio was relatively small at energies above about 15 MeV/nucleon, but larger at lower energies.

(3) Among the different element pairs, the range of flare-to-flare variation of $\delta\gamma$ and of the relative abundances are correlated, and tend to be larger for those element pairs in which the two elements have a larger difference of nuclear charge. For example, the spread of data points in both the vertical and horizontal directions increases as we move from the top left-most frame of Figure 5.3 downward, through the element pairs [C,O], [C,Ne] [C,Mg], [C,Si] and [C,Fe].

(4) The range of flare-to-flare variations of $\delta\gamma$ and of the relative abundances are not correlated with the size of the difference between the average SEP relative abundances and the photosphere abundances. For example, the element pair [Mg,O] has $\delta\gamma$ approximately equal to zero in every flare event, and the Mg/O ratio is nearly constant from flare to flare (only event ii shows a Mg/O ratio that is significantly different from the Mg/O ratio in the other events), yet the SEP Mg/O values are a factor of four to five larger than the photospheric value. On the other hand, the element pair [Fe,Si] shows large flare-to-flare variations of both $\delta\gamma$ and abundance ratio, while the average SEP Fe/Si ratio is nearly equal to the photospheric value.

In conclusion, the observations of this section suggest that the persistent differences which exist between the SEP and photospheric composition results are not due to systematic differences in SEP spectral index among the different elements, nor to systematic propagation effects which would result in time dependent abundance ratios. This suggests the other alternatives: (a) the composition of the flare acceleration site is significantly different from that measured for the photosphere and/or (b) there is a persistent acceleration bias which operates at energies outside our range of observation.

5.3 The Selection of Four Preferred SEP Events

For the purpose of studying solar composition, we concentrate on those flare events for which the measured SEP abundance ratios are approximately independent of energy/nulceon, and therefore have unique values which might equal those in the pre-accelerated plasma at the SEP acceleration site.

For each flare event, a measure χ^2 of the statistical significance of the differences among spectral indices of the various elements was calculated using:

$$\chi^2 = \frac{1}{5}\sum_{j=1}^{6}(\gamma_j-\overline{\gamma})^2/\sigma_j^2$$

The elements C, O, Ne, Mg, Si and Fe+Ni are indexed by j ; γ_j and σ_j are the spectral index and its statistical error respectively (from Table 4.12); $\overline{\gamma}$ was chosen to minimize χ^2. The results are listed in Figure 5.2. The four events with smaller values of χ^2 (i, ii, iv, and v) were chosen

for further study. The rejection of the other three events is based primarily on differences between the Fe+Ni spectral index and those of the other elements — differences which correspond to relatively large changes of relative abundance as a function of energy/nucleon. For example, the differences in spectral index of Fe+Ni and O ($\gamma_{Fe+Ni} - \gamma_O$) of about +2 and −2, in events iii and vi respectively, correspond to factors of about ten ($\approx [15/5]^2$) change in the (Fe+Ni)/O ratio over the observation interval 5−15 MeV/nucleon.

Note, in Figure 5.2, that the inclusion of flare event i in the set of preferred events is questionable because of the relatively low value of the Fe+Ni spectral index. Thus, in the next section we will consider the effect of event i on our conclusions.

In a theoretical context, the flare events in which the SEP abundance ratios were approximately independent of energy/nucleon may be those in which the various nuclei, including Fe, were fully stripped of electrons during acceleration. However, as discussed in Section 4.3, systematic time variations of the SEP (Fe+Ni)/O ratio at 5−15 MeV/nucleon, as well as direct charge state measurements at lower energies, indicate that the Fe nuclei are typically not fully stripped during their propagation through interplanetary space. For example, in flare event iv the measured energy/nucleon spectra are accurately the same among the different elements (including Fe+Ni and O), yet a systematic decrease of the (Fe+Ni)/O ratio is observed early in the event. If we assume that, in general, the Fe nuclei are also not fully stripped during acceleration, then the above selection of flare events with SEP abundances independent of energy/nucleon may

correspond to the selection of events in which the important processes were primarily velocity dependent, rather than rigidity dependent.

5.4 Systematics of Flare-to-Flare SEP Abundance Variations for Four Preferred Events

The systematics of the flare-to-flare composition variations are shown in Figure 5.4 by comparing the SEP composition results for each of the four selected flare events to the "four-flare average" composition. (The term "average" henceforth refers to the geometric or "log" average.) In each of the four flare events the deviations of the SEP abundances from their four-flare average values are approximately monotonic functions of nuclear charge Z in the range $6 \leq Z \leq 28$. In particular, the flare-to-flare abundance variations of C, N and O are correlated, as are the abundance variations of Ca, Fe and Ni; while the abundance variations of C, N and O relative to Si are anticorrelated with those of Ca, Fe and Ni. An important exception to the approximate Z ordering of the abundance variations occurs for He whose abundance relative to Si is approximately the same in all four events.

The correlations of the SEP abundances seen in Figure 5.4 suggest that the SEP composition may be described by an average composition and a systematic deviation which varies in strength, but not character, from flare to flare. In particular, the "Fe-rich" event ii does not stand out as a separate type of event, but rather may be the tail of a continuum of Z-dependent variability.

The systematics of the flare-to-flare SEP composition variations

Figure 5.4

SEP flare-to-flare composition variations. For each of the flare events i, ii, iv, and v, the SEP abundances (from Tables 4.2 and 4.3 and normalized at silicon, ■) are divided by the four-flare average abundances (from Table 5.1) and are plotted versus nuclear charge Z.

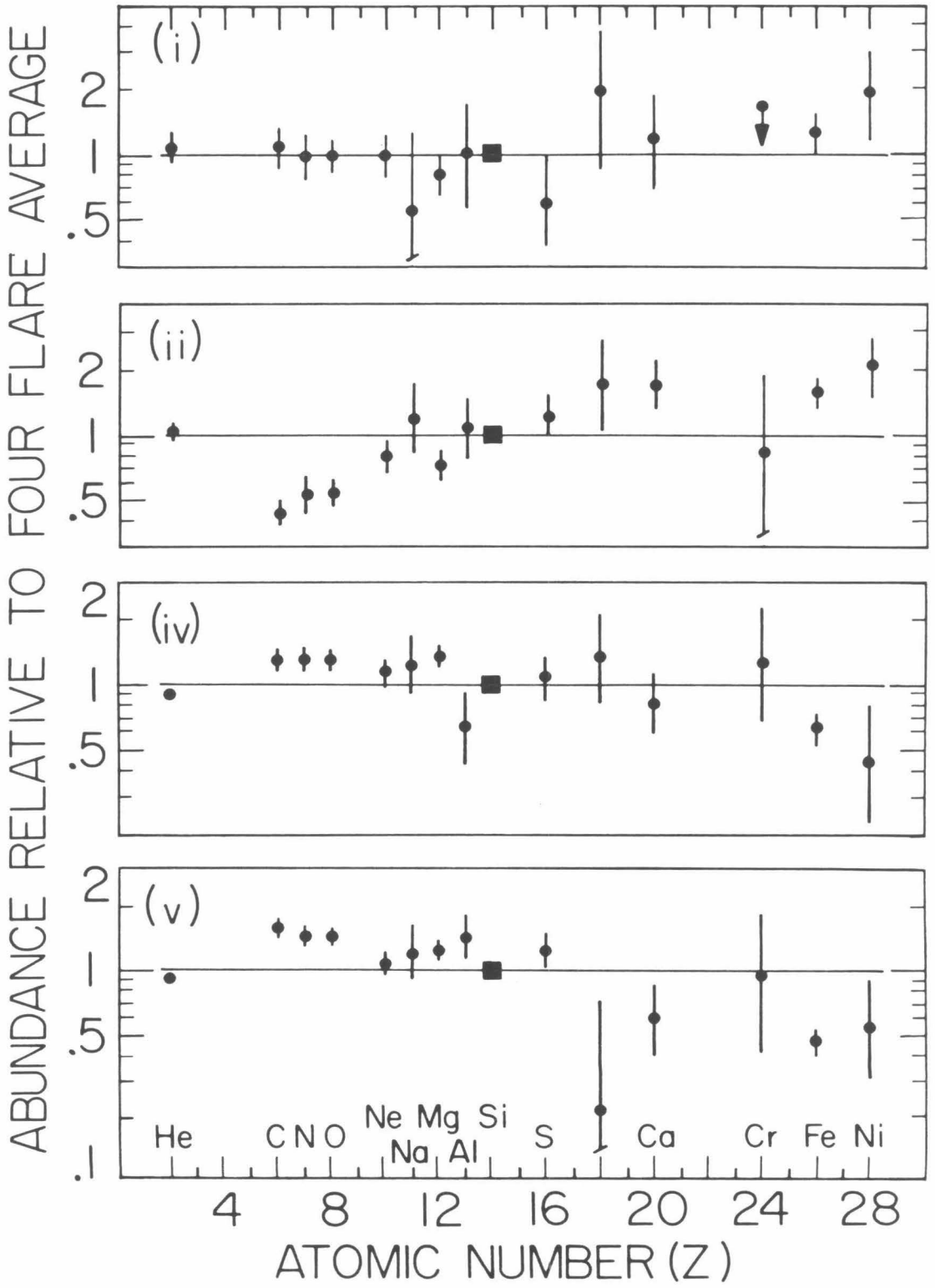
(i)
(ii)
(iv)
(v)
ABUNDANCE RELATIVE TO FOUR FLARE AVERAGE
2
1
.5
.1
He
C N O
Ne Mg Si
Na Al
S
Ca
Cr Fe Ni
4
8
12
16
20
24
28
ATOMIC NUMBER (Z)

seen in Figure 5.4 give practical significance to the four-flare average composition, since we are able (in the next section) to compare the four-flare average abundances to those from other solar sources, knowing that the same comparisons, when made separately for the four flare events, would differ only by roughly monotonic functions of Z (for $6 \leq Z \leq 28$). Further, the average SEP composition is not sensitive to our choice of this particular set of four flare events. For example, tightening somewhat the meaning of "approximately independent of velocity" excludes event i, which has only a negligible effect on the average SEP composition. On the other hand, the average composition for the entire set of seven flare events is also not significantly different from the four-flare average.

It is interesting that the selection of flare events with SEP abundance ratios that are approximately independent of energy/nucleon does not reduce the range of flare-to-flare variation of the Fe/Si ratio —the Fe/Si ratio ranges over a factor of nearly ten in both the full seven-flare and reduced four-flare sets. This is consistent with recent suggestions (Zwickl et. al. 1978; Briggs, Armstrong and Krimigis 1979) that the flare-to-flare variation of SEP elemental abundances may be largely due to variability of the composition of the pre-accelerated plasma at the SEP acceleration sites.

5.5 Comparison of the Four-Flare Average SEP Composition to Other Solar Abundance Measurements

The subject of solar composition was reviewed by Ross and Aller (1976) and updated recently by Aller (1980). The primary source of

abundance information is photospheric spectroscopy. Visible absorption line measurements, together with an atmospheric model and atomic transition probabilities, provide abundances for most of the elements — the major exceptions being Ne, Ar and the important constituent He. For most elements, photospheric spectroscopy is considered the most reliable source of solar composition information: (a) typical uncertainties in abundance measurements are estimated at less than about 30 percent, (b) the photosphere is thought to be well mixed with the outer convection zone of the sun by observed turbulent motions.

Abundance information is also available for the solar corona. Extreme ultraviolet (EUV) and X-ray emission lines are used to obtain abundances of some elements, but with typically large uncertainties of a factor of two or three. A key question concerns the compositional homogeneity of the corona, that is, the role of turbulent mixing versus fractionation processes (see, e.g., Nakada 1970, Withbroe 1976, and Mariska 1980).

A third source of abundance information is solar wind measurements. Electrostatic deflection techniques provide abundances for H, He, Si and Fe (Bame et. al. 1975). The foil collection method gives He, Ne and Ar abundances (Geiss et. al. 1972). As with the corona, there is the possibility that the average solar wind composition may differ from that of the photosphere. The solar wind He/H ratio varies with time by a factor of over ten, while the Si/H and Fe/H vary by somewhat smaller amounts (Bame et. al. 1975).

Meteorite studies provide a fourth, indirect, source of abundance information. For the non-volatile elements meteoritic abundances are in very good agreement with solar photospheric values, consistent with the idea that, for these elements, both the meteorites and solar photosphere reflect the composition of the primordial solar nebula (see Meyer 1978a, and Lambert and Luck 1978). Unfortunately, the most abundant solar constituents H, He, O, and C are volatile and, as a result, are depleted in meteorites.

In Figure 5.5 (also see Table 5.1) we compare the four-flare average SEP composition with results for the photosphere, corona and solar wind. We have taken the photospheric abundance data from Meyer and Reeves (1977) which is the most recent compilation which covers all the elements of interest here and incorporates error estimates. The photospheric abundance data of Meyer and Reeves (1977) are in close agreement with the earlier compilation of Ross and Aller (1976) and with the recent photospheric abundance determinations by Lambert (1978) and Lambert and Luck (1978) (although Lambert and Luck estimate a significantly smaller uncertainty for the Al abundance). Figure 5.5a shows that relative to the photospheric abundance data the average SEP abundances of C, N, O, and to a lesser extent S, are depleted with respect to the other elements in the range $11 \leq Z \leq 28$. The relative depletion of C, N and O in SEPs is now seen to be a persistent effect, as reported in an earlier account of this work (Cook et. al. 1979) and by McGuire, von Rosenvinge and McDonald (1979). The depletion is also present in the earlier data of Teegarden, von Rosenvinge and MacDonald (1973), Crawford et. al. (1975),

Figure 5.5

Comparison of the four-flare average SEP abundances (normalized at silicon, ■) to abundances from (a) the photosphere (● , Meyer and Reeves 1977), (b) the corona (● , Meyer and Reeves 1977, ○ Parkinson 1977, □ Withbroe 1975, and △ inferred from the N/O measurement of McKenzie et. al. 1978 and Parkinson's O/Si ratio), and (c) the solar wind (● Boschler and Geiss 1976). The ($\pm 1\sigma$) error bars include the estimated uncertainty in the photosphere, corona or solar wind abundances, and the uncertainty due to particle counting statistics in the average SEP abundances. The ($\pm 1\sigma$) estimated uncertainty in the average SEP abundances due to flare-to-flare abundance variations is indicated for carbon and iron by brackets.

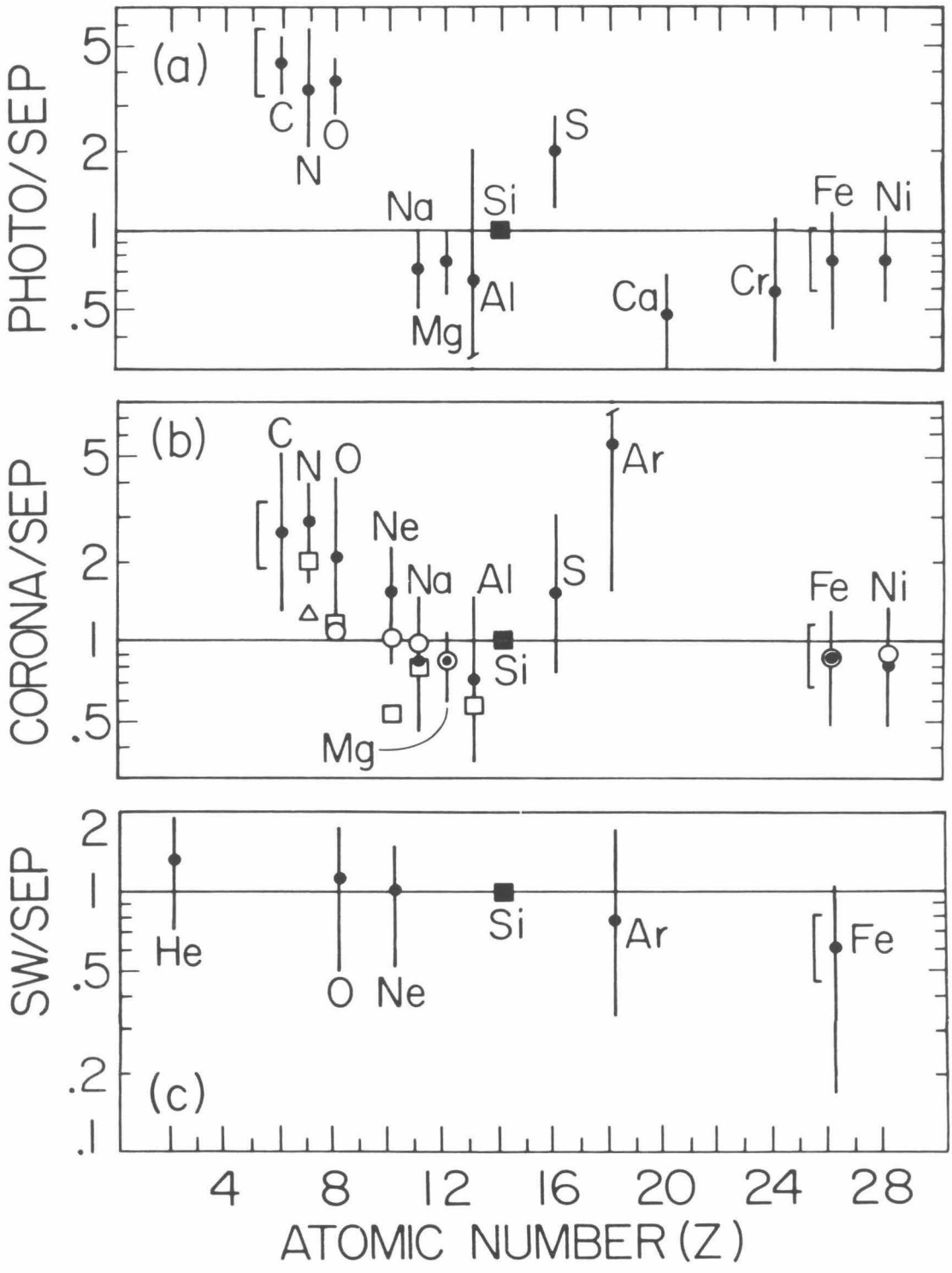
(a)
PHOTO/SEP
5
2
1
.5
C
N
O
Na
Si
S
Mg
Al
Ca
Cr
Fe
Ni
(b)
CORONA/SEP
5
2
1
.5
C
N
O
Ne
Na
Al
S
Ar
Mg
Si
Fe
Ni
(c)
SW/SEP
2
1
.5
.2
.1
He
O
Ne
Si
Ar
Fe
4
8
12
16
20
24
28
ATOMIC NUMBER (Z)

Notes to Table 5.1

(*) The geometric mean of the SEP abundances from flare events i, ii, iv and v. The ($\pm 1\sigma$) uncertainties include the effect of particle counting statistics, but not that of flare–to–flare abundance variations.

(†) Meyer and Reeves (1977).

(§) (a) Meyer and Reeves (1977), (b) Parkinson (1977), (c) Withbroe (1975).

(‡) Solar wind abundances relative to silicon were inferred from: He/H = 0.04 ± 0.01 , O/H = $(5 \pm 2) \times 10^{-4}$, Fe/H = $(5 \pm 2) \times 10^{-5}$, Si/H = $(7.6 \pm 3) \times 10^{-5}$, He/Ne = 530 ± 70 , and Ne/Ar = 41 ± 10 (Boschler and Geiss 1976)

(#) Numbers in parentheses indicate factors of error.

TABLE 5.1: RELATIVE ABUNDANCES IN SOLAR ENERGETIC PARTICLES, AND IN THE PHOTOSPHERE, CORONA, AND SOLAR WIND

Z	Element	SEP Four Flare Average*	Photosphere†	Corona§ (a)	(b)	(c)	Solar‡ Wind
2	He	416±19					530±250
6	C	2.74±0.17	12±3	7 (2)			
7	N	0.70±0.06	2.4 (1.6)	2.0±0.8		1.4	
8	O	5.80±0.34	21±5	12 (2)	6.3	6.6	6.6±3.7
10	Ne	0.97±0.07		1.5±0.7	1.0	0.5	1.0±0.5
11	Na	0.07 (1.4)#	0.052±0.008	0.06 (1.6)	0.07	0.06	
12	Mg	1.20±0.09	0.93±0.25	1.0±0.3	1.0		
13	Al	0.10±0.02	0.063 (3)	0.07 (2)		0.06	
14	Si	≡1	≡1	≡1	≡1	≡1	≡1
16	S	0.20±0.04	0.39±0.14	0.3 (2)			
18	Ar	0.03 (1.9)		0.17 (3)			0.024±0.013
20	Ca	0.12±0.02	0.057±0.010				
24	Cr	0.02 (1.8)	0.0125±0.0030				
26	Fe	1.14±0.08	0.89±0.35	1.0±0.4	1.0		0.7±0.5
28	Ni	0.06 (1.3)	0.048±0.012	0.05 (1.6)	0.06		

Pellerin (1975), Webber et. al. (1975) and Nevatia, Durgaprasad and Biswas (1977). The only SEP composition measurements which do not show the depletion are the earliest nuclear emulsion results (e.g., Bertsch, Fichtel and Reames 1972) which, according to Webber et. al. (1975), could be in error as the result of poor charge resolution and/or detection efficiency.

The comparison of coronal abundances (Figure 5.5b) from the compilation of Meyer and Reeves (1977) to the average SEP composition shows a relative depletion of SEP C, N and O which is less pronounced than that seen in Figure 5.5a. However, several recent coronal measurements show good agreement with the average SEP composition, most notably for O where large persistent depletions occur in SEPs relative to the photospheric data. Abundances of O which are low relative to the photospheric results, but consistent with the SEP values, have been found in both EUV (Withbroe 1975; Flower and Nussbaumer 1975; Mariska 1980) and X-ray studies (Acton, Catura and Joki 1975; Parkinson 1977).

Figure 5.5c shows that the solar wind and average SEP elemental abundances are in good agreement. Further, Figure 5.1 shows that the ranges of variation of the O/Si and Fe/Si ratios are similar in the SEPs and solar wind, although some of the variation of the solar wind measurements may be due to experimental errors —see Bame et. al. (1975). (While the average elemental compositions measured for SEPs and solar wind are similar, there is a puzzling difference of nearly a factor of two between the SEP and solar wind measurements of the isotope ratio $^{20}Ne/^{22}Ne$ — Dietrich and Simpson 1979 and Mewaldt et.

al. 1979.)

In Figure 5.6 we focus on the O/Si ratio where measurements are available from all four sources (SEPs, photosphere, solar wind and corona). The individual coronal measurements (EUV data, Mariska 1980) are for a wide range of different coronal environments — quiet sun, coronal hole, active region and prominence. The O/Si ratios measured in SEPs, solar wind and the corona have a comparable spread and, on the average, are all low relative to the photospheric value by slightly more than a factor of three. Although the O/Si ratios observed in SEPs, solar wind and the corona may all be low for different reasons — e.g., possible preferential acceleration of SEPs and solar wind; and possible systematic errors in the solar wind (Bame et. al. 1975) and coronal measurements (Meyer 1978b, Meyer and Nussbaumer 1979, Mariska 1980) — Figure 5.6 suggests a common cause.

The overall similarity of the average SEP elemental composition and the elemental composition measured for the solar wind and corona, and in particular the evidence for a common persistent depletion of oxygen relative to the photospheric composition results, suggests that (a) the SEPs originate in the corona and (b) both the SEPs and solar wind sample a coronal composition which is persistently different from that measured for the photosphere.

It is interesting that the Z-dependence of the ratios of photospheric abundances to four-flare average SEP abundances (seen in Figure 5.5a) is considerably different from the Z-dependence of the

Figure 5.6

Comparison of the O/Si ratio measured in the photosphere, SEPs (this work), solar wind, and corona. For the SEP data, the filled circles refer to the four preferred SEP events (see Section 5.3).

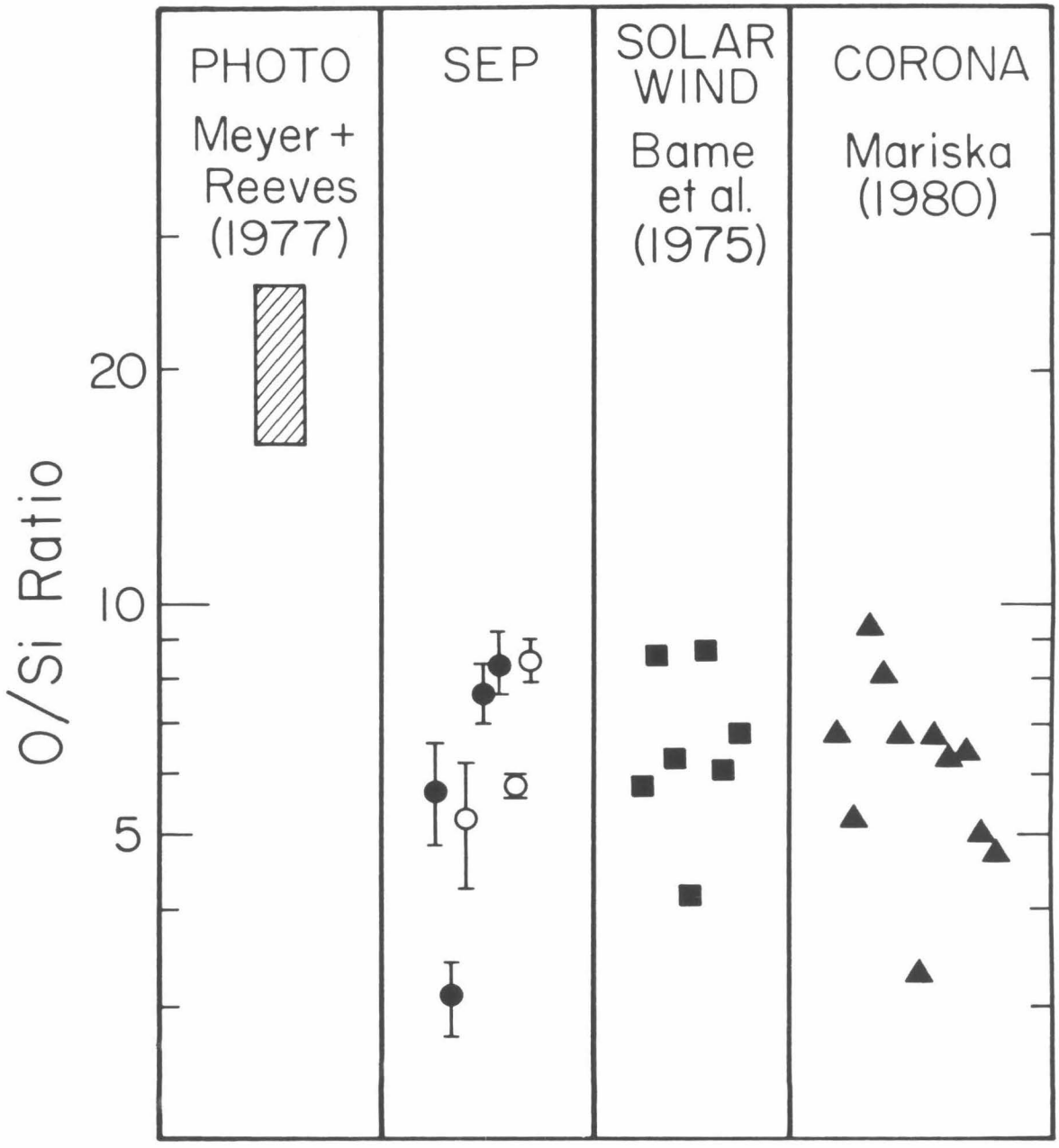
PHOTO
Meyer + Reeves (1977)
SEP
SOLAR WIND
Bame et al. (1975)
CORONA
Mariska (1980)
O/Si Ratio
20
10
5

SEP flare-to-flare abundance variations (seen in Figure 5.4). The flare-to-flare SEP abundance variations were fairly smooth monotonic functions of nuclear charge Z, for $6 \leq Z \leq 28$. In contrast, the Z-dependence of the ratios of photospheric abundances to four-flare average SEP abundances shows a sharp break between O and Mg, and a feature at S — the Z-dependence is neither smooth nor monotonic.

While the ratios of average SEP to photosphere abundances are not ordered by Z, Figure 5.7 shows that they are roughly ordered by a different atomic parameter — the first ionization potential — as noted originally by Webber (1975). Restricting attention to the portion of Figure 5.7 left of the dotted line, we see that the elements with first ionization potential less than 8 eV form a group in which there is rough agreement between the four-flare average SEP and photospheric abundances. However, the elements (C, N and O) with first ionization potential above 11 eV are depleted with respect to the elements with ionization potential below 8 eV by a factor of about five. Sulfur, with an ionization potential near 10 eV, appears in the region of transition between the two groups of elements.

The abundances of the other elements (Ne, Ar and He) with first ionization potential above 11 eV are not measured in the photosphere. However, on the right-hand side of Figure 5.7 we compare the average SEP abundances of these elements to the best available estimates (based primarily on observations of interstellar gas and hot stars) of their solar abundances from the compilation of "Local Galactic" abundances by Meyer (1978a). The average SEP abundances

Figure 5.7

Ratios of the four-flare average SEP abundances to photospheric abundances (left of the dotted line) or to "Local Galactic" abundances (right of the dotted line) plotted versus first ionization potential. All abundances are normalized to silicon ($\odot$). The "SEP uncertainty" is the ($\pm 1\sigma$) uncertainty in the four-flare average abundance, including both the effects of particle counting statistics and flare-to-flare abundance variations.

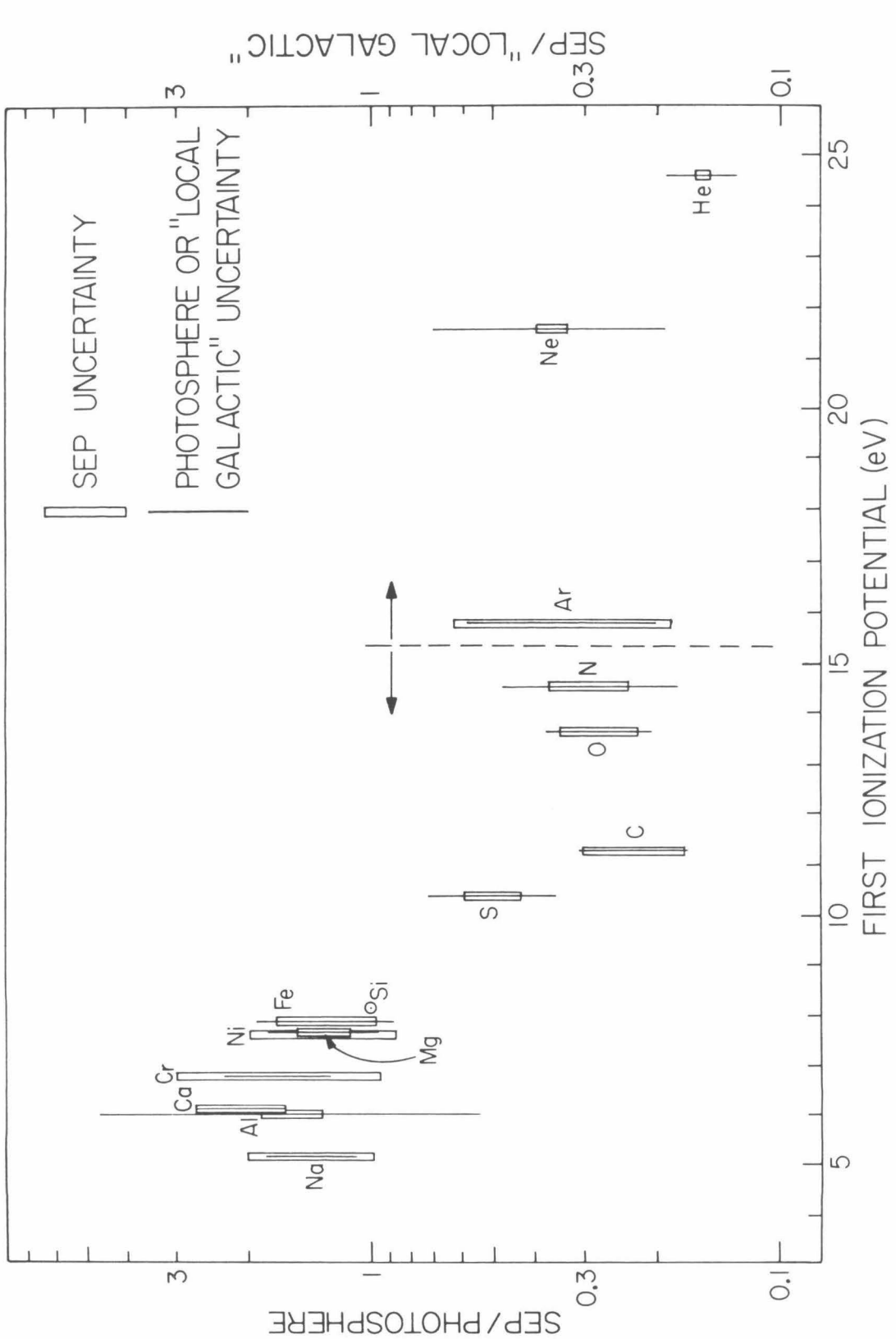
SEP/PHOTOSPHERE
SEP/"LOCAL GALACTIC"
FIRST IONIZATION POTENTIAL (eV)
SEP UNCERTAINTY
PHOTOSPHERE OR "LOCAL GALACTIC" UNCERTAINTY
3
1
0.3
0.1
5
10
15
20
25
Na
Al
Ca
Cr
Ni
Fe
Si
Mg
S
C
O
N
Ar
Ne
He

of Ne, Ar and He appear depleted similar to those of C, N and O. However, since for Ne, Ar and He, we are not comparing the average SEP abundances to solar measurements, the right hand side of Figure 5.7 should be viewed with caution.

Figure 5.7 suggests that (a) first ionization potential or some other related atomic property (such as the cross section for ionization by electron impact) plays an important role in the SEP acceleration process, and/or (b) this same property is involved in the chemical differentiation of the corona from the photosphere. The first ionization potential is of major importance in the photosphere where normally temperatures are of the order of 10^4 K. Here, elements with ionization potential less than 7 eV are predominantly ionized while elements with ionization potential greater than 13 eV are mostly neutral (e.g., see Class 1951 and Gingerich, Noyes and Kalkofen 1971). Thus, neither possibility (a) nor (b) would be surprising. For example, (a) might occur if the SEP acceleration region is initially at the relatively low photospheric temperature. Then the electromagnetic acceleration of elements with high first ionization potential would be delayed until they are ionized and this delay might cause the depletion of elements with high first ionization potential seen in Figure 5.7. Case (b) — which is suggested by the similarity of SEP, solar wind and coronal composition measurements discussed above —could conceivably result from the downward drift of neutral atoms in the photosphere–corona transition region. Neutral atoms experience the downward gravitational acceleration, but are not affected by the magnetic and electric forces which may support and accelerate the

charged component of the atmosphere. (The chemical differentiation of the corona has received some theoretical attention — see, e.g., Geiss, Hirt and Leutwyler 1970, Nakada 1970, and Shine, Gerola and Linsky 1975. However, detailed predictions of coronal composition which could be compared to our SEP abundances are apparently not available.)

Naturally, the correlation seen in Figure 5.7 must be viewed with caution since first ionization potential is related to the overall atomic structure. A search for other atomic parameters which may order the photosphere–SEP composition differences is under way —the results will be reported in a later paper. In particular, the search involves the parameters Z^*/A and $(Z^*)^2/A$, where Z^* — the average ionic charge of the nuclear species with atomic weight A —is taken from ionization equilibrium calculations (e.g. Jordan 1969) appropriate to coronal conditions and is a function of coronal temperature. The parameter Z^*/A, the charge to mass ratio, may be important if the SEP–photosphere difference results from biased electromagnetic acceleration, while the parameter $(Z^*)^2/A$ enters if frictional drag due to Coulomb interactions is important.

It is necessary to mention that the correlation seen in Figure 5.7 depends on the correctness of the photospheric abundance determinations. Meteoritic abundances verify the photospheric results only for the non–volatile elements, which are exactly those in the group with first ionization potentials below 8 eV.

5.6 Summary

The Low Energy Telescopes on the Voyager spacecraft have been used to measure the elemental composition ($2 \leq Z \leq 28$) and energy spectra (5 to 15 MeV/nucleon) of solar energetic particles (SEP) in seven large flare events. Aiming to understand the relationship between SEP elemental composition and the composition of the sun we have (a) discussed the time and velocity dependence of SEP composition in the individual flare events, (b) selected for further study four events with SEP abundances approximately independent of energy/nucleon, (c) examined the SEP flare-to-flare composition variations among the four selected flares and (d) compared the SEP composition for the selected events to solar abundance results for the photosphere, corona and solar wind.

For the four selected events, the SEP composition results could be described by an average composition plus a systematic deviation about the average. In particular, for each of the four events, the ratios of the SEP abundances to the four-flare average SEP abundances were seen to be approximately monotonic functions of nuclear charge Z in the range $6 \leq Z \leq 28$. An important exception to this pattern of Z-dependent flare-to-flare abundance variation occurred for He, whose abundance relative to Si was nearly the same in all four events.

The four-flare average SEP composition was found to be significantly different from the solar composition determined by photospheric spectroscopy. The ratios of the four-flare average SEP abundances to photospheric abundances are roughly ordered by first

ionization potential -- the atomic parameter that determines which elemental species are ionized and which are neutral in the photosphere. Compared to photospheric abundance results, the elements with first ionization potentials above 11 eV (C, N and O) are depleted in SEPs by a factor of about five relative to the elements with first ionization below 8 eV (Na, Mg, Al, Si, Ca, Cr, Fe and Ni). The abundances of the elements Ne, Ar, and He (which also have first ionization potential greater than 11 eV), are not measured in the photosphere. However, relative to "Local Galactic" abundances of these elements, the four-flare average SEP abundances are depleted similar to those of C, N, and O.

For some elemental abundance ratios, the difference between SEP and photospheric results is persistent from flare-to-flare (even among all seven events) and is apparently not due to systematic differences in SEP spectral index between the elements, nor to propagation effects which would result in a time-dependent abundance ratio in individual flare events. A striking example occurs for the Mg/O ratio. The elements Mg and O have nearly equal spectral indices in each of the seven flare events; the Mg/O ratio is approximately constant with time in each event and has nearly the same value from event to event. However, the SEP Mg/O ratio is about a factor of four larger than the photospheric result, which has an estimated uncertainty of only about 25 percent. This suggests that (a) the composition of the flare acceleration sites are persistently different from that of the photosphere and/or (b) there is a persistent SEP acceleration bias which operates at energies outside our range of observation.

The four-flare average SEP composition was found to be in good agreement with solar wind abundance results and with a number of recent coronal abundance measurements. This favors possibility (a) above. In particular, the evidence for a common depletion of oxygen in SEPs, the corona and the solar wind relative to the photosphere suggests (assuming the correctness of the photospheric results) that the SEP's originate in the corona and that both the SEPs and solar wind sample a coronal composition which is significantly and persistently different from that of the photosphere.

Appendix A

Data Processing

Data from the Voyager spacecraft are received at earth by the Deep Space Network and are processed at the Caltech Jet Propulsion Laboratory, which delivers "experiment" data (magnetic) tapes to the various Voyager science teams. The Cosmic Ray Subsystem (CRS) data are sent to the Goddard Space Flight Center and are reformatted to produce CRS "encyclopedia" data tapes, copies of which are sent to Caltech. The tapes are logged and merged to produce a set of encyclopedia tapes containing time-ordered data.

The data processing for this thesis is shown schematically in Figure A.1. The encyclopedia tapes were processed using the VSTRIP program (Aufrance and Garrard 1978) to create the "strip" tapes V1SZ01 (Voyager 1) and V2SZ01 (Voyager 2). These tapes contain LET $Z \geq 3$ and helium PHA events, together with complete CRS rate and status information, for each hour of data from September 1977 to May 1978. The "strip" tapes were processed by the program ELMER which produced (1) a printed summary of the data for each six hour period, including preliminary PHA event counts for the most abundant elements in selected energy/nucleon bins and rate information needed to normalize the event counts to obtain preliminary flux measurements, (2) the same summary information on tape, and (3) a "event" tape containing only PHA events.

An assortment of programs made use of the $Z \geq 3$ PHA events to complete the LET electronic calibration and deduce an adequate

DATA PROCESSING

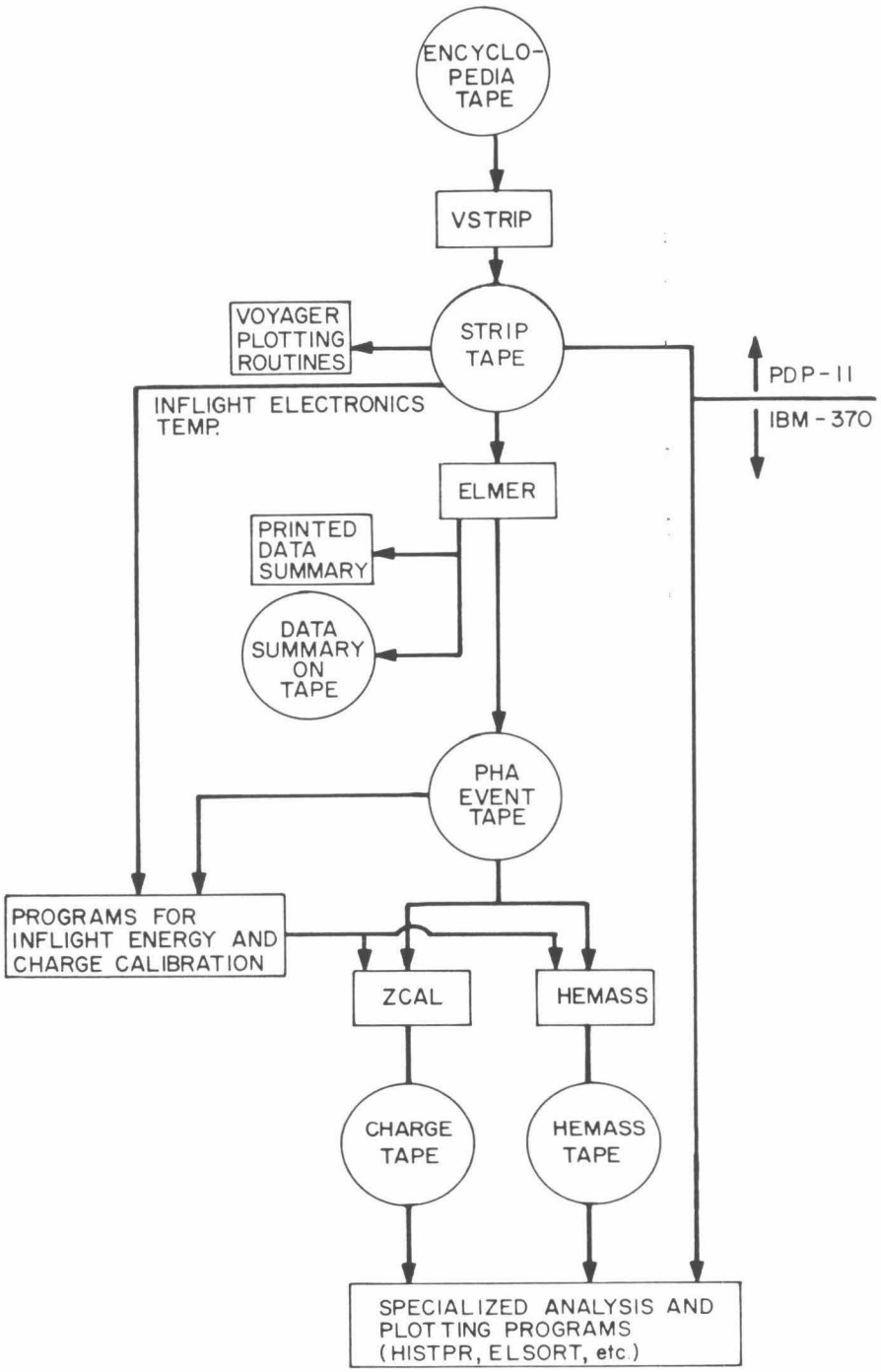

Figure A.1

generalized range–energy relation for the elements carbon through iron. These results and the L1 and L2 detector pathlength measurements were used by the program ZCAL to produce a "charge" tape which contains for each $Z \geq 3$ PHA event: (1) a number indicating the time of occurrence, (2) a number indicating which LET telescope the event was from and whether or not the L3 detector was triggered, (3) the energy (in MeV) measured in each detector, and (4) the charge measurements Z1 and, if L3 was triggered, Z2. The program HEMASS produced a similar "helium mass" tape which for every helium PHA event contains the above items (1) through (3) and the mass measurements M1 and, if L3 was triggered, M2.

A variety of specialized computer programs were used to investigate the data on the "charge" and "He mass" tapes, and to compute the flux and abundance measurements presented in Chapter 4. In particular, for each flare event, the program HISTPL was used to produce Z1 and (Z1+Z2)/2 charge histograms (e.g. Figures 3.9 and 3.10) from which the "PHA event" averaged abundances of $Z \geq 3$ nuclei (Tables 4.2 and 4.3) were obtained. The program ELSORT selected and accumulated PHA events in three hour intervals for the fluence measurements of Tables 4.4 through 4.11.

Appendix B

Problems

B.1 LET B of Voyager 1

The response of this telescope was unusual in that (1) the He mass measurement, M1, showed a relatively large energy and time dependence, (2) a relatively large "background" of events was present in the charge range near fluorine, and (3) the L1 versus L2+L3 element tracks had a uncharacteristically blurred appearance. The problem may be electronic instability, but was not investigated in detail; instead the data from this telescope were excluded from use in the measurements presented in Chapter 4, Tables 4.1 through 4.12

B.2 LET C of Voyager 2

On April 1, 1978 the L1 detector of this telescope experienced a simultaneous shift in energy calibration and increase in count rate, perhaps as the result of a light leak in the thin Al entrance window. Subsequent data from this telescope were not used in the measurements of Chapter 4, Tables 4.1 through 4.12.

B.3 Pulse Height Multiplication in the LET 35 μm Detectors

A background effect specific to the iron group nuclei was identified in Sections 3.3 and 3.5 and necessitated the further study and special handling which is discussed here. The affected PHA events were clearly seen in Figure 3.7, a plot of the charge measurements Z1 versus Z2, as a clump of points near (Z1=26,Z2=28). Inspection of the L1, L2

and L3 pulse heights of the events in this clump revealed a very specific signature:

(1) The events lie directly on the L1 versus L3 track for iron, but lie just above the L2 versus L3 iron track, indicating that the L1 and L3 pulse heights are normal, but that the L2 pulse height is abnormally large.

(2) The events have relatively small L3 pulse heights (E_{L3} less than about 170 MeV), indicating that the nuclei responsible for the events just barely penetrated detector L2.

The effect also occurs for a fraction of the iron nuclei which barely penetrate the L1 detectors. In this case, the affected events may be seen as the unusual clump of points near Z1=28 in Figure 3.6.

The above signature suggests a pulse height multiplication effect in the LET 35 μm surface barrier detectors that is very similar to one observed earlier in the response of such detectors to fission fragments. The effect (discussed by Walter 1969) occurs for nuclei which deposit a large ionization charge density in the depleted silicon near the gold electrode. The large ionization charge density is thought to induce tunneling of additional carriers (electrons) from the electrode through the thin oxide layer which separates the electrode from the depleted bulk silicon. The orientation of the LET 35 μm detectors is consistent with this multiplication hypothesis: The gold electrodes face toward the L3 detector, such that the ionization charge density near a gold electrode is largest for nuclei which just barely penetrate the detector, as in (2) above.

To further study the problem, three detector PHA events with charge measurements Z1 > 24 were re-analyzed. For each event the L1 and L3 energy measurements (E_{L1} and E_{L3}) were used to calculate a new charge measurement Z' and obtain an estimate E'_{L2} of the energy deposited in detector L2 by solving:

$$T_{L1} = R(E_{L1}+E'_{L2}+E_{L3}, Z', M) - R(E'_{L2}+E_{L3}, Z', M)$$

$$T_{L2} = R(E'_{L2}+E_{L3}, Z', M) - R(E_{L3}, Z', M)$$

taking

$$M = 2.132 \cdot Z' .$$

R is the generalized range-energy function discussed in Section 3.4. T_{L1} and T_{L2} are the mean pathlengths for the L1 and L2 detectors respectively. The results are illustrated in Figure B.1, a plot of E_{L2} (the measured L2 energy) versus E'_{L2} (the L2 energy inferred from the L1 and L3 energy measurements). Normal events lie along the diagonal, while events with abnormally large L2 energy measurements lie above the diagonal. (Events below the diagonal may be due to L2 edge effects and other processes discussed in Section 3.5.2) The abnormal events occur predominantly at large values of E'_{L2} which can only be obtained by nuclei which barely penetrate L2, consistent with observation (2) above. Figure B.2 shows two histograms of E_{L2} / E'_{L2}; one histogram for events which barely penetrate L2 (E_{L3} < 170 MeV) and one for the remaining events (E_{L3} > 170 MeV). These histograms are summed over all the LETs used on both Voyagers and indicate that (1) about 15 percent of the events with E_{L3} less than 170 MeV have L2 energy measurements which are abnormally large by an average of about 12 percent and (2) the L2 energy measurements are essentially normal

Figure B.1

A scatter plot of the L2 detector energy measurement (E_{L2}) versus the L2 energy deposition (E'_{L2}) inferred from the L1 and L3 energy measurements, for three-detector PHA events with Z1 > 24.

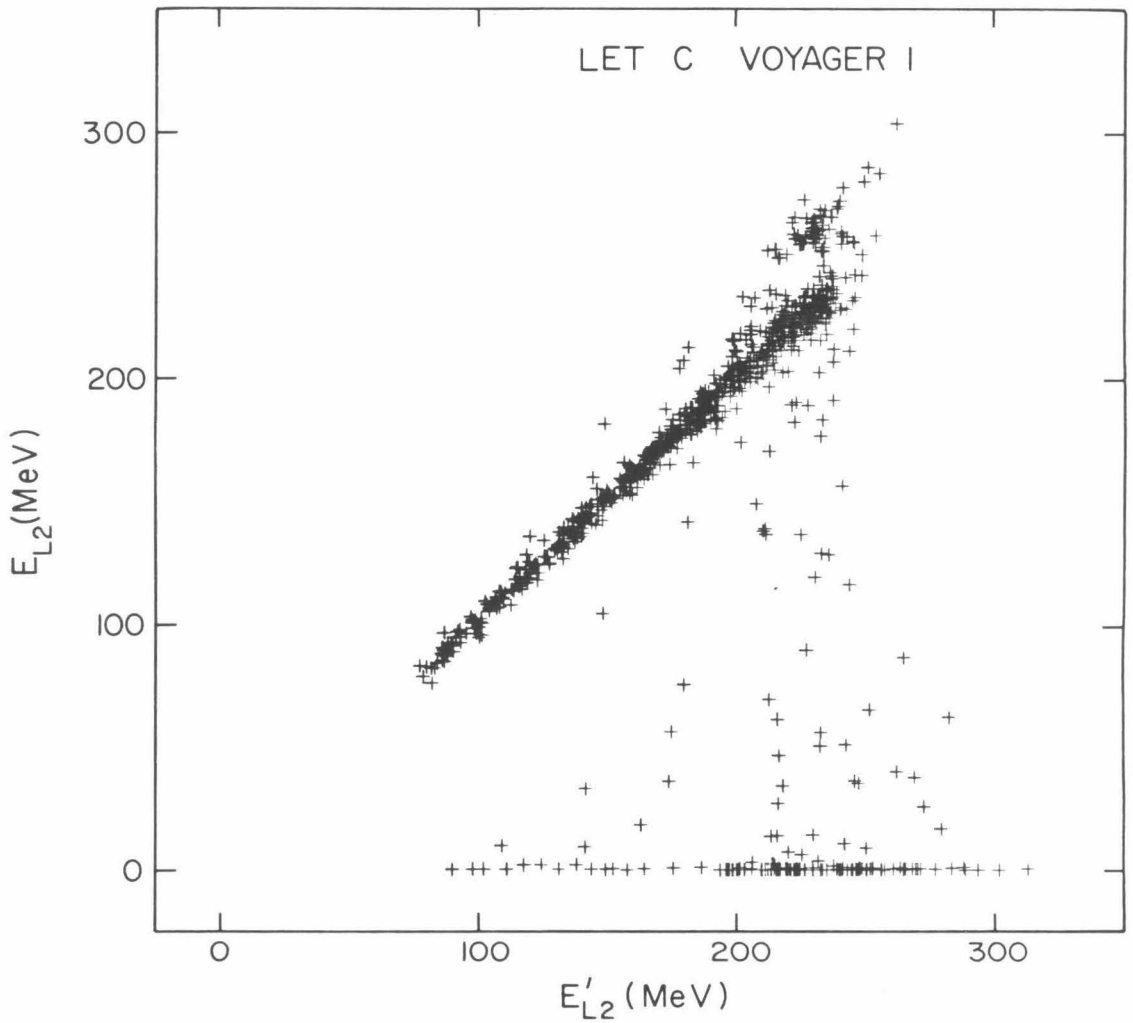
LET C VOYAGER I
300
200
100
0
0
100
200
300
E_{L2}(MeV)
E'_{L2} (MeV)

Figure B.2

Two histograms of the ratio of the L2 detector energy measurement (E_{L2}) to the L2 energy deposition (E'_{L2}) inferred from the L1 and L3 energy measurements. The histograms are summed over three-detector PHA events with Z1> 24, from all the LETs used on both Voyager spacecraft. The histogram on the left includes only PHA events corresponding to nuclei which just barely penetrate detector L2 (E_{L3}< 170 MeV), while the histogram on the right includes the remaining events (E_{L3}> 170 MeV).

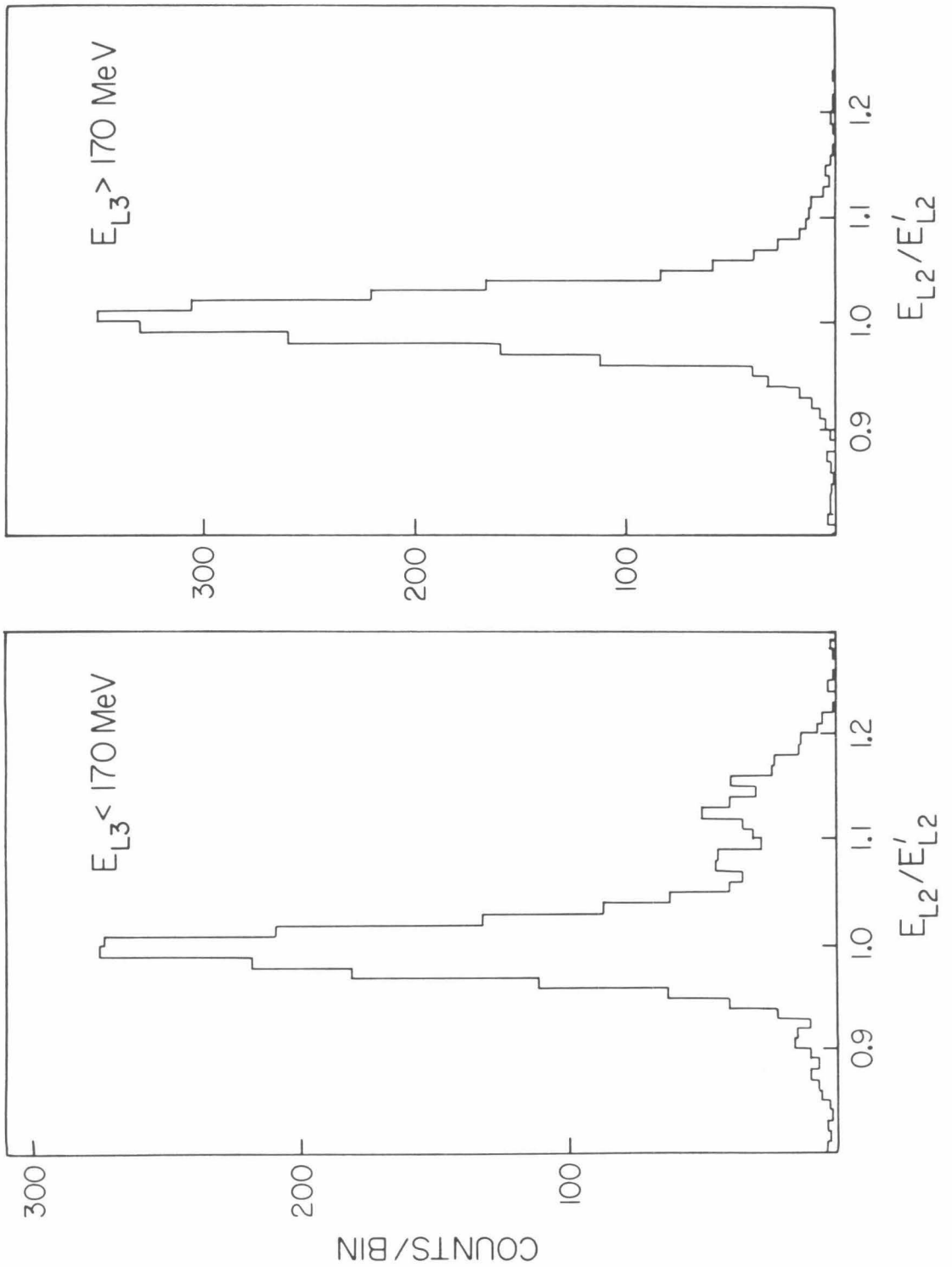
E_{L3}< 170 MeV
E_{L3}> 170 MeV
COUNTS/BIN
300
200
100
0.9
1.0
1.1
1.2
E_{L2}/E'_{L2}

for events with E_{L3} greater than 170 MeV.

The special data analysis necessitated by the multiplication effect is discussed below.

B.3.1 Three Parameter Analysis for Iron Nuclei

The results for iron nuclei presented in Table 4.2 (8.7–15.0 MeV/nucleon) are based on PHA events selected as follows:

(1) Normal iron events (i.e. those with normal L2 pulse height) were selected using the charge consistency requirement and charge boundaries discussed in Section 3.5, and were counted if the total energy measurement, $E_{L1}+E_{L2}+E_{L3}$, was appropriate to the 8.7–15.0 MeV/nucleon interval.

(2) Iron PHA events having abnormally large L2 pulse heights were identified as those events with charge measurements near (Z1=26,Z2=28). (Specifically, the requirement was $(Z1+Z2)/2 > 25$ and $(Z1-Z2) < -0.85$.) For each of these PHA events the L2 energy measurement was divided by 1.125 (the mean shift of the abnormal L2 energy measurements; see Figure B.2) to obtain a corrected value E^{*}_{L2}. Then the event was counted if $E_{L1}+E^{*}_{L2}+E_{L3}$ was within the total energy interval corresponding to 8.7–15.0 MeV/nucleon.

PHA events with abnormal L2 pulse heights constitute about 15 percent of the iron nuclei counts presented in Table 4.2. Any additional systematic error (beyond that discussed in Section 4.4.1) in the iron nuclei counts due to the abnormal L2 pulse heights should be

small. For example, if no corrections at all are applied to the abnormal L2 energy measurements (as was the case for the iron abundances reported earlier in Cook et. al. 1979 and Cook, Stone and Vogt 1980) , the resulting iron abundance measurements differ from those of Table 4.2 by less than 5 percent.

B.3.2 Two Parameter Analysis for Iron Nuclei

In the two parameter analysis of iron (for the fluence measurements of Tables 4.4 through 4.11) the multiplication effect in the L1 detectors was taken into account as follows:

(1) Iron PHA events with normal L1 pulse heights were identified as those events with charge measurement Z1 in the range 24.8 to 27.2 and were binned according to energy/nucleon as described in Section 3.4.

(2) PHA events with charge Z1 in the range 27.2 to 32.0 and L2+L3 energy measurements of less than 170 MeV are primarily due to iron nuclei with abnormally large L1 pulse heights, rather than nickel or other nuclei. Therefore, the L1 energy measurements of these events were divided by 1.125 before energy/nucleon binning. The remaining events with Z1 in the range 27.2 to 32.0 (i.e., those with $E_{L2}+E_{L3} > 170$ MeV) are mainly nickel nuclei and were included with no L1 energy adjustment. All PHA events were sorted into energy/nucleon bins as if they were due to iron nuclei, exactly as in (1) above.

In the two parameter iron analysis, no special treatment was applied to account for multiplication effects in the L2 detectors. They

do not significantly affect the Z1 charge measurement and at most shift a small fraction (about 5 percent) of the PHA events which should fall in the 7.8–8.7 MeV/nucleon interval into the 8.7–10.6 MeV/nucleon interval.

The inclusion of nickel and other nuclei ($27 \leq Z \leq 32$) increases the fluence measurements over measurements of pure iron by roughly the combined abundance of these elements relative to iron, or about 10 percent. However, the inclusion of these nuclei probably has only a negligible effect on the spectral index (γ, see Section 4.5), since the energy spectra of the various elements of the iron group are likely to be similar. (Spectral index variations among the elements appear to be roughly ordered by nuclear charge Z, such that, in a given flare event, neighboring elements have similar spectral indices; see Section 5.2. Further, the nickel to iron ratio [8.7–15 MeV/nucleon, Table 4.2] is nearly constant from flare to flare.)

The multiplication effect in the L1 detectors is potentially an additional source of systematic error (beyond those discussed in Section 4.5) in the iron fluence measurements of Tables 4.4 through 4.11 and the iron spectral index measurements of Table 4.12. Upper limits to these possible additional errors were obtained by recomputing the fluences and spectral indices without the L1 energy corrections discussed in (2) above. The changes in the iron fluence measurements were typically less than 10 percent for energy bins in the range 5.0–8.7 MeV/nucleon, and were zero for the other higher energy bins. The iron spectral indices changed by less than 5 percent. Since the actual systematic error induced in the iron

spectral indices is probably much less than 5 percent (and therefore is small compared to statistical error and the possible systematic error from other sources discussed in Section 4.5) this error is negligible.

References

Acton, L. W., Catura, R. C., and Joki, E. G. 1975, *Ap. J. (Letters)*, **195**, L93.

Aller, L. H. 1980, "The Solar Abundance Pattern", talk presented at the 4th Annual Santa Cruz Summer Workshop in Astronomy and Astrophysics.

Armstrong, T. P., and Krimigis, S. M. 1971, *J. Geophys. Res.*, **76**, 4230.

Armstrong, T. P., Krimigis, S. M., Hovestadt, D., Klecker, B., and Gloeckler, G. 1976, *Solar Phys.*, **49**, 395.

Armstrong, T. P., Krimigis, S. M., Reames, D. V., and Fichtel, C. E. 1972, *J. Geophys. Res.*, **77**, 3607.

Aufrance, T. J., and Garrard, T. L. 1979, Space Radiation Laboratory Technical Report 79–2, Calif. Institute of Technology.

Bame, S. J., Asbridge, J. R., Feldman, W. C., Montgomery, M. D., and Kearney, P. D. 1975, *Solar Phys.*, **43**, 463.

Bertsch, D. L., Biswas, S., Fichtel, C. E., Pellerin, C. J., and Reames, D. V. 1973, *Solar Phys.*, **31**, 247.

Bertsch, D. L., Biswas, S., and Reames, D. V. 1974, *Solar Phys.*, **39**, 479.

Bertsch, D. L., Fichtel, C. E., and Reames, D. V. 1972, *Ap. J.*, **171**, 169.

Bertsch, D. L., and Reames, D. V. 1977, *Solar Phys.*, **55**, 491.

Bevington, P. R. 1969, *Data Reduction and Error Analysis for the Physical Sciences*, McGraw–Hill.

Biswas, S., and Fichtel, C. E. 1965, *Space Sci. Rev.*, 4, 709.

Biswas, S., Fichtel, C. E., and Guss, D. E. 1962, *Phys. Rev.*, **128**, 2756.

Biswas, S., Fichtel, C. E., and Guss, D. E. 1966, *J. Geophys. Res.*, **71**, 4071.

Biswas, S., Fichtel, C. E., Guss, D. E., and Waddington, C. J. 1963, *J. Geophys. Res.*, **68**, 3109.

Boschler, P., and Geiss, J. 1976, Grenoble IAU Meeting, Report of Commission 12 (Solar Atmosphere).

Briggs, P. R., Armstrong, T. P., and Krimigis S. M. 1979, *Ap. J. (Letters)*, **228**, L83.

Cameron, A. G. W. 1968, in L. H. Ahrens (ed.), *Origin and Distribution of the Elements*, Pergamon Press, Oxford.

Cameron, A. G. W. 1973, *Space Sci. Rev.*, **15**, 121.

Claas, W. J. 1951, *Rech. Astr. Obs. Utrecht*, **12**, Part 1.

Coffey, H. E. (ed.) 1977–8, *Solar Geophysical Data*, U. S. Dept. of Commerce, Boulder, Colo., **398–412**.

Cook, W. R., Stone, E. C., and Vogt, R. E. 1980, *Ap. J. (Letters)*, **238**, L97.

Cook, W. R., Stone, E. C., Vogt, R. E., Trainor, J. H., and Webber, W. R. 1979, *Proc. 16th International Cosmic Ray Conf.* (Kyoto), **12**, 265.

Crawford, H. J., Price, P. B., Cartwright, B. G., and Sullivan, J. D. 1975, *Ap. J.*, **195**, 213.

Dietrich, W. F., and Simpson, J. A. 1978, *Ap. J. (Letters)*, **225**, L41.

Dietrich, W. F., and Simpson, J. A. 1979, *Ap. J. (Letters)*, **231**, L91.

Durgaprasad, N., Fichtel, C. E., Guss, D. E., and Reames, D. V. 1968, *Ap. J.*, **154**, 307.

Fichtel, C. E., and McDonald, F. B. 1967, *Ann. Rev. Astr. Astrophys.*, **5**, 351.

Flower, D. R., and Nussbaumer, H. 1975, *Astron. Astrophys.*, **39**, 295.

Gehrels, N. 1980, private communication.

Gehrels, N. 1980, Space Radiation Laboratory Technical Report 80–1, Calif. Institute of Technology.

Geiss, J., Buehler, F., Cerutti, H., Eberhardt, P., and Filleux, C. 1972, "Solar Wind Composition Experiment", *Apollo 16 Preliminary Science Report*, NASA SP–315.

Geiss, J., Hirt. P., and Leutwyler, H. 1970, *Solar Phys.*, **12**, 458.

Gingerich, O., Noyes, R. W., and Kalkofen, W. 1971, *Solar Phys.*, **18**, 347.

Gloeckler, G., Sciambi, R. K., Fan, C. Y., and Hovestadt, D. 1976, *Ap. J. (Letters)*, **209**, L93.

Goldberg, L., Muller, E. A., and Aller L. H. 1960, *Ap. J. Suppl.*, **5**, 1.

Heckman, H. H., Perkins, B. L., Simon, W. G., Smith, F. M., and Barkas, W. H. 1960, *Phys. Rev.*, **117**, 544.

Hovestadt, D., Klecker, B., Vollmer, O., Gloeckler, G., and Fan, C. Y. 1975, *Proc. 14th International Cosmic Ray Conf.* (Munich), **5**, 1613.

Hurford, G. J., Mewaldt, R. A., Stone, E. C., and Vogt, R. E. 1975, *Ap. J. (Letters)*, **201**, L95.

Janni, J. F. 1966, "Calculations of Energy Loss, Range, Pathlength, Straggling, etc.", Tech. Report AFWL-TR-65-150.

Jordan, C. 1969, *Mon. Not. R. Astr. Soc.*, **142**, 501.

Kaufman, S. B., Steinberg, E. P., Wilkins, B. D., Unik, J., Gorski, A. J., and Fluss, M. J. 1974, *Nuc. Instrum. Methods*, **115**, 47.

Lambert, D. L. 1978, *Mon. Not. R. Astr. Soc.*, **182**, 249.

Lambert, D. L., and Luck, R. E. 1978, *Mon. Not. R. Astr. Soc.*, **183**, 79.

Lanzerroti, L. J., Maclennan, C. G., and Graedel, T. E. 1972, *Ap. J. (Letters)*, **173**, L39.

Mariska, J. T. 1980, *Ap. J.*, **235**, 268.

Mason, G. M., Hovestadt, D., and Gloeckler, G. 1979, *Proc. 16th International Cosmic Ray Conf.* (Kyoto), **5**, 110.

McGuire, R. E., von Rosenvinge, T. T., and McDonald, F. B. 1979, *Proc. 16th International Cosmic Ray Conf.* (Kyoto), **5**, 61.

McKenzie, D. L., Rugge, H. R., Underwood, J. H., and Young, R. M. 1978, *Ap. J.*, **221**, 342.

Mewaldt, R. A. 1980, to be published in *Proc. of the Conference on the Ancient Sun: Fossil Record in the Earth, Moon, and Meteorites* (Boulder, Colorado).

Mewaldt, R. A., Spalding, J. D., Stone, E. C., and Vogt, R. E. 1979, *Ap. J. (Letters)*, **231**, L97.

Meyer, A., and Nussbaumer, H. 1979, *Astron. Astrophys.*, **78**, 33.

Meyer, J. P. 1978a, "The Significance of the Carbonaceous Chondrites Abundances", 22nd Liège International Astrophys. Symposium.

Meyer, J. P. 1978b, "The Neon Abundance in the Solar Neighborhood", 22nd Liège International Astrophys. Symposium.

Meyer, J. P., and Reeves, H. 1977, *Proc. 15th International Cosmic Ray Conf.* (Plovdiv), **2**, 137.

Mogro-Campero, A., and Simpson, J. A. 1972a, *Ap. J. (Letters)*, **171**, L5.

Mogro-Campero, A., and Simpson, J. A. 1972b, *Ap. J. (Letters)*, **177**, L37.

Montmerle, T. 1979, *Ap. J.*, **231**, 95.

Nakada, M. P. 1970, *Solar Phys.*, **14**, 457.

Nevatia, J., Durgaprasad, N., and Biswas, S. 1977, *Proc. 15th*

International Cosmic Ray Conf. (Plovdiv), **5**, 48.

O'Gallagher, J. J., Hovestadt , D., Klecker, B., Gloeckler, G., and Fan, C. Y. 1976, *Ap. J. (Letters)*, **209**, L97.

Parkinson, J. H. 1977, *Astron. Astrophys.*, **57**, 185.

Pellerin, C. J. 1975, *Solar Phys.*, **41**, 449.

Povlis, J. 1980, Space Radiation Laboratory Technical Report 80–2, California Institute of Technology.

Price, P. B., Chan, J. H., Hutcheon, I. D., MacDougall, D., Rajan, R. S., Shirk, E. K., and Sullivan, J. D. 1974, *Proceedings of the 4th Lunar Science Conference* (Supplement 4, *Geochimica et Cosmochimica Acta*), **3**, 2347.

Ross, J. E., and Aller, L. H. 1976, *Science*, **19**, 1223.

Russell, H. N. 1929, *Ap. J.*, **70**, 11.

Scholer, M., Hovestadt , D., Klecker, B., Gloeckler, G., and Fan, C. Y. 1978, *J. Geophys. Res.*, **83**, 3349.

Sciambi, R. K., Gloeckler, G., Fan, C. Y., and Hovestadt , D. 1977, *Ap. J.*, **214**, 316.

Shine, R., Gerola, H., and Linsky, J. L. 1975, *Ap. J. (Letters)*, **202**, L101.

Stilwell, D. E., Davis, W. D., Joyce, R. M., McDonald, R. B., Trainor, J. H., Althouse, W. E., Cummings, A. C., Garrard, T. L., Stone, E. C., and Vogt, R. E. 1979, *IEEE Trans. Nucl. Sci.*, **NS–26(1)**, 513.

Stone, E. C., Vogt, R. E., McDonald, F. B., Teegarden, B. J., Trainor, J. H., Jokipii, J. R., and Webber, W. R. 1977, *Space Sci. Rev.*, **21**, 355.

Svestka, Z. 1976, *Solar Flares*, D. Reidel.

Teegarden, B. J., von Rosenvinge, T. T., and McDonald, F. B. 1973, *Ap. J.*, **180**, 571.

Van Allen, J. A., Venketarangan, P., and Venkatesan, D. 1974, *J. Geo. Res.*, **79**, 1.

Vidor, S. B. 1975, Thesis, California Institute of Technology.

von Rosenvinge, T. T., and Reames, D. V. 1979, *Proc. 16th International Cosmic Ray Conf.* (Kyoto), **5**, 68.

Walter, F. J. 1964, *IEEE Trans. Nucl. Sci.*, **NS–11(3)**, 232.

Webber, W. R. 1975, *Proc. 14th International Cosmic Ray Conf.* (Munich), **5**, 1597.

Webber, W. R., Roelof, E. C., McDonald, F. B., Teegarden, B. J., and Trainor, J. 1975, *Ap. J.*, **199**, 482.

Wibberenz, G. 1979, *Proc. 16th International Cosmic Ray Conf.* (Kyoto), **14**, 234.

Withbroe, G. L. 1975, *Solar Phys.*, **45**, 301.

Withbroe, G. L. 1976, Center for Astrophys., Harvard College Obs. and Smithsonian Astrophys. Obs., Preprint Series No. 524.

Ziegler, J. F. 1977, *Helium Stopping Powers and Ranges in all Elements*, Pergamon Press.

Zwickl, R. D., Roelof, E. C., Gold, R. E., and Krimigis, S. M. 1978, *Ap. J.*, **225**, 281.